UNIVERSITY OF TRENTO

Doctoral School in Civil, Environmental and Mechanical Engineering

Curriculum 1. Civil and Environmental Engineering

Andrea Galletti

Detailed simulation of storage hydropower systems in the Italian Alpine Region

2020 - Doctoral thesis

UNIVERSITY OF TRENTO - Italy
Department of Civil, Environmental
and Mechanical Engineering

Doctoral School in Civil, Environmental and Mechanical Engineering
Topic 1. Civil and Environmental Engineering - XXXII cycle 2016/2019

Doctoral Thesis - April 2020

Andrea Galletti

Detailed simulation of storage hydropower systems in the Italian Alpine Region

Supervisors
Prof. Eng. Bruno Majone - University of Trento
Prof. Eng. Alberto Bellin - University of Trento

Credits of the cover image .....

ISBN (paper): ..... ; ISBN (online): .....

University of Trento
Doctoral School in Civil, Environmental and Mechanical Engineering
http://web.unitn.it/en/dricam
Via Mesiano 77, I-38123 Trento
Tel. +39 0461 282670 / 2611 - *dicamphd@unitn.it*

To my family

ABSTRACT

The water-energy nexus holds paramount relevance in the context of the transition to a carbon free energy system, being water the only renewable energy source with reliable storage capacity.
Modelling hydropower production in a large domain over a long time window represents an open challenge due to a variety of reasons: firstly, high-resolution, large-scale hydrological modelling in a context of uncertainty needs calibration, thus representing a computationally intensive task due to the large domain and time window over which calibration is needed; secondly, as stated by many works in literature, hydropower production modelling and in particular reservoir modelling is a very information-demanding procedure, and excessive simplifications adopted to face the lack of information might lead to consistent bias in the predictions.
This thesis can be subdivided into three main parts: firstly, the model that was used to perform every analysis, HYPERstreamHS, will be presented. The model is a continuous, large-scale hydrological model embedding a dual-layer MPI framework (i.e. Message Passing Interface, a common standard in parallel computing) that ensures optimal scalability of the model, greatly reducing the computation time needed. Explicit simulation of water diversions due to hydropower production is also included in the model, and adopts only publicly available information, making the model widely applicable. Secondly, a first validation of the model will be presented, and the adopted approach will be compared with some other approaches commonly found in literature, showing that the inclusion of a high level of detail is crucial to ensure a reliable performance of the model; this first application was performed on the Adige catchment, where extensive information on human systems was available, and allowed to effectively assess which information were indispensable and which, in turn, could be simplified to some extent while preserving model performance. Finally, the model setup has been applied on a relevant portion of the Western Italian Alps; in this case, two different meteorological input forcing data sets were adopted, in order to assess the differences in their performance in terms of hydropower production modelling. This latter study indeed represents a preliminary analysis and will provide stepping stone to extend the modelling framework to the Italian Alpine Region.

TABLE OF CONTENTS

CHAPTER 1

INTRODUCTION

In this chapter a general overview of the relevant topics concerning hydropower production modelling is provided, with particular attention to three topics: first, the adoption of High Performance Computing (HPC) resources in hydrological modelling applications, followed by a review of the works that include explicit simulation of streamflow alterations due to hydropower system. Finally, the role of meteorological input data sets in hydropower production modelling will be discussed.

1.1 Thesis Structure

The thesis is articulated through 6 main chapters. In Chapter 1, the relevant topics for this research are introduced and the state of the art is briefly reviewed, leading to the scientific questions and objectives of the research. Chapter 2 covers the methods adopted for the research, illustrating in detail the model and elaboration tools that were used to carry over all the activities. Chapter 3 covers the data, case studies and statistical tools for our analyses. Chapters 4 to 6 contain the main results and findings of this work. Finally, the results are summarized in Chapter 6, which provides concluding remarks as well as perspective work on this topic.

1.2 Hydropower production in the Alpine Region

The Alpine Region certainly represents one of the largest sources of freshwater in Europe, providing water to major continental catchments, such as those of the Danube, Rhine, Po and Rhone rivers. Abundant freshwater has always represented a primary requirement for human settlement, as it contributed to many important aspect of early societies, such as irrigation, breeding, transportation, personal and public hygiene and many forms of hydro-power exploitations.

While breeding, agriculture and hygiene still represent primary water usages, water is nowadays also used in industrial processes such as engine cooling or in the production of hydroelectricity. In fact, the term *hydropower* has progressively lost its wider meaning of exploitation of the mechanical energy stored in a water body, in favor of the more particular one of *hydroelectricity*, (i.e. energy obtained converting water's kinetic energy into electricity by means of turbines). The perception of water as a primary resource might have therefore changed in recent years, since traditional water usages have been concentrated and automated in several ways (e.g. municipalisation of drinking water and wastewater treatment, industrialization breeding and agricultural activities, use of fuels and electricity as the main sources of power); albeit many forms of water usage have changed through the course of history, freshwater availability still

plays a key role in every society. Furthermore, the steady increase in world population corresponds to an increase in demand for food and energy, which are both closely linked to water availability. It is therefore clear that water should be in many circumstances regarded to as a scarce resource to be preserved proactively, rather than as a disposable good.

In the context of optimizing worldwide resource usage, freshwater certainly holds capital importance since its usage is at the foundation of countless activities (i.e. hydro-power exploitation, agriculture, manufacturing, touristic and recreational uses, to cite the most relevant ones) (Beniston, 2012; Meissner and Relier, 2005). In particular, hydropower contributes for more than 19% to the worldwide electricity demand (Akpinar, 2013; IEA), and storage hydropower currently represents the only renewable energy source that ensures reliable, long-term energy storage capacity (Barton and Infield, 2004), though technology is rapidly advancing in this sector and scenarios with progressive decommissioning of dams in favor of a more diffuse use of solar energy have been recently envisioned (Waldman et al., 2019). Nevertheless, hydropower can be expected to cover a key role in the near future energy market, helping to ensure a smoother transition to a low-carbon footprint energy market, and its contribution should be therefore planned with utmost care.

Many studies on climate change expect temperature to be generally higher in the near future (Brunetti et al., 2009; Jasper et al., 2004; Keiler et al., 2010); on the other hand, predictions on precipitations and of their effects on hydrologic regimes are closely linked to the topography of the domain.

Nowadays, environmental regulators all around the world are drawing guidelines and/or enforcing prescriptions aimed at a more sustainable water usage, acknowledging the scarcity of the resource. In a climate-change context, this calls for models that are able to deal with all levels of uncertainty, from the one embedded in future climate, to hydrological uncertainty, all the way up to all kinds of water usage, which potentially carry the largest amount of uncertainty, being them related to economy and influenced by human decision making.

1.3 Large-scale hydrological modelling and HPC

In the last decades, the renewed awareness for issues related to water availability has favored the development of a wide set of modelling tools, commonly referred to as Earth System Models (ESM), which are usually operated at the continental scale in order to reproduce the interactions between land and climate; however, high temporal and spatial resolution are required to render the relevant physical processes related to the water cycle with sufficient detail, which in turn results in higher computational loads. The complex orography that characterizes mountain regions, which are for obvious reasons the most advocated to provide hydroelectric energy (due to the naturally available geodetic jumps available below most reservoirs), makes it difficult to adopt General Climate Models to correctly represent runoff with the needed spatial and temporal resolution. These difficulties notwithstanding, Climate Models provide important insights on pattern of changes, both in space and in time, that are expected due to climate change. (Bavay et al., 2013; Beniston, 2012; Gobiet et al., 2014).

Climate change impact assessment studies have made wide use of hydrological modelling throughout the last decades, to support water resources management by developing new adaptation plans (see e.g., Kundzewicz et al., 2007). However, the simulation of hydrological processes typically requires a high spatial and temporal resolution; indeed, sufficiently high spatial resolution is mandatory in order to properly reproduce the main dynamics of key hydrological variables such as e.g., snow accumulation (Scipión et al., 2013) and soil water storage (Rojas et al., 2008). On the other hand, dealing with climate change analyses requires simulations run over a sufficiently wide time period (Todd et al., 2011). Due to the aforementioned requirements, it can be easily understood that the execution of distributed hydrological models over medium-to-large catchment necessarily involves higher computational loads, in terms of both run time, which is needed by the hydrological kernel to simulate hydrological processes over such high-resolved domains, and of instantaneous memory allocation, due to the large amount of data that are processed during each step

of the simulation (Liu et al., 2013; Vivoni et al., 2011).

Another factor that should be always kept into consideration when simulating the spatial variability of hydrological fluxes is the inherent uncertainty involved in the process, whose main causes can be sought after in: i) structure of the conceptual model (i.e., epistemic uncertainty), ii) model parametrization, and iii) input data uncertainty (like e.g. errors in observed meteorological input forcing data and/or flaws in the spatialization techniques applied to the raw input meteorological observations). Indeed, many approaches have been proposed when it comes to the quantitative assessment of uncertainty associated its these different sources acknowledging the relevance of the subject (see e.g., Montanari et al., 2009, for a review). When it comes to the model's parameters, the optimal set can be identified by either adopting a calibration procedure that aims directly at the recognition of the single optimal set of parameters, or within a formal/informal Bayesian framework, where the a-posteriori probability distribution of the parametrization is computed (see e.g., Beven and Binley, 1992; Liu and Gupta, 2007; Vrugt et al., 2003). However, regardless of the choice of parametrization procedure, a specified sampling scheme to explore parameters' space is required, such scheme being informed by an appropriately chosen performance metric computed at the end of every simulation (Madsen, 2000). It appears therefore evident that model calibration and uncertainty analyses both require a rather large number of *forward* runs of the model. This, in conjunction this with the computational load which is inherent to highly resolved (in space and time) simulations, motivated and led to a growing interest in the use of High Performance Computing (HPC) for applications in hydrological modelling (Li et al., 2011; Vivoni et al., 2011).

Thanks to the linearity of most governing processes in hydrological models, the first and most intuitive way to exploit a high computational capacity, is to execute those processes in parallel (i.e., have distinct CPUs treat different parts of the model, after appropriately subdividing the computational domain and/or workload). Indeed, different parallelization strategies have been applied to distributed hydrological models, aimed at reducing the overall runtime as

well as improving the management of large amount of data; among the most common parallel-computing protocols are Message Passing Interface (MPI, MPI Forum, 1994) and Open Multi-Processing (openMP, Dagum and Menon, 1998) . Examples of application of the MPI standard to hydrological model are the works from Wu et al. (2013) and Li et al. (2011), where a parallel framework (MPI) was implemented into the SWAT and DWM hydrological models, respectively: the study area was partitioned into smaller sub-domains (i.e., subbasins), and the computation of the hydrological processes relative to each sub-area was assigned to a different processor and performed independently. Due to its better computational performance (albeit more expensive), GPU-based (Graphics Processing Unit) parallel computing has also found numerous applications in distributed hydrological modelling. In the work from Ortega and Rueda (2010), GPU parallel computed has been adopted to compute the drainage network of large river basins corresponding to the Digital Elevation Model (DEM) provided as an input. Qin and Zhan (2012) and Rueda et al. (2016) applied the parallel GPU standard to streamflow accumulation process. Finally, Le et al. (2015) implemented GPU-based parallel computing into the GCS-flow model, simulating surface-sub-surface flow interactions.

The application of parallel computing framework to distributed hydrological modelling brings unquestionable advantages but, along with those, some known limitations should be taken into account. In particular, the speed-up (i.e., the improvement in run time execution due to parallelization) does not increase once the number of processors exceeds a certain threshold (Amdahl, 1967); such threshold characterizes the *scalability* of a model, i.e. its ability to efficiently subdivide its workload on as many processors as there are available, hence increasing its performance. The limitation of a model's scalability is generally due to a variety of factors: i) tasks interdependencies; ii) time spent for communication between parallel threads; and iii) load imbalance, i.e., the uneven distribution of computational workload between the available processors. Although load imbalance issues can be reduced, or even removed, through a mindful coding of the parallelization scheme, the first two elements are inher-

ent to parallel computing; hence, no model can achieve ideal scalability. In addition to the endemic limitations of parallel computing, most of the existing hydrological models include parts of the code that must be carried out serially due to the nature of the phenomena being represented, further capping the theoretical scalability (i.e. the maximum achievable speed-up of the model) regardless of the number of processors used (Amdahl, 1967). This kind of limitation is particularly evident in models that adopt explicit hydrodynamic routing through the numerical solution of the mass and momentum conservation equations (i.e., the *de Saint-Venant* equations), but also for models adopting cell-to-cell routing algorithms, which are also based on mass conservation and relationships between river-channel storage and streamflows (de Paiva et al., 2013; Yamazaki et al., 2011). Liu et al. (2013) and Wang et al. (2012) computed the maximum (hence, theoretical) run time acceleration that can be achieved in distributed hydrological models, by adopting either grid or sub-basins as simulation units for the parallelization framework, respectively.

Since the bottleneck due to the serial execution of processes associated to streamflow routing along the river network is inevitable, other works focused their attention on a different concept of single layer parallelization, in which single (forward) model executions adopting different sets of parameters are dispatched to multiple processors: this is usually the case of calibration procedures, where multiple forward runs are required. Calibration of hydrological model parameters adopting HPC systems is indeed promising and can in fact significantly reduce the computational time required in this phase. For example, in the work from Kan et al. (2018), the OpenMP standard was implemented onto a calibration algorithm based on the Shuffled Complex Evolution Method and then used into the XAJ hydrological model. Likewise, the calibration module of the SWAT hydrological model was parallelized by assigning different forward runs (i.e. each adopting a different set of parameters) to different processors in the work from Rouholahnejad et al. (2012). Finally, Tristram et al. (2014) adopted GPU parallelization for parameters' uncertainty estimation into (Pitman, 1973)'s hydrological model.

In all of the cited works, a single-layer parallelization of hydrological models is proposed, either based on the spatial decomposition of the domain or on the decomposition of the parameters' space, which are then taken as computational units. Recently, multi-layered parallelization strategies have also been explored to improve the exploitation of HPC resources. Indeed, adding one layer in the logical subdivision of the workload implies that no serial dependencies exist between jobs assigned to different layers, thus allowing to employ a larger number of CPUs for performing single jobs, as opposed to applications where only one level of parallelization can be adopted.Liu et al. (2013) proposed a layered approach to parallel computing for FSDHM distributed hydrological model in which simulation units are divided into layers according to flow direction by guaranteeing that no upstream or downstream relationships are present within each individual layer. Liu et al. (2016) presented a two-level parallelization method for the same FSDHM hydrological model by dispatching parallel tasks in a multi-nodes cluster first at a sub-basin level and then, within each node, at the grid cell level using a shared-memory configuration. Zhang et al. (2016) introduced a double-layer parallel system for the calibration of DYRIM hydrological model: the second layer adopted a MPI framework to simulate hydrological process at the sub-basin scale, while the parallelization in the first layer was achieved by running simultaneous hydrological simulations with different sets of parameters generated by a genetic search algorithm.

Layered parallelization strategies are therefore particularly appealing in the field of distributed hydrological modelling, although the examples of application remain limited in number. Furthermore, in all the cited studies the influence of antropic activities that affect the natural water cycles are neglected; examples of such include water supply systems, pumping stations, irrigation networks, storage reservoirs, diversion channels, etc. Indeed, water storage and transfer network related to human activities have implications on the water cycle and security, and their feedbacks on climate are effective both at the local and at the regional-to-global scales (see e.g., Destouni et al., 2010, 2013; Panday and Huyakorn, 2004). An integrated hydrological model able to encompass

into a single holistic model multiple water-related processes is therefore advisable to provide full coupling between the natural hydrological processes and alterations to water fluxes and storage due to human systems (Hwang et al., 2019; Refsgaard et al., 2010). The topic becomes particularly relevant for large scale hydrological models, since the detailed inclusion of different kinds of water usages at a scale significant and informative for water management (i.e. regional scale or larger) is challenging due to the amount of technical and operational details that need to be retrieved (see e.g., Nazemi and Wheater (2015a,b) for a review on the issues associated to the inclusion of water resources management modules into Earth System Models). For example, the presence of diversion channels alters the natural direction of streamflows, as well as requiring a specific modelling approach for solving the associated water mass balance equations (see e.g., Bellin et al., 2016). Indeed, the presence of human water uses alters the natural stream network topology, with repercussions on the modelled hydrology (Gregory, 2006). All things considered, the simulation of non-natural infrastructures adds a non-negligible burden to the overall workload, because it introduces upstream-downstream dependencies in transfers along the river network that must be solved serially, hence impairing the full parallelization of the code and limiting its scalability.

1.4 Explicit simulation of streamflow alterations due to Human Systems

Water cycles are often represented using Earth System Models (ESM), which seek to simulate many relevant aspects of the global environment. These models are set to operate on a large scale following physical constraints, allowing a good coupling with Climate Models. However, a comprehensive analysis of the water cycle should encompass the interactions between the natural streamflows and different kinds of anthropogenic water usages causing all sorts of alterations such as modifications in timing, magnitude of peak flows, as well as modifications to flow velocity and water quality (Poff et al., 2015), hence requir-

ing a deeper insight on the relevant phenomena (Clark et al., 2015). For these reasons, accurate regional scale models including anthropogenic streamflow alterations are needed to test and compare different water management strategies. As far as the Italian Alpine Region is concerned, hydropower-related water uses exceed in diverted volumes all other kinds of water usage (agricultural, recreational and industrial). In particular, large hydropower plants (i.e. with installed power greater than 3MW, according to the Italian definition) constitute about 80% of the diverted volumes yearly (TERNA,2015).

The inclusion of hydropower systems in a meso-scale (or larger) hydrological model is often challenging from a modelling perspective, as it requires that the relevant characteristics of each system are adequately described (Nazemi and Wheater, 2015a,b). While operations of run-of-the-river hydropower plants could be assimilated to natural streamflow committing relatively little mistake, due to their limited storage volume, reservoir hydropower most likely do introduce changes in downstream flows and must therefore be modelled in peculiar ways that account for operational constraints (Ashraf et al., 2018; Bonnema and Hossain, 2017). Assessing the changes brought by reservoirs to downstream flows calls for new data, which include reservoirs' stage-storage-surface area curves, geometrical information on the outlets and their capacity, and most importantly the operational rules specific to each reservoir, which are difficult to acquire because they are often kept confidential by the hydropower companies. Models dealing with hydropower-related water diversions thus involve a trade off between the extension of the domain and the level of detail at which human systems are modelled, allowing to draw a coarse subdivision in two categories: firstly, works focused on detailed hydropower modelling, who usually adopt a simplified hydrological model and focus their effort on a highly detailed model of the systems of interest (see e.g. Beheshti et al. (2019); Koch et al. (2016)). Conversely, models typically applied to large spatial scales and used for climate change impact assessment studies, simplify hydraulic infrastructures and their connections: in their work, Shin et al. (2019) developed and implemented a reservoir operation module over the CONUS (Contiguous U.S.) region, in order

to improve the representation of catchment dynamics, explicitly modelling storage and release mechanics for around 1900 reservoirs around the U.S.: however, no information on other hydraulic infrastructures potentially altering river continuity was included in the simulation.

It is however worth noticing that attempts have already been made to develop modelling framework that take into account both the natural water cycle and its alterations due to hydropower-related activities: as an example, Fatichi et al. (2015) analyzed the potential effects of climate change on hydropower production on a system of 14 reservoirs located in the Upper Rhone basin (Switzerland); Amjath-Babu et al. (2019) coupled the WEAP hydrological model (Yates et al., 2005) with an economic optimization model, to test the benefits brought to the food-water-energy nexus by the development of a system consisting of 11 reservoirs located in the central part of the Koshi river basin (south Asia). However, to date and to the best of our knowledge, existing works that model hydropower production are in fact impact analyses that focus on variations between different future scenarios, one of which is defined as baseline, or with gross hydropower potential estimates, (defined as the hydropower that could be produced if all the water flowing in the area of investigation could be turbined at sea level) (Lehner et al., 2005). Exception to this procedure is the work by Qin et al. (2020), where daily hydropower time series are used to develop a detailed daily reservoir regulation scheme for the Three Gorges Reservoir (China). This low number of works that attempt to validate their modelled hydropower production against historical data might be explained by the fact that hydropower production is strongly influenced by exogenous factors such as energy market and decision making, and is therefore hard to grasp within any purely physically-based model; in fact, while the overall hydropower production (e.g. annual average) is more related to water availability, the *timing* of said production is closely related to reservoir management strategies, which are confidential wherever electricity is not a service provided by the Nation itself. Likewise, the validation data themselves (i.e., time series of turbined water discharge or hydropower production) are treated as confidential by the

hydropower companies, as revealing them would unveil reservoir management strategies thus jeopardizing company's competitiveness in the market;.

Reservoir operations do therefore represent a major source of uncertainty in the modelling chain, becoming one of the unknowns of the model themselves. This problem is sometimes circumvented by introducing in the model objective functions that include turbined flow as their unknown. Optimizing such objective functions while complying with several constraints (e.g. environmental flows, estimated downstream water demands, etc.) allows to create optimized discharge time series that are often applied to multi-purpose reservoirs(see e.g. Anand et al., 2018). However, this kind of practice involves a particularly high computational load and is rarely applied to complex systems or to large simulations. On the other hand, if some level of information concerning the hydropower systems is available, deterministic reservoir management rules are usually preferred, to cope with larger simulations: in this case, reservoir discharge is enforced directly by the model and follows physical and operational constraints. While only inducing a marginal effect on the modelled catchment hydrology, the repercussions of reservoir operation on modelled hydropower production can be considerable.

A wide set of deterministic approaches to reservoir operation modelling can be found in literature: hedging curve rules seek to satisfy all sources of downstream demand, according to prioritization rules set by the user. In order to do so, several scaling factors (one for each different component of the downstream demand) are computed, depending on current reservoir filling and/or drought/flood foresights (see e.g. Guo et al., 2013; Shrestha et al., 2014; Tu et al., 2003). This approach is able to account for the seasonality of water inflows by appropriately modulating its scaling factors throughout the year, and might indeed provide good results: the main limitation to the performance of this approach lays in the definition of the downstream demand, which has to be known precisely for every system being modelled, while at the same time strongly relying on a proper definition of the hedging thresholds and demand scaling coefficients. Another deterministic reservoir operation scheme that is

commonly found in literature as well as in many well-established water resource management tools is the target volume approach (see e.g. Fatichi et al., 2015; Finger et al., 2012): in this case, 365 (daily) target stored volume values are assigned to each reservoir. The model can be based either on averaged daily volume observations if available, or on typical target volume curves derived from reservoir geometry. Within this approach, turbined flows are determined in such a way that makes the current volume tend towards the target volume for the day. This methods represents an easily applicable, yet accurate alternative where detailed volume time series are available; however, the same cannot be stated about the adoption of generalized target volume curves: in fact, this does not allow to consider the specificity of each individual system, which is crucial to ensure proper hydropower production modeling. This approach therefore relies heavily on the availability of reservoir volume time series, which are in many countries protected by industrial secret, due to the reasons already explained in the previous paragraph. Despite the potential of being extended to a wide number of systems, adopting normalized target volume curves obtained by averaging time series of other reservoirs could introduce further uncertainty in modelled hydropower production, as different reservoirs might have different usage regimes (some reservoirs are emptied and refilled weekly, some monthly or seasonally, etc.): therefore, the same normalized curve will suit only partially the systems being modelled. A common assumption made in works dealing with hydropower reservoirs is that the downstream (hydroelectric) demand is always equal to the system capacity (i.e., the maximum water discharge that the turbines can elaborate), except for drought periods when MVF (Minimum Vital Flow, depending on local regulations) is guaranteed as a priority (Turner et al., 2017; Wagner et al., 2016). This relatively parsimonious approach performs well at the global scale and suits well large scale impact assessments, in fact as already stated hydropower production is strongly linked to water availability (see also Jabbari and Nazemi, 2019). However, when modelling mesoscale catchments in order to test the effects of different management strategies and environmental regulations in terms of e.g. water budget, hydropower production, and impact of said strategies on the natural habitat downstream of the

power plants, a higher level of detail is necessary, in order to fully grasp the complex interactions between the hydrological cycle and the different water uses (Zhang et al., 2018).

1.5 Implications of uncertainties in meteorological input forcing on hydropower production forecasts

The great effort devoted to hydrological modelling in the last decades is not just aimed at gaining a deeper understanding of the relevant phenomena involved in the water cycles and of their interactions; rather, it stems from the perspective forced by climate change. In this regard, the best possible modelling tools need to be developed in order to minimize the uncertainty involved at each level of the modelling chain (the *uncertainty cascade* concept was firstly introduced by Wilby and Dessai (2010)). When it comes to climate change impact assessment on hydropower production, the sources of uncertainty are multiplied, as the initial uncertainty inherent to Climate Models is then amplified by the subsequent steps of the modelling chain, such as the hydrological model and the hydropower system operation models, not to mention the uncertainty involved in the evolution of the energy market itself.

Sperna Weiland et al. (2015) Highlighted how the meteorological forcing constitutes a major source of uncertainty, compared to the minor effects brought by hydrological models' parametric uncertainty. Indeed, uncertainty in meteorological input forcing is well-acknowledged, as many studies have tried to assess the impacts of uncertain meteorological forcing on the estimation of water balance (see e.g. Clark et al., 2016, for a review). This is particularly true when dealing with catchments characterized by a complex topography, since small difference in climate forecast can result in larger differences in the hydrological response of the catchment (Kotlarski et al., 2014; Majone et al., 2012; Tuo et al., 2016). This notwithstanding, adopting a single meteorological input dataset

not questioning the uncertainty it might add to the model is a rather common practice (Yang et al., 2014). Conversely, with an ever-increasing computational capacity at hand, one might be tempted to just perform ensemble runs with several different CMs, ending up with an unreasonably wide set of 'plausible' scenarios, but in this case the uncertainty would be strongly inflated, making the result itself less relevant.

It is therefore clear that where a high degree of accuracy is required throughout the modelling chain, *democracy* should not be the leading criterion when it comes to the selection of input data sets (using the words of Knutti (2010)). Following this concept, Laiti et al. (2018) developed a goal-oriented approach to climate dataset benchmarking, by means of which different dataset can be classified based on how well they can reproduce observed streamflows in the catchment of interest. Several works attempted to assess the impact of different climate data sets on hydropower production (see e.g. Carvajal et al., 2017; Majone et al., 2016; Oyerinde et al., 2016): as it can be expected, the range of uncertainty associated with future hydropower is often rather wide with projected changes covering a range of 50% or more; furthermore, in all the aforementioned works it can be observed that variation patterns in hydrologic response (i.e. runoff, streamflows) are not strictly followed by the variations in modelled hydropower production and/or potential: this is due to the complexity inherent to hydropower systems, in particular when it comes to reservoir hydropower where decision making and market strategies play a key role.

In light of the above considerations, goal-oriented approaches to input selection represent an appealing way to reduce the inherent uncertainty in hydropower production modelling, where the initial uncertainty interacts and is amplified by a number of factors, hence reducing the uncertainty of the final results.

1.6 Aim of the study

In this thesis we would like to contribute to the aforementioned research topics by addressing three distinct issues. Firstly, we would like to develop a suitable hyydrological modelling framework called HYPERstreamHS, that is able to exploit HPC resources and to be executed on large catchments at a sufficiently spatial and temporal resolution, by means of an efficient subdivision of the workload. Secondly, we included detailed and explicit simulation of Human Systems in the modelling framework, by means of specific modules reproducing the behavior of some of the main water infrastructures related to hydropower (i.e. reservoirs, diversion channels, restitution points), constraining them with intensive information. We chose to only adopt publicly available information to inform our model, so that the same framework could be applied in any domain (at least in Italy). Finally, the role of different meteorological input datasets in terms of modelled hydropower production will be investigated.

Once the modelling framework is set, we firstly applied it on the Adige river catchment, a large catchment located in the Eastern Alps; here the model has been tested for performance in terms of scalability and in terms of its ability to reproduce hydropower production and streamflow time series. Moreover, we tried to "deteriorate" the input information to the model in a way that resembles some assumptions commonly made in reservoir operation modelling. This was done in order to understand the effect of some common simplifications and assumptions in terms of hydrological- and hydropower production modelling. Finally, the model was applied to a second domain, composed by five catchments located in the Western Alps; in this case, after validating the model for hydrological- and hydropower production modelling, we studied the differences in the model's output caused by using different meteorological input forcing datasets.

CHAPTER 2

THE HYDROLOGICAL MODELLING FRAMEWORK: HYPERSTREAMHS

In this Chapter a detailed description of the HYPERstreamHS model, that has been used to perform all of the analyses contained in this work, will be provided: the description will cover the hydrological component of the model, the Human System modules as well as the parallel computing features embedded in the model in order to improve its scalability.

This Chapter is based on:
Avesani, D., Galletti, A., Piccolroaz, S., Bellin, A., Majone, B. A Dual layer MPI continuous large-scale hydrological model including Human Systems, Environmental Modelling & Software, ***SUBMITTED***

HYPERstreamHS inherits the core features of the HYPERstream routing scheme recently presented in the work from Piccolroaz et al. (2016), while improving it by means of a dual-layer MPI framework and the inclusion of explicit modelling of streamflow alterations due to Human Systems (hence, the HS suffix to the model's name). HYPERstream is a multi-scale streamflow routing method based on the Width Function Instantaneous Unit Hydrograph (WFIUH) approach; this approach has been specifically designed for reliably simulating the relevant horizontal hydrological fluxes preserving the geomorphological dispersion of fluxes and thus being able to perform well at different scales, from a single catchment to the meso-scale. The routing scheme is prone to parallelization, due to the fact that the routing processes are linear and are independent from the runoff generation module adopted in the simulation unit (grid cells in this case). Indeed, developing improved routing schemes to model horizontal fluxes achieving a good trade off between accuracy and computational effort has been pointed out as one of the priorities for the improvement of state-of-the-art large-scale hydrological models (see e.g., for a review Clark et al., 2015). Specifically, HYPERstream has been coupled with continuous modules for surface and subsurface flow generation, as well as adding to it specific routines modelling the alterations introduced by infrastructures related to hydropower, like e.g. reservoirs and diversion channels. Human System modules are inserted in the stream network as nodes, in each of which specifically constrained water mass balance equations are solved during every timestep. Furthermore, a dual-layer parallelization strategy based on the MPI standard was adopted in the HYPERstreamHS framework, allowing for an optimal exploitation of the domain decomposition, both in terms of geographic domain (computation of horizontal fluxes) and of the parameters' space (model calibration). In particular, the first level of parallelization subdivides among the available CPUs the simulation of the physical processes acting in each grid cell of the domain. The presence of a high number of hydraulic infrastructures in the hydrological conceptual model affects model scalability by increasing the point-to-point dependencies (and as a consequence the sheer number of communications needed between processors); to cope with this bottleneck, a

second layer of parallelization is introduced, this one handling the workload due to model calibration and uncertainty analyses: a new increase in scalability can be achieved by subdividing the available processors in sub-sets, each one managing an independent simulation of the hydrological model (forward run, performed by the so-called first layer) adopting a given set of parameters, hence speeding up the exploration of the parameters' space.

In the present Chapter, all the main components of HYPERstreamHS will be covered: firstly, the natural and artificial modules of will be described. Afterwards, the algorithms embedded in the model and used for the identification of the hydrological model's parameters will be presented. Finally, the parallelization strategy adopted in HYPERstreamHS using the MPI standard will be illustrated.

2.1 HYPERstreamHS model components

2.1.1 Natural hydrological system

The natural component of HYPERstreamHS hydrological model is obtained by coupling HYPERstream routing scheme (Piccolroaz et al., 2016) and a model for the generation of vertical fluxes (presented in Laiti et al., 2018). The model is characterized by 12 parameters, 11 of which pertaining to the soil moisture accounting procedures and one adopted in the routing model. In the following paragraphs only the key aspects of the natural hydrological model will be illustrated. For a more comprehensive overview of the domain decomposition and of the flow generation, snow melting, soil moisture accounting and routing modules embedded in HYPERstreamHS, please refer to the Appendix A.1.

2.1.1.1 Computational grid

The modelling framework relies on two key geometric objects (see Figure 2.1): i) *macrocells* (i.e., grid cells), groups of DEM cells to which the same meteorological forcing is assigned and the vertical water fluxes are evaluated

(Figure 2.1a), and ii) *nodes*, in which streamflow is computed.

The computational domain is firstly partitioned into M macrocells of equal shape and size (Figure 2.1b), which can be defined in such a way so that the hydrological model grid can be exactly superimposed to an overlaying climate model or gridded dataset providing the input meteorological forcing. Afterwards, N nodes are identified: nodes correspond to the locations in which streamflow is computed (Figure 2.1a). The nodes are arbitrarily distributed along the river network, and are typically located in correspondence of existing gauging stations where streamflow observations are available (such locations are often used for the calibration and validation of the hydrological model), as well as in relevant locations where anthropogenic alterations to the streamflow are present, which will be simulated by the Human System module (see Section 2.1.2).

A one-time geometrical pre-processing step is run prior to model execution: during this phase, the geometrical information needed to implement the streamflow routing scheme are processed based on input data. The DEM is analyzed in order to extract the river network, according to one of the several criteria available for the identification of the hillslope-channel separation (e.g., Lazzaro, 2009; Tarboton et al., 1991), as well as the drainage characteristics of the study area, and to derive the corresponding geomorphological width functions for each macrocell-node pair (see Figure 2.1b): indeed, runoff generated in each macrocell flows towards one or more downstream nodes; therefore, each connection between a portion of macrocell and the node it directly contributes its runoff to is defined as macrocell-node pair. In virtue of this definition and as it can be seen in 2.1b each macrocell (large squares) contributes to several nodes and, vice-versa, each node receives runoff contributions from several macrocells, as well as from the river network. Furthermore, the necessary parameters for vertical fluxes' evaluation (e.g., average elevation, soil use and type, crop coefficient etc., which are further explained in Section 3.1) are computed and assigned to each macrocell, by means of an analysis of the available DEM and land-use/land-cover spatial maps. A detailed example

of macrocell-discretization and width functions derivations can be found in Piccolroaz et al. (2016).

2.1.1.2 HYPERstream routing scheme

HYPERstream is a multi-scale hydrological routing scheme based on the width function instantaneous unit hydrograph (WFIUH) theory (see, e.g., Rodríguez-Iturbe and Rinaldo, 1997). The model has been designed in order to preserve the geomorphological dispersion of the river network (Pilgrim, 1977; Rinaldo et al., 1991), independent of the grid resolution providing the meteorological forcing, and therefore is well suited for multi-scale applications, from the catchment up to the meso-scale. This is achieved by deriving the geomorphological width functions from the fine-scale spatial structure of the drainage basin embedded in the digital elevation model (DEM) of the study area. As a result, the routing of the horizontal water fluxes is grid-invariant, and a "perfect upscaling" of the river network geomorphological dispersion is achieved (Piccolroaz et al., 2016). The approach allows to use grid cells (hereafter referred to as macrocells) of any shape and size, thus making the model particularly suitable for the coupling with gridded datasets, such as e.g. climate models outputs (Laiti et al., 2018).

2.1.1.3 Simulation of vertical water fluxes

Vertical fluxes (i.e., water storage and runoff generation processes) are modelled adopting the approach proposed by Laiti et al. (2018). In particular, surface flow generation module relies on a continuous soil moisture accounting procedure (Michel et al., 2005) based on the SCS-CN methodology (U.S. Soil Conservation Service, 1964), coupled with a nonlinear bucket model for soil moisture depletion (Majone et al., 2010), a linear bucket model for the base-flow component, Hargreaves and Samani (1982) model for the computation of potential evapotranspiration, and a degree-day model for the snow dynamics (see also Bellin et al., 2016; Majone et al., 2016; Piccolroaz et al., 2015, for similar flow generation modules successfully applied in Alpine catchments). A schematic of the vertical water flux generation model and routing scheme is depicted in Fig-

ure 2.1a. The information derived from the DEM is used to build the probability density function (pdf) of the flow path lengths (i.e., width function) connecting the hillslope-channel transition sites of a macrocell to the first downstream node. A width function is evaluated for each macrocell-node pair (Figure 2.1b), and then it is rescaled through a constant stream velocity to obtain the pdf of the travel times required by the WFIUH routing scheme. The assumption of constant stream velocity makes the transfer process linear and hence the routing model highly parallelizable. In this regard, it should be noticed that the assumption of a constant stream velocity is supported by previous experimental measurements (see e.g., Pilgrim, 1977) and is coherent with the evidence that varying flow velocity along the network (i.e., stream hydrodynamic dispersion, Rinaldo et al. (1991)) is largely dominated by geomorphological dispersion (Rodríguez-Iturbe and Rinaldo, 1997), expecially under high flow conditions.

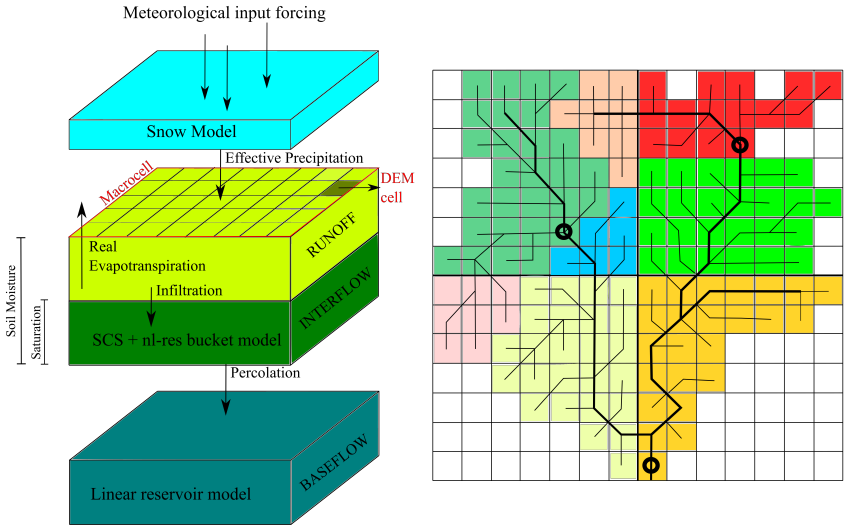

Figure 2.1 *Schematic of the natural hydrological system used in this study, coupling a vertical fluxes generation module (a) with the HYPERstream routing scheme (b). The details of the vertical fluxes generation module are the same as in Laiti et al. (2018). Each one of the (8) colors in panel (b) identify the portions of a specific macrocell contributing to each node, therefore said colors are as many as the macrocell-node pairs.*

2.1.1.4 Model's parameters

A total of 12 model parameters is used, 11 pertaining to the vertical water flux generation module and 1 to the HYPERstream routing scheme. Parameters of vertical water flux module are assumed as spatially uniform, with the spatial heterogeneity of hydrological processes being delegated to the different values of S and K_c (respectively: soil water storage and cultural coefficient) assigned to the different macrocells: these values are derived from available infiltration capacity and soil use maps, and are computed as weighted averages of the values at each DTM cell contained in a given macrocell. Routing scheme requires the definition of a single parameter, the stream velocity V_c, which is assumed constant over the domain, thus making the model linear and easily

Table 2.1 *List of the calibration parameters with their range of variation. T_s and T_m: temperature thresholds for snow precipitation and snow melting; c_m: snow melting factor; c_s and c_a: parameters of the rainfall excess model; q_{ref} and μ: parameters of the nonlinear reservoir mimicking the dynamics of the unsaturated zone; c_{fc} and c_r: coefficients for field capacity and residual soil moisture; k: mean residence time of the baseflow linear reservoir; : α partition coefficient for leakage flux; V_c: stream velocity.*

Parameters	Range of variation	Unit
T_s	$-2 \div 6$	$[^\circ C]$
T_m	$-2 \div 6$	$[^\circ C]$
c_m	$0 \div 10$	$[mm^\circ C^{-1} d^{-1}]$
c_s	$0.1 \div 10$	-
c_a	$0.01 \div 1$	-
q_{ref}	$10^{-7} \div 10^{-3}$	$[mm\ s^{-1}]$
μ	$0.5 \div 300$	$[mm]$
c_{fc}	$0 \div 1$	-
c_r	$0 \div 0.25$	-
k	$200 \div 1000$	$[day]$
α	$0 \div 1$	-
V_c	$0.2 \div 4$	$[m\ s^{-1}]$

parallelizable. The list of the 12 calibration parameters, with their units and range of variation is presented in Table 2.1.

2.1.2 Human Systems modules

Streamflow alterations due to the presence of human infrastructures are modelled by adding specific nodes to the network, in each of which a set of rules is enforced when computing the water mass balance. These rules are derived following the way human systems are operated and are the main factor that alters natural flow regime. From a modelling perspective, this is achieved constraining water mass balance to physical, geometrical or operational properties of the described system. The water mass balance performed at each node during every time step leads to different partitioning of the inflows, depending on the ability of the node to store water (reservoir only) and on a variable prioritization of the outflow based on node functionality. Simulation of human systems is performed in HYPERstreamHS by means of a suite of object types which are described in the following subsections.

2.1.2.1 type-Reservoir nodes

Reservoir nodes are the only nodes where storage can occur. As it can be seen from Figure 2.2, each reservoir is subdivided into three volume pools: flood control, active and inactive volume. The deterministic release scheme associated to each reservoir (due to hydropower and environmental needs) is fully met whenever the current stage falls inside the active storage. If the current stage is outside this portion of the reservoir, either pool conservation measures or flood control measures (i.e., water spilling) are taken, and the resulting set of releases will differ from the default scheme. As a result of reservoir constraints and operation schedules, a water mass balance following the general formulation of Eq. (2.1) is performed at each reservoir and at every time step:

$$\Sigma Q_{IN}(t) - \Sigma Q_{DIV}(t) - Q_{OUT}(t) - Q_{spill}(t) = \frac{dV}{dt} \tag{2.1}$$

where $\sum Q_{IN}$(t) is the total inflow to the reservoir, $\sum Q_{DIV}$ is the total flow diverted from the reservoir for hydropower or agricultural water uses, Q_{OUT}

is the flow released to the downstream river network including the Minimum Ecological Flow (MEF, which is set for each reservoir and computed according to existing regulations), Q_{spill} is the flow that is spilled when the maximum regulation level is exceeded during flooding events, and finally V is the reservoir volume at time t. The summation in the first two right hand terms of Eq. (2.1) indicates that the reservoir may receive water from more than one source (for example the river network upstream and a second river network connected through a channel deriving water from lateral streams intercepted at a level higher than the reservoir level) and may feed more than one source, though this last situation is unlikely.

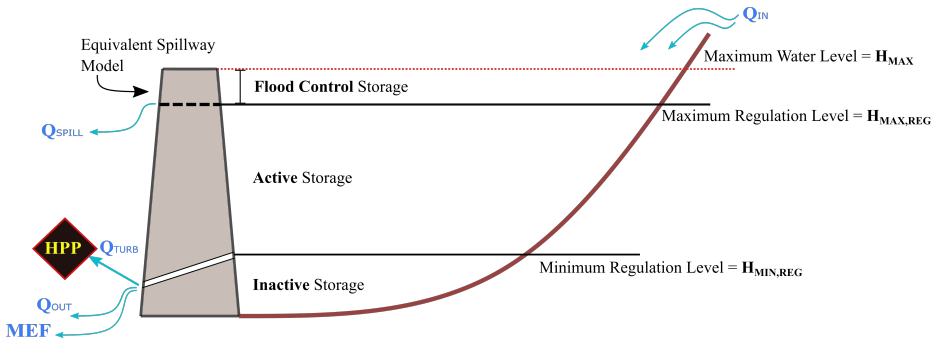

Figure 2.2 *Sketch of the partitioning of the reservoir volume and the corresponding operational water levels.*

Mass balance described by Eq. (2.1) is applied by considering the following priority of releases:

a. *Minimum Ecological Flow*: local environmental regulations determine the amount of water that must be released to the downstream river network by reservoirs. MEF is released with absolute priority, only releasing a lower amount of water if current reservoir stage is below the minimum regulation level.

b. *Spillways*: they are activated when reservoir water level is above the maximum regulation level $h_{max,reg}$ and water is released in the downstream river. The reservoir is equipped with one or more spillways such as to release a given maximum discharge when the maximum water level h_{max} is reached. Often spillways are equipped with gates, which allow flexibility in dealing with

flood events since timing of the release can be, to some extent, decided by the operator. Considering that spillways operate seldom, only during major events, and given the impossibility of predicting operator's decisions we introduced an equivalent spillway in each reservoir, which is unmanned and starts to release at the maximum regulation level and discharges the maximum water discharge at the maximum water level. In doing this we impose that the cumulative released volume is respected, but the exact timing of the release is not captured. The water spilled from the reservoir is therefore computed as follows:

$$Q_{spill}(t) = L_{eq} c_q \sqrt{2g} \left(h(t) - h_{max,reg}\right)^{3/2} \tag{2.2}$$

where c_q is a coefficient of discharge, and L_{eq} is the equivalent length of the spillway, computed by imposing that it releases the maximum water discharge ($Q_{spill,max}$) when the water level is at its maximum (h_{max}):

$$L_{eq} = \frac{Q_{spill,max}}{c_q \sqrt{2g} \Delta h_{fc}^{3/2}} \tag{2.3}$$

In Eq. (2.3), $\Delta h_{fc} = h_{max} - h_{max,reg}$ is the maximum hydraulic head. Due to the rapid variability of flow during flood events, the time step Δt adopted for solving Eq. (2.1) is set in such a way to obtain good accuracy in the computation of the level into the reservoir and discharge. For example, in our simulations the adopted time step is of 1 h for the hydrological kernel of HYPERstreamHS, which is reduced to 1 minute for the computation of water balances depicted in Eq, (2.1).

c. *Release scheme*: whenever the water stage is above the minimum regulation level, a specific release scheme is applied to the reservoir. The derivation scheme is a deterministic time series that must be set by the user prior to the simulation. Further detail on the development of the release scheme adopted in this work is provided in upcoming Section 2.1.2.5.

2.1.2.2 type-Diversion Channel

Diversion channels divert water from the natural stream network by means of an intake and route it to a downstream restitution point. These objects are fully characterized by the channel length and a celerity describing how fast the water can move along the artificial channel. Celerity is assumed as constant throughout the simulation and can be set by the user prior to the simulation.

2.1.2.3 type-Intake nodes: diversions, restitution points and confluences

In our modelling scheme intake points are locations where water is diverted from the natural stream network by means of artificial channels (see Fig. 2.3). Furthermore, intake nodes can be used to model other human infrastructures, such as restitution points and confluences between tunnels. In each of these situations, a specific water mass balance is performed as described in the ensuing paragraphs.

Diversion points are locations at which water is withdrawn from the river network and sent to channels or tunnels, both for hydropower uses. Similarly to reservoirs, diversions from river network (Fig. 2.3a) must obey to MEF and operational constraints:

$$\begin{cases} Q_{IN,nat}(t) = Q_{OUT,nat}(t) + Q_{DIV,art}(t) \\ Q_{OUT,art}(t) = Q_{DIV,art}(t) + Q_{IN,art}(t) \end{cases} \tag{2.4}$$

In the above equations, contributions to the water mass balance are distinguished between natural (flows related to the stream network) and artificial (related to the channel). It should be also noted that all terms refer to the location of the diversion point. $Q_{DIV,art}$ (first line of Eq. 2.4) represents the portion of natural streamflow that is diverted from the stream network after the MEF requirement has been met at the diversion node; moreover, this portion of flow is limited by the capacity of the downstream artificial channel as well as from the portion of flow already present in it, $Q_{IN,art}$ (second line of Eq. 2.4); by virtue of this constraint, the flow to be routed downstream along the diversion

channel, $Q_{OUT,art}$, will never exceed the channel's capacity. In other words, if the maximum channel capacity is reached before the diversion point in object, this will not divert any more water from the natural stream network.

In the case of a *restitution point*, water mass balance between all natural ($\Sigma Q_{IN,nat}$) and artificial ($\Sigma Q_{IN,art}$) incoming flows is performed (Fig. 2.3b), with the resulting flow being routed downstream along the natural network, without any further constraint:

$$Q_{OUT,nat}(t) = \Sigma Q_{IN,art}(t) + \Sigma Q_{IN,nat}(t) \tag{2.5}$$

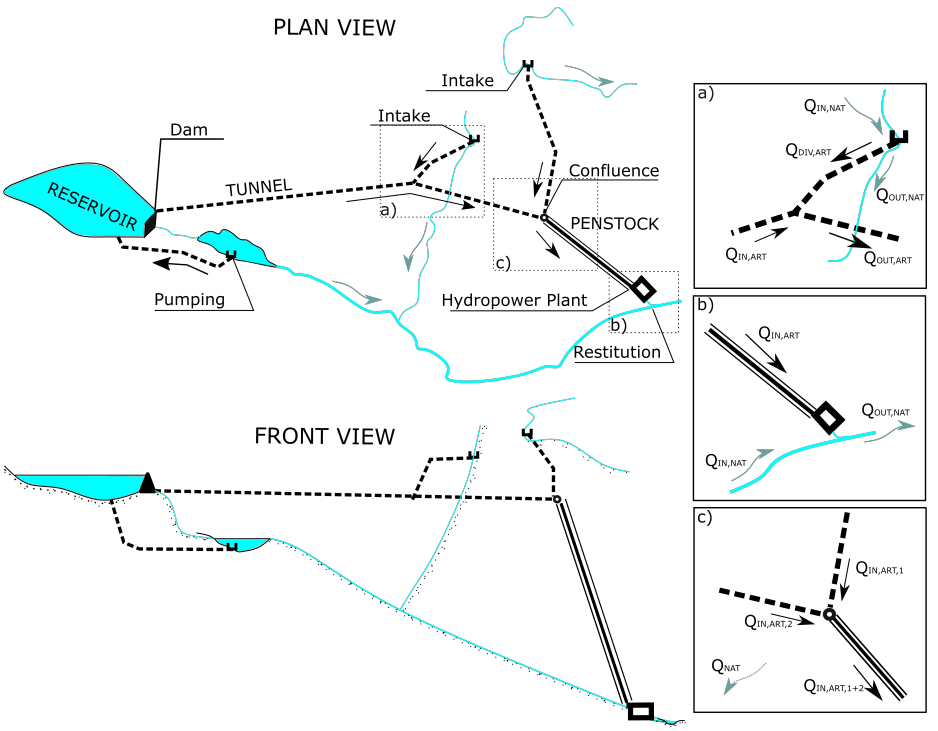

Figure 2.3 *Schematic of the infrastructures simulated in the Human System module of HYPERstreamHS. Insets in the lower panel detail a particular structure that can be simulated with the object type-intake: diversion (a), restitution point (b) and confluence between tunnels (c).*

Finally, intake points are also used to model *confluences* between tunnels, in situations like e.g. the one depicted in Fig. 2.3c: in this case, only artificial flows

are accounted for, as there is no water exchange between the natural stream network and the tunnels at these locations:

$$Q_{OUT,art}(t) = \Sigma Q_{IN,art}(t) \tag{2.6}$$

As it can be seen from Eq. (2.6), water incoming from upstream tunnels is conveyed to the downstream tunnel without any constraint.

2.1.2.4 type-Hydropower Plant nodes

Power plant elements act similarly to restitution points illustrated in the previous paragraph, where all the incoming contributions are summed up before being routed downstream. Before performing the water balance, the contributions incoming from penstocks are used to compute hydropower production by means of a hydropower production function that applies to each inflow to the power plant, and computes hydropower production (HPP) at every time step, as shown in Eq. (2.7):

$$HPP(t) = \eta \sum_{i=1}^{N} \gamma Q_{TURB,i} \Delta H_i(t) \tag{2.7}$$

where $Q_{TURB,i}$ and ΔH_i represent the turbined flow and the hydraulic head for each water inflow (i) to the plant (hydropower plants may have more than one inflow), respectively. The hydraulic head is computed as the difference between the reservoir stage at timestep t and the turbine axis level, in the case of reservoir hydropower. In the case of run-of-the-river plants, it is just assumed equal to the constant value declared by the system owning company. Furthermore, η represents the turbine efficiency, which we assumed constant and equal to $\eta = 0.8$ for every plant on the basis of efficiencies data available at some plants located within the case study.

2.1.2.5 Derivation of the deterministic reservoir release schemes

In type-reservoir nodes, whenever the water stage is above the minimum regulation level, a specific derivation scheme is applied to the reservoir. We developed a deterministic reservoir operating rule that proportions the average reservoir derived discharge on the expected mean annual production of the i-th hydropower system, as illustrated in Eq. 2.8:

$$Q_{AVG,i} = \frac{HP_{EXP,i}}{\gamma \Delta H_i \eta * 24 * 365} \tag{2.8}$$

where $HP_{EXP,i}$ is the expected average annual production declared by the plant operating company, ΔH_i represents the nominal head for the plant (this quantity is often declared by plant owners, available in public concession acts etc.), and η is the plant efficiency, which in our applications was set constant and equal to the average of the efficiencies of the hydropower plants for which it was available (further detail on this provided in Chapter 3). This is justified from the similarity in the hydraulic characteristics of the power plants. The final value for the hydropower discharge rule is obtained by modulating this value using three coefficients representing different factors that influence decision making and reservoir operating routines, as shown in Eq. 2.9:

$$Q_{TURB,i} = Q_{AVG,i} k_m \delta_w \phi_e \tag{2.9}$$

In the previous equation, the coefficient $k_m = HP_{prov,m}/HP_{prov,ann}$ represents the ratio between monthly average production and yearly average production in the province of interest (detailed motivation for this choice can be found in Section 3.3). Therefore, k_m will assume 12 different values throughout the year. Furthermore, k_m is computed for each province belonging to the study area, and each plant will adopt the set of coefficients related to the province it belongs to. δ_w is a user-set variable controlling the variation of the production during weekdays, while $\phi_e = P_{avg,3}/P_{avg,month}$ is computed comparing the 3-day moving average of electricity price with the average price for the current

month, reflecting short-to-medium term adjustments to management strategies. A similar approach has been adopted by Schaefli et al. (2007), where a stochastic component was added to a deterministic water demand, in order to model stochastic processes such as the evolution of demand or perturbations in electricity market.

The resulting deterministic hydropower production rule depicted in Eq. 2.9 varies in time (due to the daily variability of ϕ_e and to the monthly variability of k_m) and and space (due to k_m assuming a different set of values for each province), differing from typical target volume approaches where an average year is defined and then repeated for the entire simulation. An example year of deterministic hydropower discharge scheme is shown in Figure 2.4. The turbined discharge varies monthly according to variation of incoming flow and shows daily fluctuations according to the energy price. Particularly relevant is the shutoff of production during the weekends, achieved by setting $\delta_w = 1$ during weekdays, and to 0 otherwise.

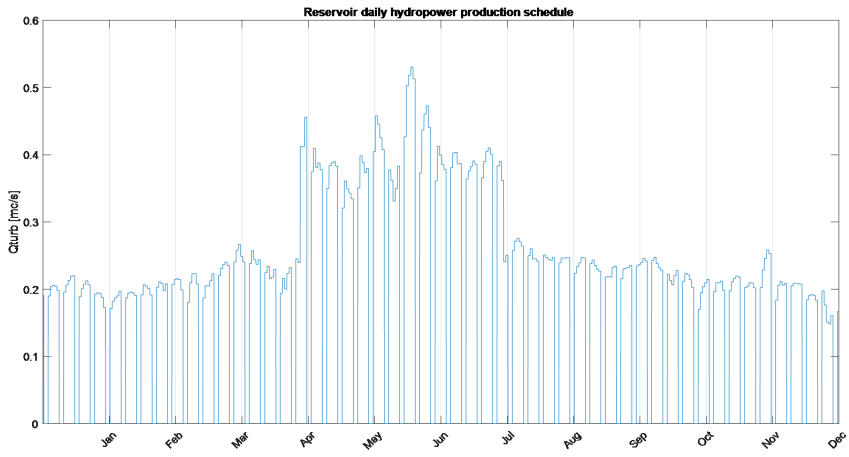

Figure 2.4 *Example of deterministic discharge scheme for hydropower reservoirs. Discharge is influenced by current month, electricity price and weekday, as well as from the location of the reservoir*

2.2 Parameter Identification

As it was already mentioned in Chapter 1, the parameters of the hydrological model (cfr. Sec. 2.1.1) can be computed by either a conventional-deterministic approach or in a more general-statistical Bayesian framework. While in the first case, the single optimal set of parameters is sought after (optimality here defined as the parameters set that allows to minimize the error between model predictions and measure data), on the other hand, Bayesian approaches aim to quantify the uncertainty of model predictions and the a-posteriori distributions of the parameters.

In light of this distinction, HYPERstreamHS is equipped with two calibration procedures belonging to the aforementioned approaches: the Particle Swarm Optimization (PSO) algorithm (Castagna and Bellin, 2009; Kennedy and Eberhart, 1995; Majone et al., 2010; Robinson and Rahmat-Samii, 2004) and the Monte Carlo analysis in conjunction with Latin Hypercube Sampling (LHS) technique (McKay et al., 1979), respectively. PSO is a robust stochastic genetic optimization technique based on the movement of a swarm of *bees*, which represent the parameters set in the space of parameters. The application of this algorithm is particularly suited to calibration procedures in the presence of a large number of parameters since it is insensitive to both initial conditions and the shape of the objective function. On the other hand, uncertainty evaluation generally holds that all parameters sets of a system shall be retained until they are rejected (Wagener, 2003). The set of plausible models obtained by different parametrizations is used to construct confidence intervals for model outputs. According to the concept of "equifinality" (Beven and Binley, 1992), which states that many parameter sets within a given modelling framework are capable to simulate reliably a given output, a likelihood value can be assigned to each parameter set to indicate how well the given set of parameters provides a behavioural simulation of the observed variable. Here we adopted the LHS sampling scheme as the technique to adequately explore the entire parameters space.

In both cases, the inverse modelling procedures were based on the maximization of the Nash-Sutcliffe Efficiency (NSE) index (Nash and Sutcliffe, 1970) for streamflow time series evaluated at chosen nodes of the river network:

$$NS = 1 - \frac{\sigma_e^2}{\sigma_o^2}, \tag{2.10}$$

where σ_o^2 is the variance of the observed streamflow time series, σ_e^2 is the variance of the residuals, i.e. the difference between observed and simulated streamflow. Nevertheless, other efficiency metrics used in the hydrological literature could well be implemented (like e.g., the Kling-Gupta efficiency, KGE, (Gupta et al., 2009)) without any loss of the generality for the proposed modelling framework (e.g., see Laiti et al. (2018); Piccolroaz et al. (2015)).

2.3 Parallelization strategy

In the present work, the MPI standard has been adopted in order to implement a dual-layer parallelization scheme into HYPERstreamHS. Each parallelization layer contributes to the model's scalability, either reducing the computational time associated to each run of the hydrological model (first-layer) or improving the workload subdivision during model calibration or uncertainty analyses procedures (second-layer). In addition to this, the parallelization enables the use of multiple CPUs (which can have multiple processors) with their own and independent memory access: this allows in order to overcome the volatile memory allocation issues due to the simultaneous managing of a large amount of data, which is typical in hydrological modelling applications.

MPI standard has been preferred over a standard scheduler approach (Zhang et al., 2016) due to its flexibility and portability (i.e. it can be used in different computing platforms, Musiał et al. (2008)). In fact, MPI can interact with every kind of processor memory configuration (i.e. shared, distributed or distributed-shared), and it can work with processors using either fast or slow communication networks.

Furthermore, the use of MPI standard allowed to implement a master-slave architecture. Figure 2.5 shows an illustrative example of such architecture, considering $n_p = 16$ processors hypothetically available in a HPC system. Before parallelization, all the processors p_k belong to the same group, named as MPI_GROUP_WORLD, and are associated to its corresponding communicator, termed according to the MPI terminology as MPI_COMM_WORLD: a simple distinction between groups and communicators lays in the fact that groups are entities that represent a set of processes, whereas a communicator is a set of processes that are able to communicate with each other and may consist of processes from a single group or from multiple groups. More detailed definitions of the terms MPI groups, communicators and topology can be found in MPI Forum (1994) and Gropp et al. (1996). When the parallelization is performed, the global group and its communicator are split in n_g sub-sets, here named MPI_LOCAL_COMML, where each sub-set has $n_s = n_p/n_g$ processors. The processors are then renamed $p_{i,k}$, according to the group they belong to.

Each sub-set constitutes now an univocal set of processors and defines the first level of the MPI parallelization, where independent simulation runs are performed. In the illustrative example (see Figure 2.5) the total number of $n_p = 16$ processors is divided into 4 sub-sets, i.e. $n_g = 4$, with each set accounting for 4 processors (see dashed black lines in Figure 2.5). The Figure also highlights that each sub-set has its own local communicator, MPI_COMM_LOCAL, and its own local identifier $p_{i,k}$ for the processor id. The definition of a group of processors that interact by means of a communicator establishes the first parallelization level.

The second parallelization layer is obtained having multiple groups communicate with each other. From Figure 2.5 it can be noticed that a $master$ processor is defined in each sub-set; the $master$ processor coordinates the activity of other processors within its sub-set. These non-master processors are usually referred to as $slaves$, and it should be noticed that each $master$ also performs $slave$ tasks within its own sub-set. The second level of paral-

lelization is achieved by creating a new group, *MPI_MASTERS_COMM* (see continuous black line in Figure 2.5), which gathers the master processors of all sub-sets together with its own communicator. The master processors are in charge of subdividing the workload during the parallel computation involved in the inverse modelling procedures described in Section 2.2, while the slaves perform the parallel computations associated to each given run of the hydrological model identified by their own master from a different set of parameters.

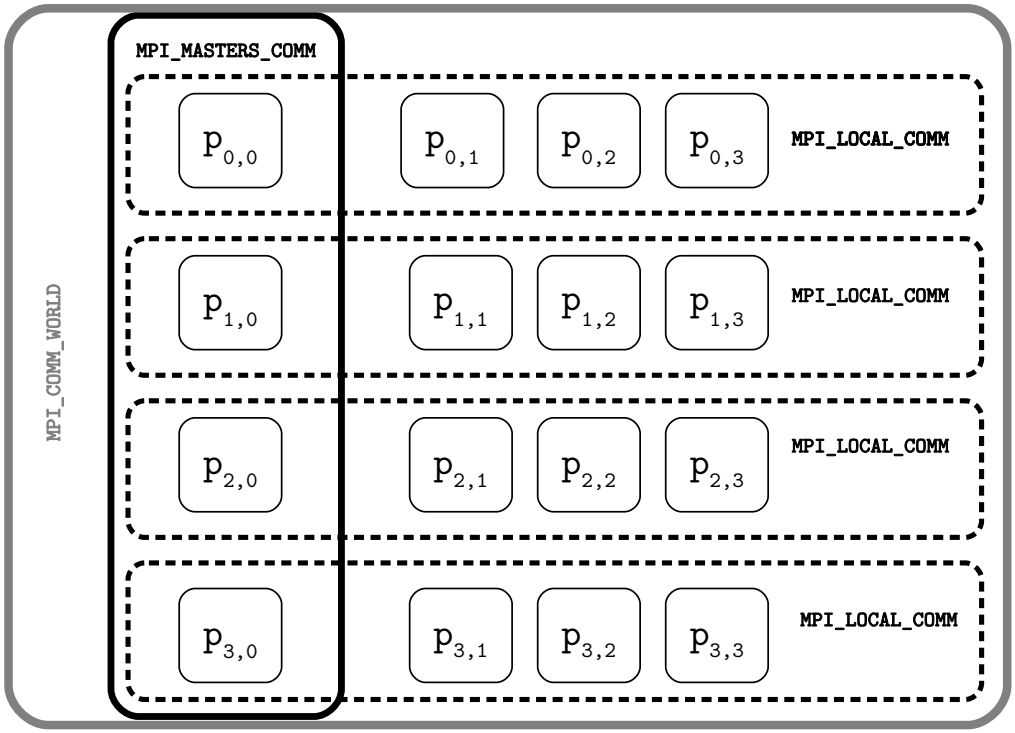

Figure 2.5 *Illustrative example of the MPI dual layer parallelization The original set of* 16 *processors is subdivided in* 4 *local sets (dashed line), each one provided with its local communicator MPI_LOCAL_COMM. Each processor has its local identifier* $p_{i,k}$*, where* $i \in [0..3]$ *identifies the group and* $k \in [0..3]$ *represents the local numbering within the sub-set. Notice that* $k = 0$ *identifies the master of each set. The additional set composed by masters of each group with its communicator MPI_MASTERS_COMM is also presented as continuous black line.*

2.3.1 First parallelization level

As discussed in Section 2.1.1, many of its features make HYPERstreamHS inherently highly parallelizable: i) subdivision of the computational domain in independent macrocells, each of which is assigned its corresponding properties and input meteorological forcing; ii) vertical water fluxes are computed independently for each macrocell; and iii) the WFIUH approach allows to apply the superposition principle at the node itself. when transferring the specific runoff generated in each portion of the macrocell to the corresponding downstream node using the HYPERstream routing scheme (Piccolroaz et al., 2016). The serial computations foreseen in HYPERstreamHS are indeed associated only to the transfers along the river network of the streamflows generated at the node level. In light of these considerations, the first level of parallelization scheme assigns the parallel tasks based on the number of macrocell-node pairs identified by the geometric pre-processor (see Section 3.1). Figure 2.6 illustrates the parallelization approach adopted in the first MPI level: the processed being carried over can be broken down into four separate phases, represented by the horizontal panels shown in the Figure:

a. *Reading of Input Data*: at the beginning of the simulation each processor stores the hydrological model parameters and the network topology;

b. *Macrocell-node Splitting*: afterwards, the macrocell-node pairs are evenly subdivided between the available processors, and the corresponding macrocell-node width functions and input meteorological forcing are read, limited to the subset of macrocell-node pairs pertaining to each processor;

c. *Hydrological Kernel*: afterwards, each processor computes the hillslope runoff time series of the assigned macrocells and transfers the streamflow contribution to the connected downstream node. A first water mass balance is then performed at each network node by summing up all the pertaining contributions to each node coming from different macrocells;

d. *HS Modules and Final Routing*: once macrocell-node streamflow contributions have been aggregated at each node, a single processor is designed to

perform the serial computations envisioned in the code: i) enforcement of the constraints on natural water budget imposed by the presence of the human infrastructures (see Section 2.1.2); and ii) routing along the natural and artificial network of the resulting fluxes simulated at the nodes.

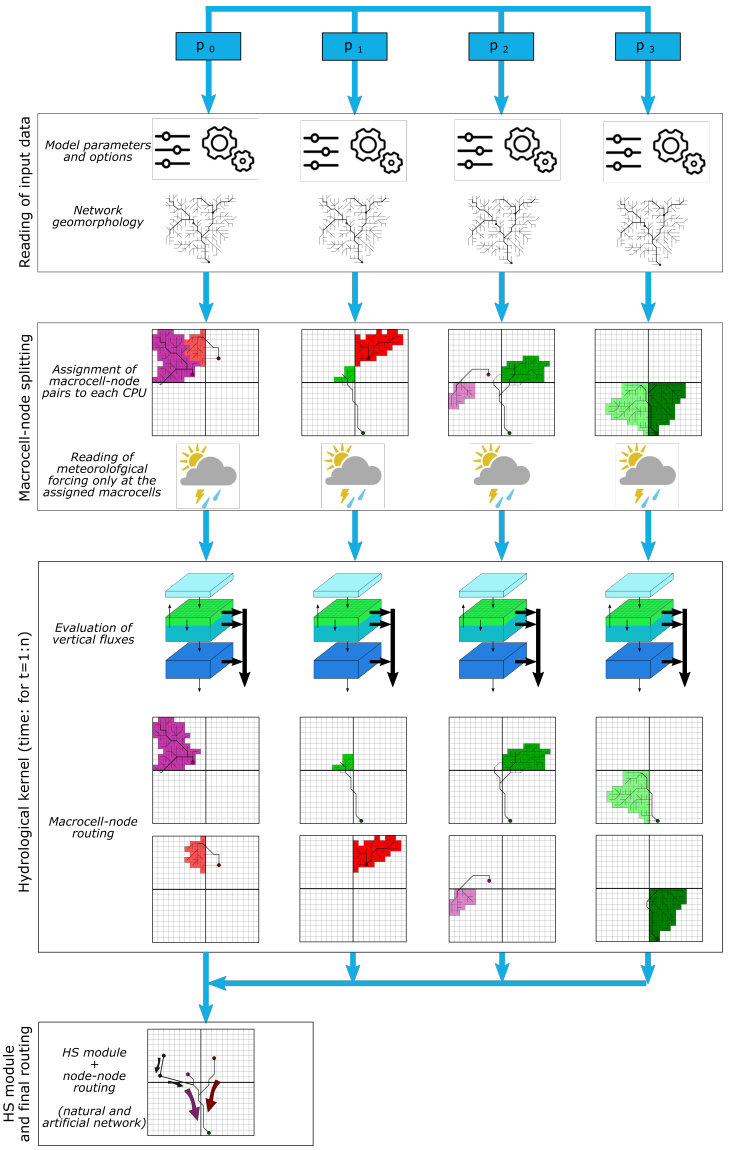

Figure 2.6 *Illustrative example of the first parallelization level considering* 4 *processors. Each processor reads river topology and model parameter, then macrocell-node pairs are assigned to processors which read the corresponding input meteorological forcing and evaluate vertical fluxes and the macrocell-to-node routing. Finally, a single processor solves the water balance equations imposed by the presence of HS and performs the final routing along the entire natural and artificial network.*

2.3.2 Second parallelization level

The second level of parallelization has been applied to the parameters identification schemes described in Section 2.2: the Latin Hypercube Sampling (LHS) and the Particle Swarm Optimization (PSO). Figure 2.7 and 2.8 illustrate a schematic of the implemented dual layer framework for LHS and PSO, respectively.

2.3.2.1 Latin Hypercube Sampler - LHS

The LHS calibration procedure allows an easy and direct implementation of the parallel scheme. At the beginning of the simulation a given number of sets of parameters are randomly generated; afterwards, these sets are equally subdivided among the master processors. Each master and its slaves perform a simulation run of HYPERstreamHS and evaluate model performance corresponding to each given set of parameters. In the case of the LHS algorithm, the second MPI layer is onlyactivated at the beginning of the calibration procedure, and no further communications between masters are required. An illustrative example of the LHS scheme functioning is depicted in Figure 2.7; firstly, one processor (termed as master of masters, with local identifier $p_{0,0}$) generates all the sets of parameters according to the LHS scheme and subdivides such sets equally among the 4 masters ($p_{0,0}$, $p_{1,0}$, $p_{2,0}$, $p_{3,0}$). Each master coordinates the cycling over the assigned subset of parameters, having its slaves run the hydrological model a number of times equal to the number of the sets of parameters assigned to the sub-set. The cycling over the parameter sub-set assigned to each master is depicted with a red box in Figure 2.7.

2.3.2.2 Particle Swarm Optimization - PSO

Differently from the LHS, the PSO is an evolutionary computation technique characterized by the presence of a population of potential solutions, called particles, exploring the multi-dimensional parameters space in order to find the optimal solution of a given inverse problem. After a preliminary step in which particle positions are generated randomly and independently, each particle

starts to explore the parameters and updates its own position considering both the memory of its own best position and the knowledge of the overall best position (i.e., the location visited by one among all the particles that achieved the highest efficiency metric up to now). It can be easily noticed that the parallelization strategy in the case of PS must differ from the LHS case (see Figure 2.8). Even in this case, the master of the masters ($p_{0,0}$) generates randomly the initial locations in the parameters space of a given number of particles, which are then assigned evenly to all the masters. Afterwards, each master ($p_{i,0}$) and the associated slaves perform a number of runs of the hydrological model equal to the number of particles assigned to each master. At the end of each PSO iteration step, the masters must share information in order to recognize the best-scoring particles, and then to update the positions of all particles based on the performance achieved at the previously explored locations.

This is clarified in Figure 2.8 where the PSO scheme in the dual-layer framework is illustrated. As it can be noticed, the PSO configuration shares some similarities with LHS: in both cases the master of masters initializes the population of candidate solutions, and then subdivides them among the masters. Thereafter, the LHS and PSO differ: while in PSO the 4 masters are forced to communicate at each step in order to track the best solution among all the population, communication in LHS occurs only at the very end of the process.

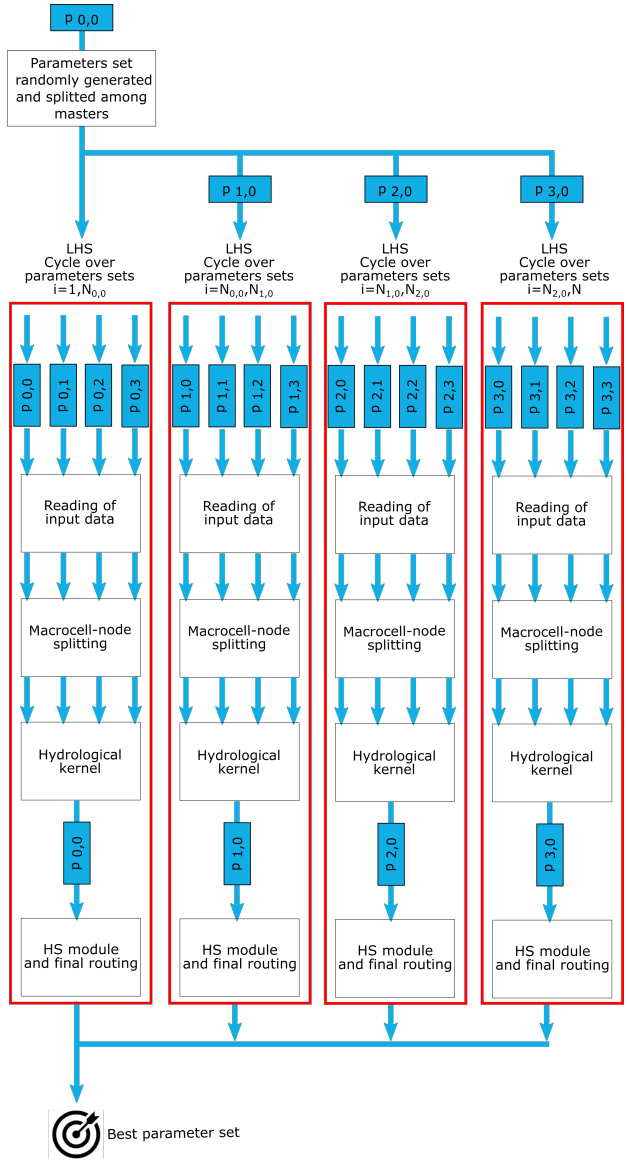

Figure 2.7 *LHS double-layer parallelization scheme. The master of the masters ($p_{0,0}$) computes the parameters and divides them equally between other masters. Each masters runs the parallel hydrological model with its own slaves.There is no communication between masters until the end of the process. The cycling over the parameter sub-set assigned to each master is depicted with a red box.*

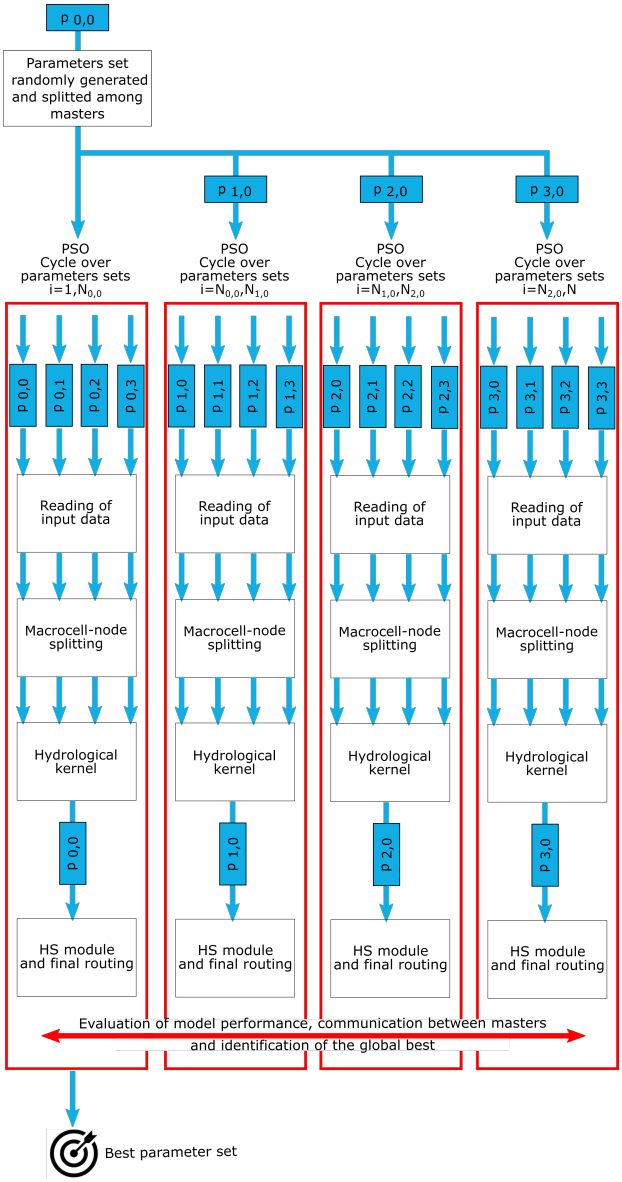

Figure 2.8 *PSO double-layer parallelization scheme. The master of the masters ($p_{0,0}$) computes the parameters and divides them equally between other masters. Each masters runs the parallel hydrological model with its own slaves, and at each iteration step the masters communicate in order to find the best global solution (red horizontal arrow). The cycling over the parameter sub-set assigned to each master is depicted with a red box.*

CHAPTER 3

DATA, CASE STUDIES AND STATISTICAL TOOLS

In this Chapter an overview of the information required to characterize the model is presented. Then, a detailed presentation of the different case-studies is provided and finally the statistical tools adopted in Chapter 5 are illustrated.

Inputs to HYPERstreamHS can be subdivided into three main categories:

a. Geometric information: required for preprocessing the domain, hence defining the computational grid and stream network, as well as assigning soil characteristics to each macrocell;

b. Meteorological input forcing: spatialized rainfall and temperature time series are provided as input to the model;

c. Nodes characterization: this category includes both observed streamflow time series obtained at relevant stream gauging stations, as well as a wide set of information required to characterize HS nodes that will be further detailed in the upcoming sections.

While geometrical data and meteorological input are already available over the entire Alpine Region, collection of Human System information is an ongoing task. However, it has already been completed for the first two applications of HYPERstreamHS, the first of which is the Adige catchment, located in the Eastern Italian Alps, and the second case study being located in the Western Alps, composed of 5 catchments, namely the Dora Baltea, Orco, Stura di Lanzo, Dora Riparia and Pellice river catchments. Both domains are depicted in Figure 3.1.

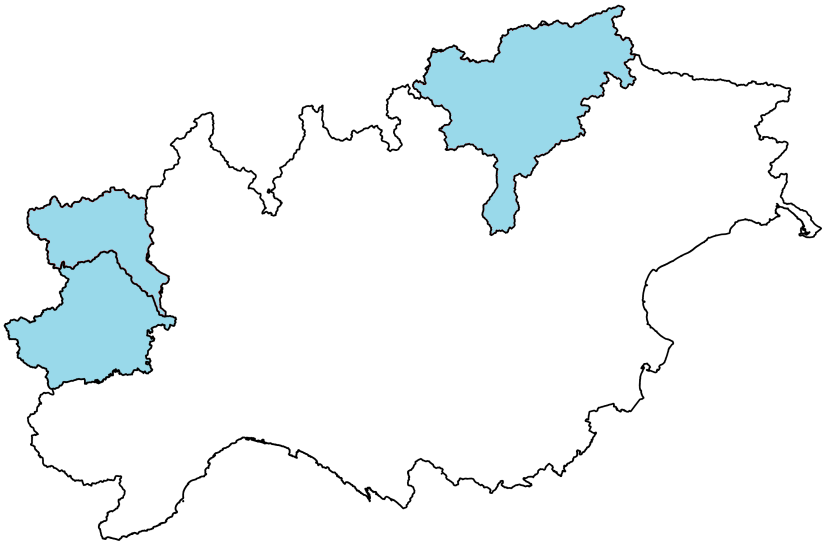

Figure 3.1 *Location of the two case studies investigated in this thesis. The Adige catchment is located in the Eastern portion of the Italian Alps. In the Western part of the map is the second domain, which was further subdivided within two areas during its implementation: the upper portion is the Dora Baltea catchment, while the lower one contains the Orco, Stura di Lanzo, Dora Riparia and Pellice catchments.*

3.1 Geometry and Soil information

As anticipated in Section 2.1.1, a preliminary geometric processing is required to set up the simulation. Four raster files are required as input: the DEM (Digital Elevation Model) of the area, a Drainage Direction file, which can be computed starting from the DEM by means of a GIS analysis (or can be provided otherwise), a Crop Coefficient raster map, useful for the determination of the S parameter adopted in the SCS-CN infiltration model, and finally a Stream Network raster file, which again can be computed by means of a raster GIS or provided otherwise. Along with the input raster files, a text file containing the coordinates of the nodes, grid information (macrocell size, and top-left grid corner coordinates), and the sampling width for the definition of the widthfunction is provided. The key outputs from the geometrical preprocessing are indeed files that contain node-to-node dependencies based on drainage directions and

stream network, macrocell infiltration data, and widthfunctions computed for each macrocell-node pair: these files are suitable for use from HYPERstreamHS. The raster input files are shared between all of the analyses presented in this thesis (and will also be adopted in the upcoming ones) and are the following:

a. DEM: the 30m EUDEM Digital Elevation Model was used; the DEM has then been reconditioned in order to comply with the official stream network;

b. Land use information and crop coefficients were extracted from the Corine dataset (https://www.eea.europa.eu/publications/COR0-landcover).

c. Stream Network provided by the Superior Institute for Environmental Protection and Research (ISPRA, available at http://www.sinanet.isprambiente.it/it/sia-ispra/download-mais/reticolo-idrografico/view).

3.2 Meteorological Input Forcing

Gridded meteorological forcing is also provided as an input. Temperature (minimum, mean, and maximum) and precipitation time series are required. Temperature dataset is also used to compute PET (Potential EvapoTranspiration) gridded dataset. The meteo forcing grid should overlap with the computational grid (i.e. macrocell grid): therefore, a preliminary reprojection of the dataset might be necessary. The input meteorological information is then processed and associated to each macrocell, together with the soil infiltration properties presented in the previous Section. As already introduced, two separated case studies were investigated: the chosen input forcing was different for each case, as detailed in the following.

3.2.1 Meteorological input forcing for the Adige catchment

The ADIGE dataset (Mallucci et al., 2019) was used for this case study. The dataset consists of daily readings taken at 244 and 350 gauging stations for precipitation and air temperature respectively, which have then been spatialized on a 5x5km grid by means of Ordinary Kriging with External Drift (OKED),

adopting terrain elevation as the secondary variable (Gooaverts, 1997). The portion of the ADIGE dataset that was used in our analyses covers the 1989-2013 time window. This dataset was employed in the analyses presented in Chapters 4 and 5.

3.2.2 Meteorological input forcing for the Dora Baltea, Orco, Stura di Lanzo, Dora Riparia and Pellice catchments

The analysis carried over in this second case study was aimed at the validation of HYPERstreamHS hydropower production model against historical observations, as a first application of the framework that later will be applied to the entire Alpine Region. For this study, the COSMO datasets for temperature and precipitation were adopted, limited to the 1995-2008 time window, in order to match the data availability for model characterization. COSMO (Bollmeyer et al., 2015) is a weather prediction model whose results have been improved by means of a data assimilation, i.e. the inclusion of heterogeneous observations to improve the prediction of COSMO's physical model. The improvement brought by the data assimilation was assessed through a dynamical downscaling experiment (i.e. comparing model results with and without data assimilation) COSMO provides both temperature and precipitation time series, and data over the 1995-2008 time window were used in this case study.

3.2.3 Temporal and Spatial disaggregation of the inputs

The spatial resolution for the data sets of both case studies was set to 5x5 km, hence overlapping the macrocell grid and allowing to assign different input at each macrocell; the time window covered by the two datasets allowed to perform the simulations over the 1995-2008 time window, adopting daily measurements that were disaggregated to the hourly scale, in order to match simulation time step. Disaggregation procedures were linear, hence assuming the same temperature throughout each day and partitioning evenly the daily precipitation among the 24h.

3.3 Node characterization

3.3.1 Streamflow time series

Streamflow time series for many Northern Italian rivers were retrieved from multiple sources as a part of a concurrent activity of this project, as described in Todaro (2020). Streamflow observations are available at a daily time step at 388 locations, as displayed in Figure 3.2. The accuracy and time span of the measurements vary substantially, however a follow-up analysis on the data set showed that measurements at many stations cover more than 90% of their entire time span; stations with extensive measurement coverage and reliable measurements represent the ideal candidate locations for model calibration and validation.

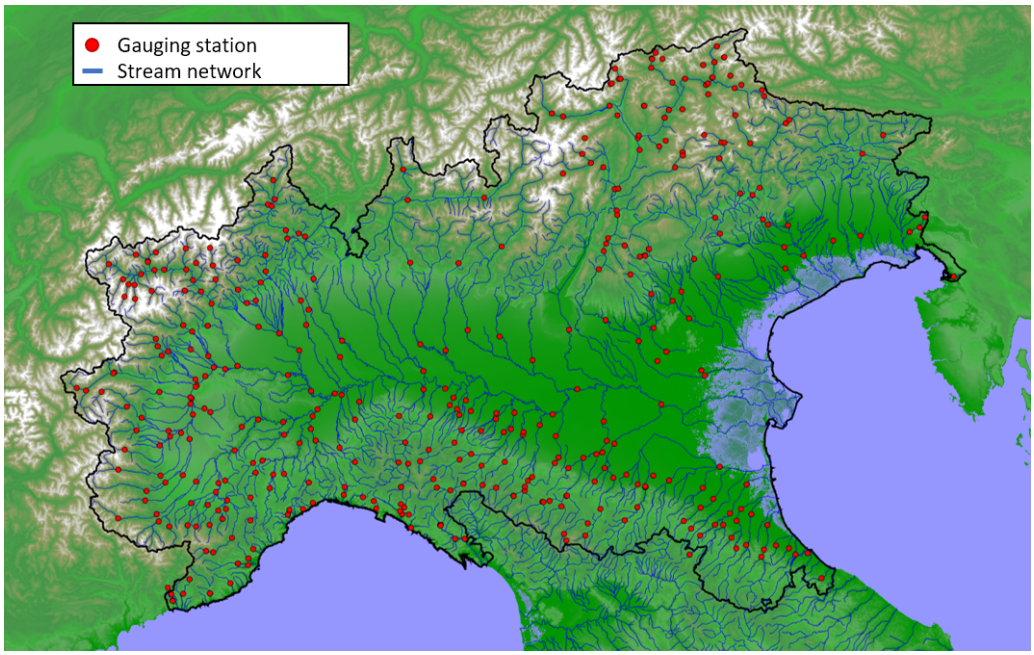

Figure 3.2 *Location of the 388 stream gauging station provided by several Environmental Agencies in Italy. Streamflow time series at relevant locations are used to calibrate and validate HYPERstreamHS.*

3.3.2 Human System Nodes

The approach to modelling hydropower-related infrastructure required a particularly high level of detail. Firstly, as many information as possible were collected to characterize human systems; then, after a phase of model tuning it was possible to define the modelling strategy, thus refining and reducing the required input information to an optimal and minimal set. Since global database do not contain detailed information about Italian hydropower systems, and since key information concerning reservoir operation are rather often protected by industrial secret, we chose to model human systems only adopting data that are typically available to the public without any particular agreement: since no standard dataset is available for this kind of information, an in-depth, site-by-site search was carried over in order to progressively fill the input dataset; the information required to characterize and constrain the HS nodes in HYPERstreamHS is synthesized in Table 3.1. Information concerning the location, structure and operation of the hydropower systems, as well as network topology information, was collected and structured in a GIS database during the EoCoE2 (https://www.eocoe.eu/water-for-energy/) project, which is visually displayed in Figure 3.3. Due to the sheer number of information it includes, the completion of the data set often requires system-specific investigation and is therefore ongoing. It has, however, already been completed over the three catchments already investigated in our analyses, which are depicted in Figure 3.1.

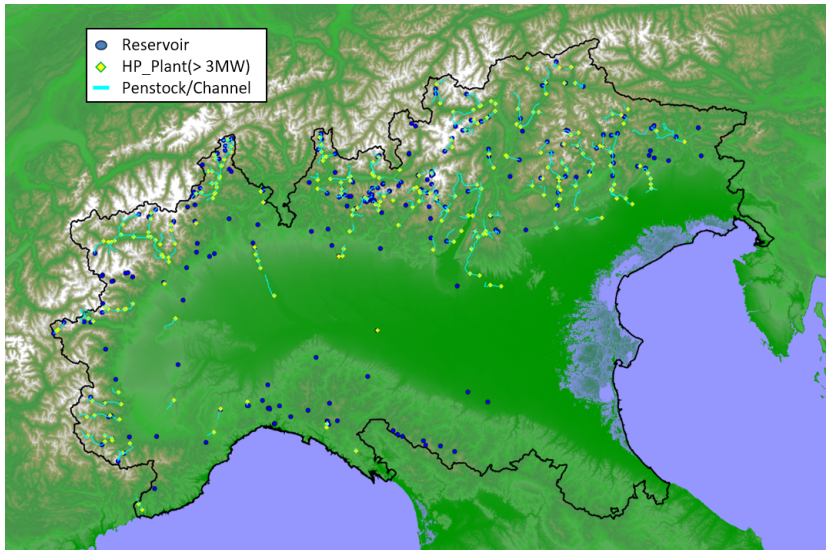

Figure 3.3 *Current state of completion of the Human System database for the Alpine Region. The database is organized in a GIS platform and each node is characterized according to Table 3.1*

Table 3.1 *Data requirements to fully characterize HS nodes in HYPER-StreamHS. All the information contained in this Table (with the exception of the location, which is accounted for during the geometric preprocessing) is provided as-is to the model, with the exception of the HPP schedule, which is computed offline and then provided as input.*

Reservoir		
Characteristic	Description	Data type [units]
x_{res}, y_{res}	Location	CRS: WGS 84-UTM 32 N [m]
$Q_{spill,MAX}$	Spillway capacity	[m^3s^{-1}]
$V(H)$	Stage-Storage curve	array [m a.s.l. vs. Mm^3]
$h_{min,reg}$	Minimum regulation stage	[m a.s.l.]
$h_{max,reg}$	Maximum regulation stage	[m a.s.l.]
$h_{max,inv}$	Spillway crest elevation	[m a.s.l.]
$Q_{turb,MAX}$	Maximum turbined flow	[m^3s^{-1}]
$MEF(t)$	Minimum Ecological Flow	[m^3s^{-1}]
$q_{turb}(t)$	HPP schedule	time series [m^3s^{-1}]
Intake		Data type
Characteristic	Description	Data type [units]
x_{itk}, y_{itk}	Location	CRS: WGS 84-UTM 32 N [m]
$Q_{max,chann}$	Intake capacity	[m^3s^{-1}]
$MEF(t)$	Minimum Ecological Flow	[m^3s^{-1}]
Hydropower Plant		Data type
Characteristic	Description	Data type [units]
x_{plt}, y_{plt}	Location	CRS: WGS 84-UTM 32 N [m]
H_{plant}	Elevation	[m a.s.l.]
ΔH_{plant}	Head (run-of-the-river only)	[m]
P_{ann}	Mean annual production	[MWh/y]
W_{inst}	Installed power	[MW]
η	Plant efficiency	-
Channel		
Characteristic	Description	Data type [units]
id_{UP}	Upstream node ID	Node attribute
id_{DOWN}	Downstream node ID	Node attribute
$typen_{UP}$	Upstream node type	Node attribute
$typen_{DOWN}$	Downstream node type	Node attribute
l	Length	[m]
u_{art}	Celerity	[m^3s^{-1}]

3.3.3 Hydropower production time series

Hydropower production data were made available upon request by the Manager of the Italian electricity grid, TERNA (http://www.terna.it/). Hydropower production time series are publicly available at a monthly time scale and aggregated by-province (Figure 3.4), and cover the 2000-2015 time window with no gaps. Moreover, data are subdivided between small and large hydropower plants (3 MW installed power threshold), in line with the classification commonly adopted in Italy and inherited from the present work (Figure 3.5). In order to validate the model, hydropower production time series produced by the model must be comparable with observations. Since provinces do not constitute hydrologically independent units (except by coincidence, like it happens for the upper portion of the Adige catchment which falls in- and covers entirely in the province of Bolzano), setting up the model to directly reproduce a province's production could be troublesome and not significant. Conversely, we decided to scale the available observations so that they could represent the hydropower production of any catchment of interest. The production from a catchment was therefore estimated through the following relationship:

$$HPP_{catchment} = \Sigma HPP_{prov,i} w_i \tag{3.1}$$

Where $HPP_{prov,i}$ represents the hydropower production related to each province in which the catchment has at least one hydropower plant, and being w_i a weighting factor computed as the ratio between the total hydropower capacity installed in the portion of the province belonging to the catchment and the installed capacity of the entire province. This procedure requires the knowledge of single plant capacity of both the plants pertaining to the catchment of interest and of the plants belonging to provinces partially touched by the catchment. Under the hypothesis that the all hydropower systems are operated similarly, we can consider the so-obtained values as observations, and are able to use them for comparison with the model's predictions during validation.

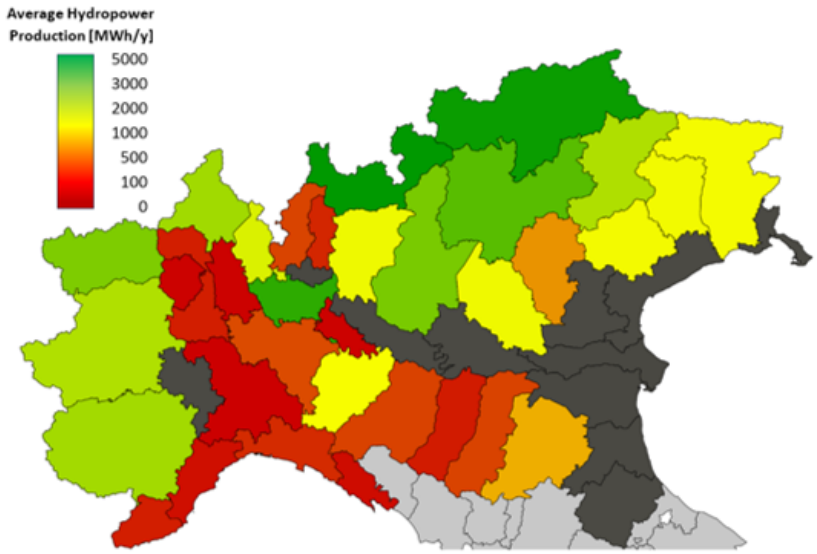

Figure 3.4 *Distribution of the average annual hydropower production due to large hydropower plants in the provinces of Northern Italy. The average is based on the available observations (years 2000-2015). Gray provinces mean that no large hydropower plants are known to belong to the province.*

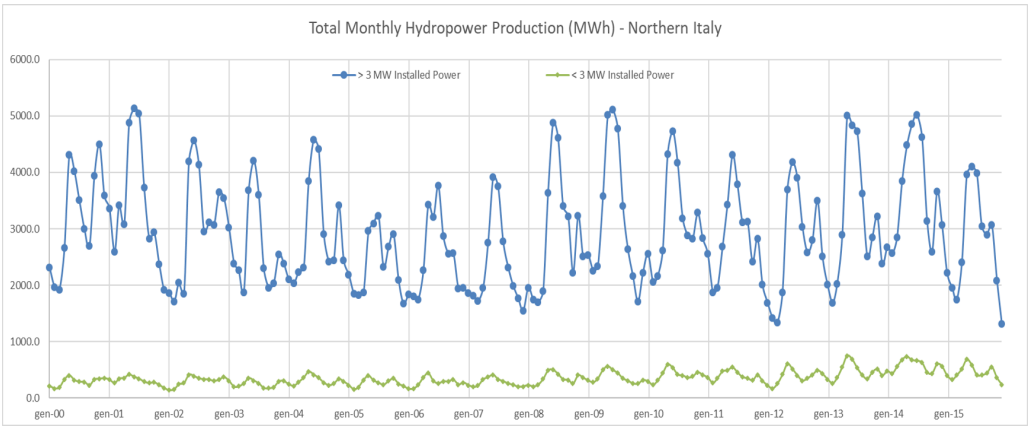

Figure 3.5 *Total monthly hydropower production in Northern Italy. The two series represent the contribution to the total from large (blue) and small (green) hydropower plants; the distinction is based on the 3MW installed power threshold.*

3.4 Case studies

As anticipated, the modelling framework illustrated in Chapter 2 has been applied to two different domains. The Adige domain was the first application, and both scalability testing of the model and hydrological/hydropower modelling and validation were performed on this catchment: their results will be illustrated in Chapters 4 adn 5, respectively. The second case of study is composed by five catchments located in the Western Alps: Dora Baltea, Orco, Stura di Lanzo, Dora Riparia and Pellice. Together with usual hydrological and hydropower production modelling and validation, this second case study served for an analysis of the role of different meteorological input data sets in hydropower forecasts, which will be presented in Chapter 6.

3.4.1 The Adige catchment

The Adige catchment is the second widest of all the Italian river catchments and is located in the eastern portion of the Italian Alps. It is a mesoscale basin (around 10600 square kilometers, considering the catchment closed at the Vo Destro stream gauging station); it includes a wide variety of topographic characteristics ranging from small, mountainous catchments to larger basins, resulting in a variable geomorphology and hydrologic regime throughout the catchment, that reflect themselves on different reservoir management strategies for hydropower production. As anticipated in Section 3.2, the ADIGE dataset provided temperature and precipitation input forcing for the simulation: the distribution of average rainfall and temperature are depicted in Figures 3.6 and 3.7, respectively.

In the Adige river basin, as many as 40 large hydropower plants are present, with installed power ranging from 3 to 230 MW and 30 of them being fed by as many 30 reservoirs, which operational volume ranges between 0.48 and 200 Mm^3. A rather extensive network of diversion channels with capacity ranging from 0.3 to 203 m3/s is feeding the whole system. The total average production

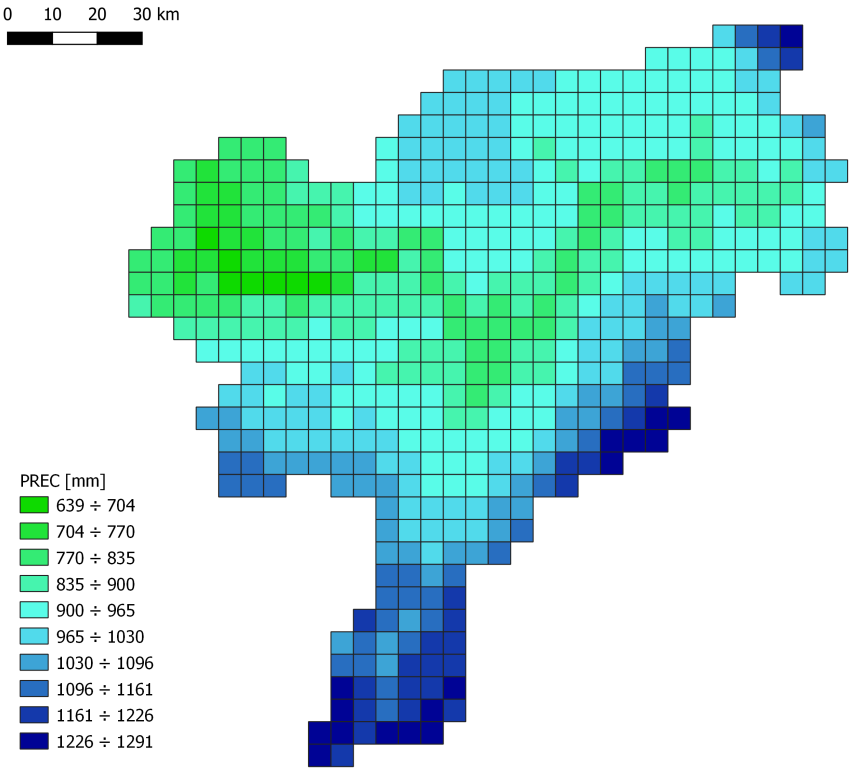

Figure 3.6 *Average rainfall provided by the ADIGE data set over the reference period 1989-2013 in the Adige river basin.*

of the Adige large hydropower plants is around 6609 GWh/y, according to data available from the hydropower companies operating in the river basin, thereby contributing to more than 14% of the yearly Italian hydropower production (TERNA, 2015). The resulting conceptual model for the Adige catchment includes 146 nodes 30 of which represent reservoirs, 41 intake, 40 hydropower plants and 35 nodes that include stream gauging stations or nodes inserted for modelling purposes; this setup is depicted in Figure 3.8.

As anticipated in Table 3.1 the Italian law prescribes a minimum value of the streamflow that must remain in the river network at each water usage location, called Minimum Environmental Flow (MEF). This threshold often varies seasonally, and its definition pertains to Regional authorities. Detailed prescriptions for MEF at each water diversion were retrieved from the Public

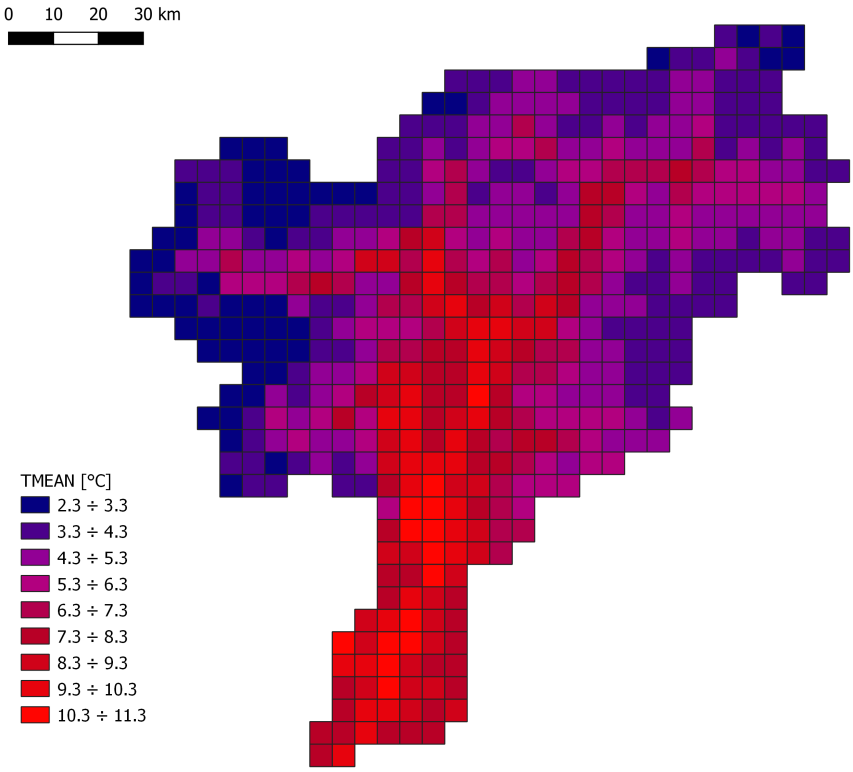

Figure 3.7 *Average temperature provided by the ADIGE data set over the reference period 1989-2013 in the Adige river basin.*

Water Usage Plans of the Trento and Bolzano autonomous provinces, ensuring complete coverage of the Adige catchment (Piano Generale di Utilizzazione delle Acque Pubbliche, available at http://www.pguap.provincia.tn.it for Trento, and at https://ambiente.provincia.bz.it/acqua/piano-generale-utilizzazione-acque-pubbliche.asp for the Bolzano province).

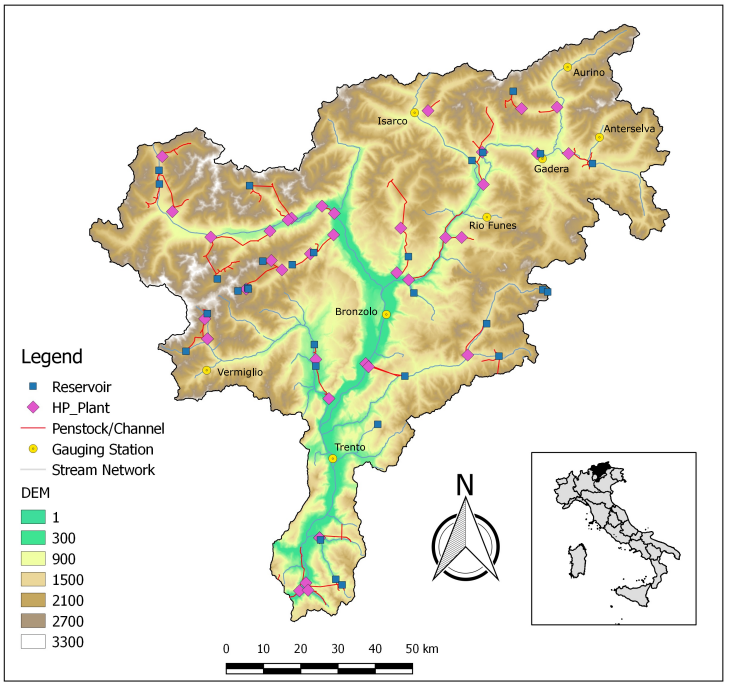

Figure 3.8 *Map of the Adige river basin closed at the Vo' Destro section. In the figure are indicated the locations of the relevant streamflow gauging stations (yellow dots), reservoirs, hydropower plants, artificial channels network connecting the main hydropower systems and intake points. The inset recalls the position of the catchment in Italy.*

3.4.2 The Dora Baltea, Orco, Stura di Lanzo, Dora Riparia and Pellice catchments

For the analyses presented in Chapter 6, a different domain was used. The choice of the domain has been driven by the progress in the completion of the HS nodes database: the availability of HS node characterization on a sufficiently large region allows for a significant application of the model, which is mainly made to be applied at the regional scale. The final choice of the domain was performed accounting for a set of adjacent river catchments in which the HS dataset was completed.

Dora Baltea is the fifth tributary of the Po river, and its catchment area mea-

sures roughly 3850 square kilometers. The river is fed by a number of glacial, mountainous creeks and this gives it the unique trait among the major Italian rivers of having a nivo-glacial hydrologic regime. Few reservoirs can be found in the mountainous portion of the catchment, while the majority of the hydropower activities are concentrated on the main body of the river by means of run-of the river plants. Orco, Stura di Lanzo, Dora Riparia and Pellice rivers are four tributaries of the Po river, wose catchments are located immediately South of the Dora Baltea catchment. These catchment present a similar morphology, all having a mountainous region located to their western side. Indeed, the hydrological regimes of the rivers are also the same and mainly exhibit a pluvio-nival characteristic. The joint surface area of these catchments is around 4100 square kilometers. The Pellice catchment is only mildly influenced by hydropower activities, while the other three catchment are influenced by the presence of many hydropower plants, all concentrated in the mountainous region of the catchment.

As anticipated, one of the purposes of the analyses performed on this domain was to assess the effects of different climate data sets in terms of modelled hydropower production. Therefore, two combinations of data sets were adopted, all in the 1995-2008 time window. Firstly, COSMO was used to provide both temperature (Figs. 3.9a and 3.9b) and precipitation (Figs. 3.9c and 3.9d).

Observed streamflow time series at 17 relevant stream gauging stations were selected among those available at the Superior Institute for Environmental Protection and Research website (ISPRA, http://www.isprambiente.gov.it); measurements were taken at a daily scale, and all the records showed a relatively low share of missing observations (i.e. 30% or lower).

As mentioned in the previous paragraph, most hydropower plants in this study area are run-of-the-river plants: among 63 hydropower plants, only 18 are served by upstream reservoir. The declared mean annual production for this area is around 4496 GWh//y. A relatively complex network of intake points and tunnel serves the hydropower systems present in this area, resulting in 119 modelled intake nodes. The total conceptual model hence includes 18

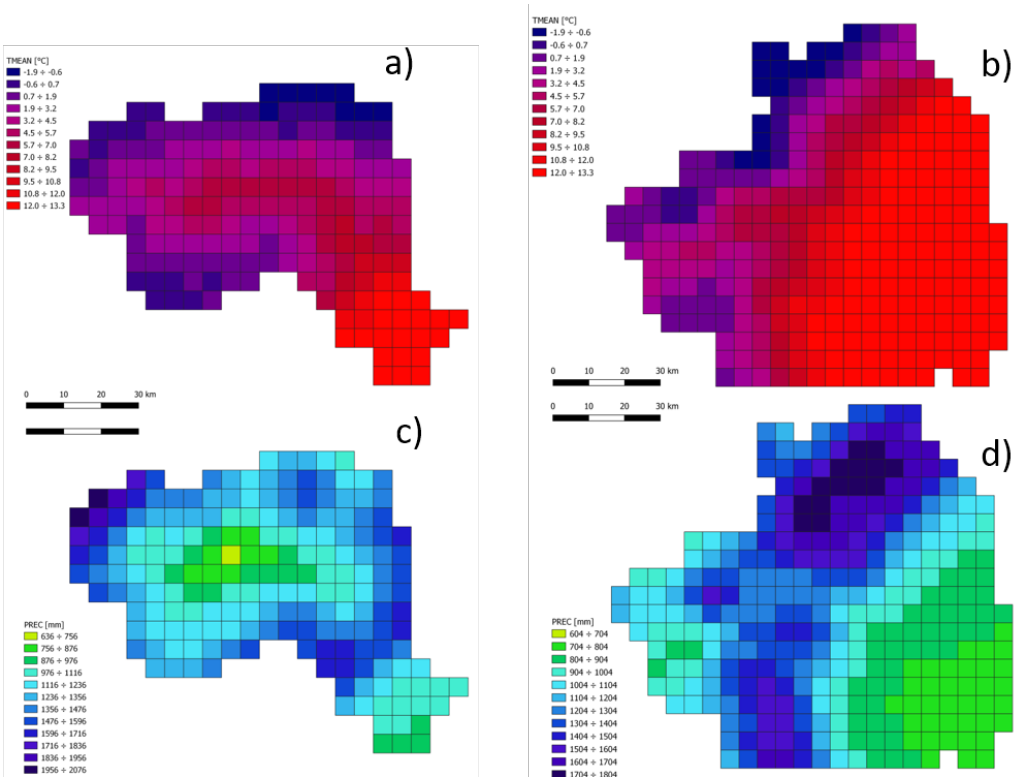

Figure 3.9 *Average annual temperature and precipitation over the 1995-2008 time window int the two subsets of the domain: the left column is relative to the Dora Baltea catchment while the right column is referred to the Orco, Stura di Lanzo, Dora Riparia and Pellice river catchments. In the rows are shown respectively: COSMO average temperature (a,b) and precipitation (c,d)*

reservoirs, 119 intakes, 63 hydropower plants and 17 stream gauging station locations, for a total of 217 nodes. The resulting model is shown in Figures 3.10 a and b, split in two as usual for sake of clarity.

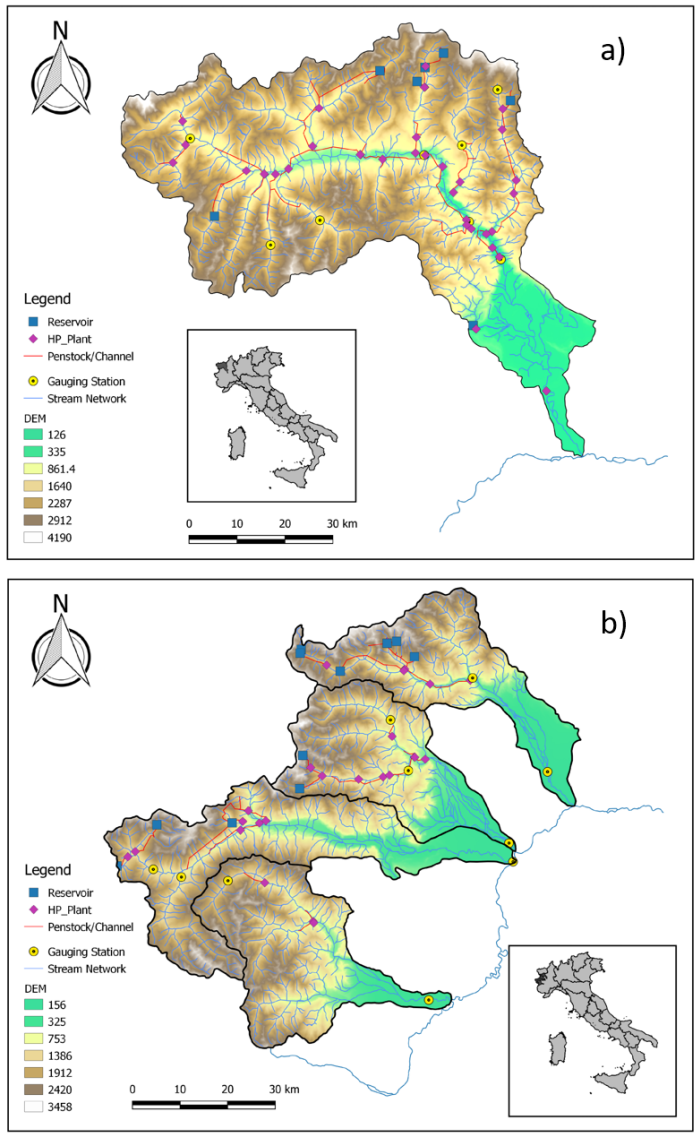

Figure 3.10 *Map of the Dora Baltea (a) and Orco, Stura di Lanzo, Dora Riparia and Pellice (b) river catchments, with indicated the location of the outlet and the relevant streamflow gauging stations (yellow dots), reservoirs, hydropower plants, artificial channels network connecting the main hydropower systems and intake points. The insets recalls the position of the catchments in Italy.*

3.5 Clustering analysis tool

In order to perform the additional analyses presented in Section 5.3, a standard clustering analysis was performed. To this aim, the *kmeans* algorithm was used: the algorithm is based on Lloyd (1982) clustering algorithm: in this procedure, the number of clusters must be guessed by the user prior to the partitioning (based e.g. on expected results or just by trial-and-error); at the first iteration, k cluster centroids are chosen at random, and each data point is assigned to the cluster with the closest centroid. At the start of the second iteration, k new centroids are computed based on the locations of evry data point belonging to their cluster; subsequently, data points are assigned to a new cluster, again based on the closest centroid. This procedure is repeated until convergence (i.e. the centroids do not move between iterations) or when the maximum number of iterations is reached. For our analysis, three normalized indicators were taken into account:

$$H(i) = \frac{H_{res,max}(i) - H_{res,min}(i)}{H_{sys}(i)} \tag{3.2}$$

Where H_{res} represent the maximum and minimum regulation stage of the $i-$th reservoir, respectively and H_{sys} represents the average geodetic jump of the hydropower system (i.e. from reservoir to turbine axis in case of storage hydropower plant, or the jump declared by the plant operator in the case of run-of-the-river hydropower plants). This indicator accounts for the relevance of the reservoir geodetic head compared to the overall geodetic head of the system.

$$HPP(i) = \frac{HP_{sim}(i) - HP_{ref}(i)}{HP_{ref}(i)} \tag{3.3}$$

Where HP_{sim} represents the simulated hydropower production obtained in the current scenario at the $i-$th plant and HP_{ref} represents the reference hydropower production for the same plan, as computed by means of our standard simulation setup (further detail provided in Section 2.1.2.5).

$$Q(i) = \frac{Q_{rule}(i)}{Q_{in,avg}(i)} \tag{3.4}$$

This third indicator accounts for the ratio between the average turbined flow at reservoir i in the current scenario, Q_{rule}, and the average inflow to the same reservoir ($Q_{in,avg}$). The results of the k-means clustering analysis are shown in Section 5.3.

CHAPTER 4

HYPERSTREAMHS SCALABILITY PERFORMANCE

HYPERstreamHS is a developed version of the HYPERstream model. The main additions to the previous version were parallel computing and explicit simulation of Human Systems related to hydropower. In this Chapter the results concerning the computational performances of the model will be covered.

This Chapter is based on:
Avesani, D., Galletti, A., Piccolroaz, S., Bellin, A., Majone, B. A Dual layer MPI continuous large-scale hydrological model including Human Systems, Environmental Modelling & Software, ***SUBMITTED***

4.1 Model calibration and setup

The scalability of HYPERstreamHS was tested in a real case which was considered suitable for its application. The Adige was selected due the extensive knowledge of the hydropower systems of the area, and to well-organized publicly available of in-depth information, which have been fundamental to guarantee a reliable development and implementation of the Human Systems module. Specifications on the case of study, its conceptual model and on the input data set are provided in detail in Section 3.4.

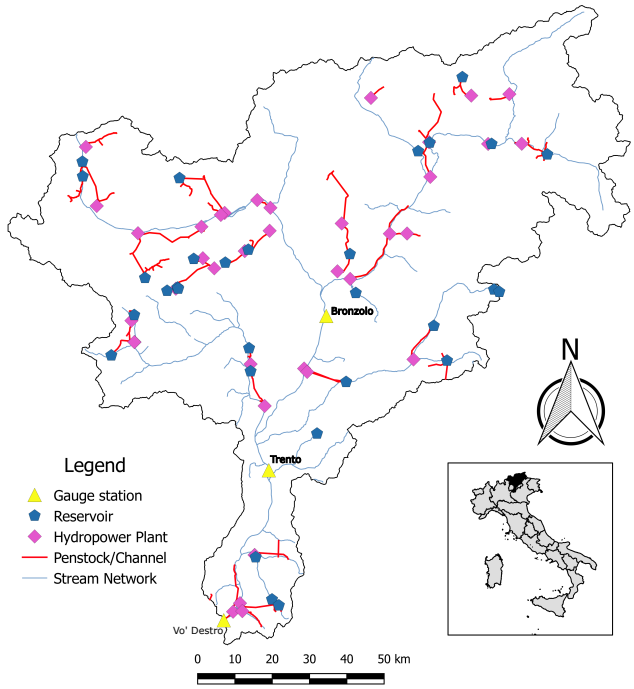

Figure 4.1 *Map of the Adige river basin with indicated the locations of the Vo' Destro outlet section and the streamflow gauging stations of Trento and Bronzolo (yellow dots), reservoirs, hydropower plants, artificial channels network connecting the main hydropower systems and intake points. The inset shows the geographic location of the Adige river basin within the Italian territory.*

All the simulations were conducted at a hourly time step during the 1989-2006 time window using a $5x5km$ computational grid. Streamflow time series

collected at the Trento and Bronzolo gauging stations (see Figure 4.1 for node's location and Section 3.3 for further details on streamflow time series) were used as observations in the inverse modelling procedures. The first two years of simulations were used as a spin-up and thus were excluded from the computation of the NSE efficiency index. In the forward simulations the parameters characterizing the natural hydrological component (see Section 2.1.1) were assumed as equal to the values obtained during one of the optimization experiments described in previous applications of HYPERstream to the Adige catchment (Laiti et al., 2018).

Although sharing the same stream network closed at the Vò Destro section (included in the setup just as catchment closing section but not as a calibration node), two different sets of network nodes were used, in order to create two similar cases with different computational complexity involved.

a. **Full Setup**: The first node setup represents the "complete" setup, and envisions the implementation of all the relevant human infrastructures present within the Adige river basin, resulting in 30 storage reservoirs, 37 intake points and 36 hydropower plants, for a total (including all available streamflow gauging stations) of 138 nodes. It should also be noted that 35 nodes representing streamflow gauging stations were included in this setup, though only 2 of them were effectively used for model parameters inference (i.e., Trento and Bronzolo).

b. **Simplified Setup**: In a second configuration we considered a simplified representation of the human system in which only 5 nodes were considered, composed by 2 storage reservoirs, the two aforementioned streamflow gauging stations adopted for parameters calibration and the Vò Destro outlet section.

Given the $5 - km$ grid spacing adopted and the number of implemented nodes, the two setups yielded a different number of macrocells-node pairs; this quantity is indeed relevant during the parellelization of the HYPERstreamHS model. In particular 569 and 1167 macrocells-node pairs for the 5-nodes and 138-nodes cases, respectively. According to the parallelization strategy described in Sect. 2.3, in the following Sections the computational performances

of HYPERstreamHS and its scalability are tested considering both a single and a dual layer decomposition schemes. In the case of the dual layer implementation we considered 500 runs for LHS and 10000 for PSO (specifically 100 iterations and 100 particles). Under this perspective, it is worth to clarify that we are not interested either in evaluating the convergence to the global optimum in the PSO scheme or in a full uncertainty assessment of the posterior parameters distribution in the LHS, but rather to evaluate how HYPERstreamHS scalability can be influenced by the adopted parameters sampling scheme (see Section2.2). It is also worth mentioning that, despite being tested on a realistic case, the aim of this first application was not to measure the performance of the model in terms of reproducing streamflow time series, which has indeed been already demonstrated in previous applications (see e.g. Laiti et al., 2018; Piccolroaz et al., 2016), but rather to show the peculiarities of the holistic approach implemented in the HYPERstreamHS model.

4.2 Scalability of the single-layer MPI implementation

As previously clarified, the first MPI layer only handles the workload related to macrocell-node pairs and to the computation of their fluxes. Therefore, single-layer parallelization performance is tested in *forward* mode, adopting the same parametrization as in Laiti et al. (2018), since the investigated catchment is the same (the only difference being the explicit simulation of Human Systems) and since hydrologycal performance is beyond the scope of these tests anyway. Testing on the first MPI layer has been performed with reference to the 5 and 138 nodes cases already described in Section 4.1. Moreover, the two test cases have been further differentiated: each one has been run both in *natural* and *artificial* mode, meaning that a natural scenario which does not account for the presence of artificial infrastructure is simulated in the first mode, while in the second one all hydraulic works are modeled, mimicking river flow alteration and requiing a higher number of computations; this further distinction resulted in a total of four configurations. These four cases were expected to show a trend of the relative impact of node numerosity and of the simulation of artificial systems on the overall scalability. Indeed, a low number of nodes requires both a low number of macrocell-node width function computations and likewise lowers the required inter-processors communications. Conversely, a higher number of nodes not only increases the number of width function computations (performed in parallel) but also increases inter-processors communications due to the increased number of upstream-downstream dependencies that necessarily have to be carried out serially without relying on parallelization. Likewise, the artificial infrastructures add up to the overall computational time, requiring the computation of complex water mass balances for each node representing a hydraulic work .

In Figure 4.2 is depicted the speed-up of HYPERstreamHS achieved with a single level of parallelization: the computational time is plotted against the number of processors in a logarithmic scale. In particular, the computational

time using a different number of processors (1,2,4,8,16,32,64) is compared with the theoretical 100% speedup as represented by the dashed lines in Figure 4.2, which means that doubling the number of processors would halve the computational time. the four theoretical speedup curves represent the four combination of node number and artificial/natural mode explained previously. As it could be expected, the number of nodes strongly influences scalability: the test case with 5 nodes exhibits a better scalability than the case with 138 nodes in both cases, with relatively small differences between the natural and the artificial scenario. Indeed, in the 5 nodes case the serial part of the hydrological model is limited to the streamflow routing between the 5 nodes themselves and to the computations of the water balances at the 2 reservoirs (i.e., simulation of the water storage in the two reservoirs and partitioning of outflows). The presence of reduced serial computations also explains why there are negligible differences in the theoretical speed-up curves between the natural and artificial scenario in the presence of 5 nodes.

On the other hand, in the 138 nodes cases the scalability drops evidently after 8 processors are used, ultimately showing a negative trend when 64 processors are used. Indeed, the presence of 138 nodes increases significantly the serial computations to be performed. Similarly, the presence of 103 artificial nodes (see Section 4.1) explains the larger difference in the computational time between the natural and artificial scenarios (see green lines in Figure 4.2) as opposed to the 5 nodes test cases. In fact, when the number of human infrastructures increases, a larger amount of time has to be spent in order to solve the continuity equations for all the hydraulic works present in the system, following the rules detailed in Section. 2.1.2.

Drops in scalability implied by the serial computations required in streamflow routing are a well-acknowledged issue in parallel computing which is typical of single-layer decomposition schemes (see e.g. Wang et al. (2012) and Zhang et al. (2016)). Nevertheless, it should to be kept in mind that a first layer of parallelization of the hydrological model already reduces the computational time with respect to a single-processor run and, more importantly, eases the

simultaneous handling of large amounts of data, overcoming the allocation problems typical of shared memory codes. According to Lai et al. (2018), this is a mandatory feature in order to handle big earth data in large scale simulations. While the results for dual-layer implementation will be presented in next Section, it should be noticed that these results constitute a preliminary step for the following analysis, as they allow to define the optimal number of processors to be used as slaves in the dual layer MPI implementation, as using too many slaves might result in a net loss of scalability for most realistic applications.

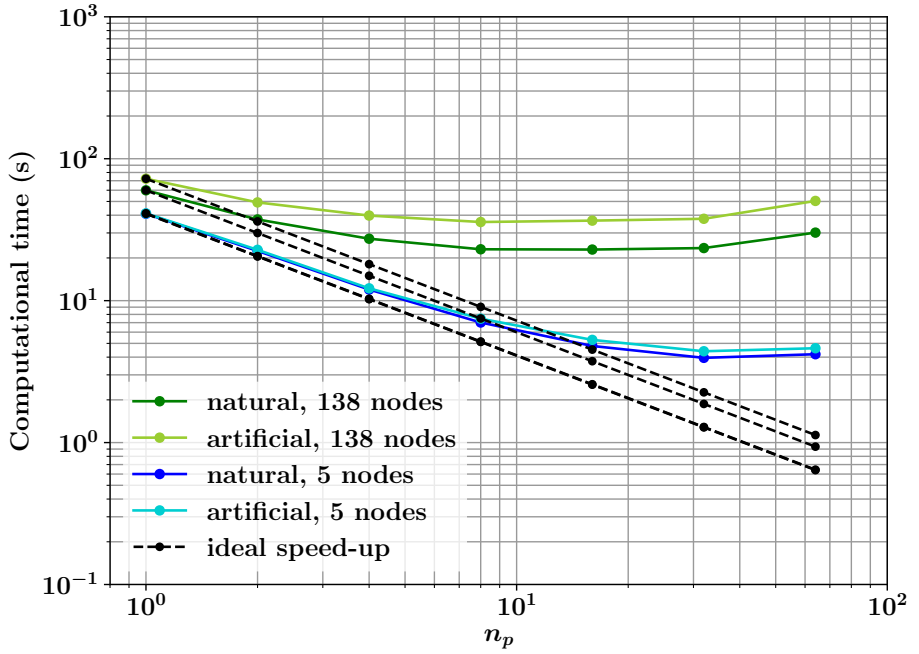

Figure 4.2 *First MPI layer parallel scalability of the hydrological model considering* 5 *and* 138 *network nodes and the presence of artificial structures. Ideal (100%) scalability is represented with dashed lines.*

4.3 Scalability of the dual-layer MPI implementation

As anticipated by the end of the previous Section, optimal results in terms of scalability of a dual-layer parallelization can only be achieved with an appropriate subdivision of the workload between the two layers; in order to achieve the best results from the dual-layer MPI implementation, we explored different configurations between the number of slaves and the number of masters, (for definitions please refer to Section 2.3). These configurations are applied to both LHS and PSO calibration procedures (described in Section 2.2), and range between two opposite situations: the first, where only one master in the first MPI layer and one slave in the second level are used (i.e. $n_p = 1$); and the second, which considers 32 masters (i.e. $n_p = 32$), each associated with a single slave. The first case represents the condition in which the run is performed without parallelization as the master coincides with the slave. Consequently, this can be considered as the benchmark test for speedup measurements. On the opposite, the second case represents a simulation in which only the second MPI layer is active and all the hydrological simulation are run as a serial code. In between these two configurations, different master-slave combinations have been tested, with a number of total processors ranging from 1 to 64 (in particular, n_p = (1,2,4,8,16,32,64), see Figures 4.3 and 4.4).

Similarly to the first layer performance analysis (Sect. 4.2), we consider both the 5 and the 138 nodes configurations, although we limit the analysis to the artificial scenarios in which all hydraulic infrastructures are considered, since the second parallelization layer is not affected by the hydrological model setup. The model's scalability in both cases is depicted in Figures 4.3 and 4.4. For a better visual recognition of the actual improvements introduced by dual-layer MPI strategy, on the x-axis is shown the total number of processor used (computed as the number of masters multiplied by the number of assigned slaves) and contain the speed-up curves drawn for an increasing number of masters (different coloured lines in Figures 4.3 and 4.4).

With reference to Figure 4.3, the computational time considering the LHS sampling scheme and using both 5 and 138 nodes, are displayed. The performance results are indeed satisfactory, with the efficiency of the parallel scheme approaching the ideal speed up line as the number of masters increases. It can also be noted that the configuration adopting a single master achieves a plateau in the speed-up with reference the 5 nodes test and even a negative scalability in the 138 nodes case. This result is a confirmation of the results presented in Figure 4.2, since for this configuration the second MPI layer is deactivated. A similar behavior is also exhibited in the 2 and 4 masters configurations in the 138 nodes setup (Figure 4.3b).

The master-slave configurations that were explored in the case of PSO sampling scheme were the same analyzed for LHS; this time, each configuration was tested on performing 100 Montecarlo realizations adopting 100 particles, for a total of 10000 forward HYPERstreamHS runs. Furthermore, Figure 4.4 shows the scalability performances for 5 and 138 nodes, respectively; it can be seen that with respect to the configuration using a single master (green lines), the configurations with 2 and 4 masters (marked with blue and red lines, respectively), achieve scalability performances progressively closer to the ideal speed-up, which resembles the results achieved by the LHS scheme. However, once the number of masters further increases (purple, blue and gray lines), the performances deteriorate and the scalability diverges from the ideal one.

The differences between the dual-layer parallelization strategy applied to LHS and PSO schemes can be explained by the different nature of the two algorithms: while LHS presents a naturally parallelizable structure, in the case of PSO the masters are forced to communicate multiple times in order to update the best solution at each iteration. It is therefore clear that the number of communication is not fixed, but rather it scales with the number of masters in use. Therefore, a successful exploitation of the dual-layer parallelization strategy using the genetic PSO algorithm can only be achieved seeking the optimal balance between the number of masters to be used in second layer and the number of slaves in the first level should be identified. To this, aim, the

considerations made in Section 4.2 come in handy, showing that the network topology and the number of macrocell-node pairs strongly define the scalability threshold, regardless of the number of available processors. Combining the information derived from the two analyses makes it possible to exploit the ideal master/slaves configuration in the case of PSO calibration. This result is clarified even further by the plots displayed in Figure 4.5. The figure focuses the attention on a 64-processors configuration, applied only to the 138 nodes, artificial case to both PSO and LHS algorithms. The plots display the computational time in the two cases as a function of the number of masters (and consequently of slaves, given the fixed total of 64 processors). In the case of LHS (Figure 4.5a) the total computational time drops rapidly as the number of masters increases from 1 to 32. On the contrary, for PSO (Figure 4.5b) an increasing number of masters (i.e. 32) does not correspond to a decrease in computational time. In particular, the computational time decreases until the number of master increases to 8, and then starts to increase after this number of masters is surpassed, meaning that the time loss due to communication is larger than the time gain due to workload splitting.

To briefly summarize the main findings of this chapter, HYPERstreamHS shows good scalability on single-layer parallelization, which can be furter improved by activating the second parallelization layer. However, while the LHS scheme presents increasingly good performances as the number of masters is increased at the expenses of the slaves, (the only limit being represented by memory allocation issues), PSO cannot exploit as many processors as there are available due to its structure, and instead requires preliminary scalability analyses which are peculiar to the case of study, aimed at the identification of both the optimal number of slaves dealing with the forward runs (i.e. first MPI layer) and of masters handling the inverse modelling procedure (i.e., second MPI layer).

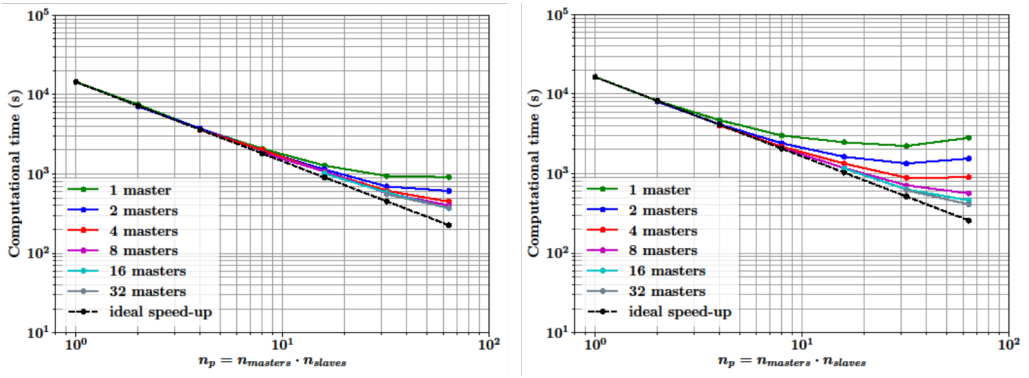

Figure 4.3 *Speed-up test cases for LHS in the case of a) 5 and b) 138 nodes.*

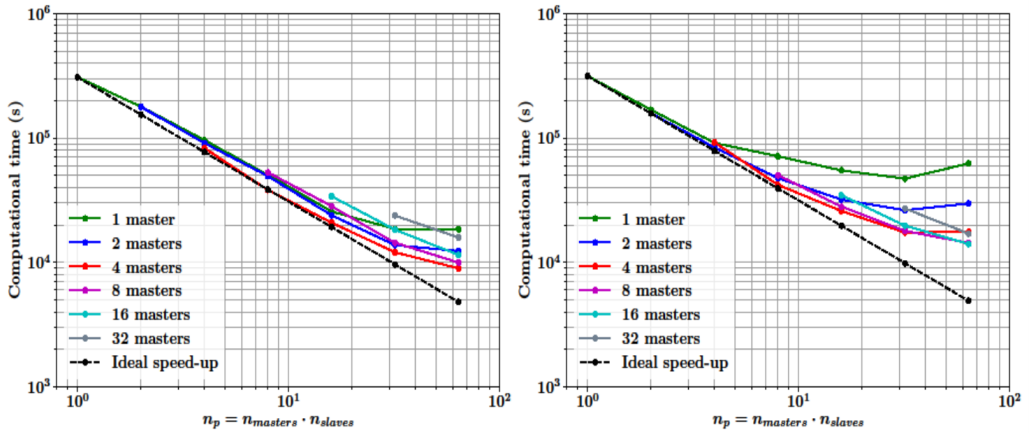

Figure 4.4 *Speed-up test cases for PSO in the case of a) 5 and b) 138 nodes.*

4.4 Conclusions

In this Chapter we presented the development of HYPERstreamHS, a hydrological model that explicitly models alterations due to Human Systems when simulating natural streamflows, and is also able to exploit HPC resources by mean of a dual-layer MPI implementation.

The scalability tests that were performed on both the single-layer and on the dual-layer parallelization schemes highlighted that the hydrological model (forward simulation) has some inherent bottlenecks that limit its scalability, in

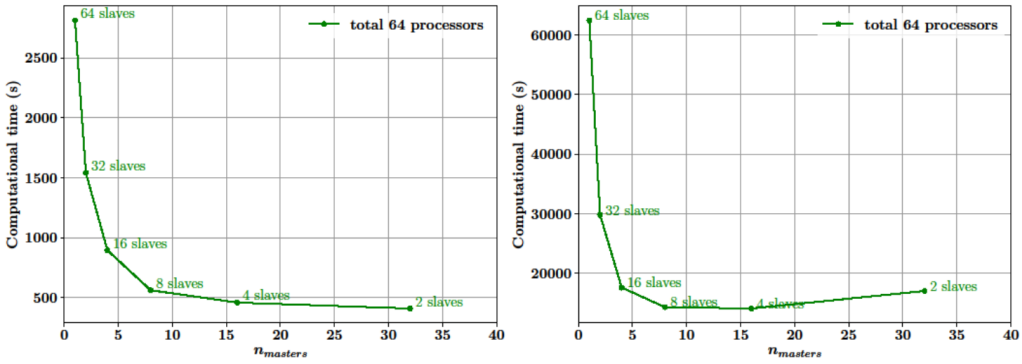

Figure 4.5 *Computational time of the dual-layer system applied to HYPERstreamHS in the LHS scheme (a) and PSO scheme (b) with a fix number of* 64 *processors and different masters and slaves configurations applied to the* 138 *nodes case.*

which case only a small portion of the computational resources can be exploited. Such limitations are circumvented by implementing a second parallelization layer that speeds up calibration procedure and uncertainty analyse, which indeed require the majority of the computational time in hydrological simulations; this allowed to push further the scalability limit of the model, achieving close-to-ideal scalability up to 32 processors, with the appropriate workload subdivision between masters and slaves.

CHAPTER 5

DETAILED SIMULATION OF STORAGE RESERVOIR AND HYDROPOWER PRODUCTION IN A MESOSCALE CATCHMENT

The Adige catchment was used as the first case study to test the performance of the HYPERstreamHS model; a reservoir-specific hydropower production schedule was developed and tested for consistency prior to its application to the entire catchment. This Chapter will present the results in terms of hydrological and hydropower production modelling, as well as a robustness analysis that was conducted in order to assess the influence of detailed input information on both modelled hydrology and hydropower production.

This Chapter is based on:
Galletti, A., Avesani, D., Bellin, A., Majone, B. Detailed simulation of storage hydropower systems in a large Alpine watershed, in preparation for Water Resources Research

5.1 Model calibration and setup

In this study, HYPERstreamHS was applied on the Adige river basin in order to test the capabilities of our modelling framework in terms of hydrological and hydropower production modelling. In fact, hydrological modelling of this catchment is challenged by its widely variable topography and by the presence of numerous hydropower systems which affect the natural water cycle. Furthermore, we would like to provide a complete benchmarking of the framework developed and explained in Section 2.1.2 by also validating the hydropower production model. For specifications on the case of study, its conceptual model and on the input data set please refer to Section 3.4.

The model was calibrated using the PSO algorithm adopting a 2-masters, 8-slaves configuration of the parallel scheme. NSE was chosen as the objective function for the calibration algorithm, in order to achieve an optimal solution while preserving a good correlation between observed and simulated streamflows. The choice of the calibration nodes was different from the one adopted in the previous Chapter, and was mainly led by two considerations: firstly, the adoption of the outlet node as model calibration site in large catchments often leads to large errors in the upstream sub-catchments, because the calibration fails to capture the spatial variability of model's parameters and instead suffers the disturbing effect of streamflow alterations due to water usages (Bombelli et al., 2019). Secondly, a multisite calibration of the model is suggested by Zhang et al. (2008) in order to increase the spatial reliability of the calibrated parameters. Since most hydropower plants are located at intermediate elevations, accurate modeling of streamflow in the higher sub-catchments is crucial. The aforementioned recommendations resulted in the choice of three gauging stations at the outlet of undisturbed mountainous sub-catchments as calibration nodes: the Aurino station, the Gadera station and the Vermiglio station (see Figure 3.8). A multi-site calibration was performed in the time window 1989-2013 where the first two years were used as spin-off (i.e., they are not accounted for when computing the objective function), adopting the average NSE among the three gauging stations as the objective function for the PSO algorithm. During

the calibration, artificial water diversions have been turned off in order to focus on natural flows.

It is worth noticing that our chosen calibration procedure does not represent an absolute best, but rather our preference to improve some aspects of the model, potentially sacrificing its performances elsewhere. For instance, the choice of upstream sections as calibration nodes ensures a better reproduction of upstream hydrology, but cannot ensure that hydrology is properly reproduced downstream, due to the disturbing effect of hydropower systems and to different hydraulic soil properties. Furthermore, the NSE objective function tends to avoid high errors, hence reproducing better high peaks, rather than low flows, as opposed, for instance, to KGE which focuses more on mid-to-low flows. This translates into the fact that our model will be more likely to reproduce high flows with little bias, and also that it won't achieve absolute accuracy in reproducing lower flows.

5.2 Hydrological and Hydropower production modelling performances

The hydrological performance of the model was measured by computing the NSE index for 5 gauging stations not used in the calibration, along with those that were used to calibrate the model. The two downstream gauging stations of Bronzolo (catchment area: 7400 km^2) and Trento (9000 km^2) were taken as benchmark to evaluate the overall performance of the model. The position of these two gauging stations within the Adige catchment is shown in Figure 3.8, while the corresponding simulated and observed streamflows are shown in Figures 5.1 (Bronzolo) and 5.2 (Trento). The resulting NSE values ranged between 0.49 and 0.81, which according to Moriasi et al. (2007) can be considered a satisfactory result (NSE>0.5); as it can be observed in Table 5.1, the introduction of human systems' effects in the model improved the NSE at the gauging stations of Trento and Bronzolo, highlighting the fact that the introduction of the hydraulic infrastructures adds relevant information to

Table 5.1 *NSE values obtained in calibration and validation. The introduction of human systems in the simulation improved the NSE at downstream nodes (Trento and Bronzolo), showing that positive information was introduced in the model*

STATION	$NSE_{cal,nat}$	$NSE_{val,nat}$	$NSE_{val,art}$
Isarco		0.49	0.49
Aurino	0.59	0.59	0.59
Anterselva		0.59	0.59
Gadera	0.71	0.71	0.71
Rio Funes		0.59	0.59
Vermiglio	0.60	0.60	0.60
Bronzolo		0.79	0.81
Trento		0.73	0.75

the model, though the improvement is somewhat limited. Furthermore, this result is in agreement with the findings from Dang et al. (2020), where the introduction of reservoir simulation improved the performance of the hydrological model (also measured in terms of NSE). All things considered, the results are encouraging, given that the introduction of the hydraulic infrastructures was finalized to obtain a reliable model for hydropower production, not to improve the hydrological model.

The hydropower production model was validated against hydropower production time series for the Trento and Bolzano provinces; data were compared over the 2000-2013 time window, where both modelled and observed data were available. The comparison was performed at the catchment scale, adopting the procedure described in Section 3 to obtain consistent datasets. Figure 5 shows the comparison between modelled and observed hydropower production, at a monthly time scale, for the entire Adige catchment. The mean annual production for each hydropower plant was also compared with the value declared by the owners. The mean modelled annual production in the Adige catchment differed by only -4.7% from the observations (6469 GWh/y against 6786 GWh/y), with the computed production of run-of-the-river systems differing from the amount declared by the producer by +4% (3285 GWh/y against 3164 GWh/y)

and reservoir hydropower by -8% (3184 GWh/y against 3466 GWh/y). The results showed a good performance of our modelling framework in terms of hydropower production modelling; the framework itself can be considered an improvement with respect to most studies related to hydropower production, that limit themselves to confronting model output against baseline scenarios, without seeking validation against observed data.

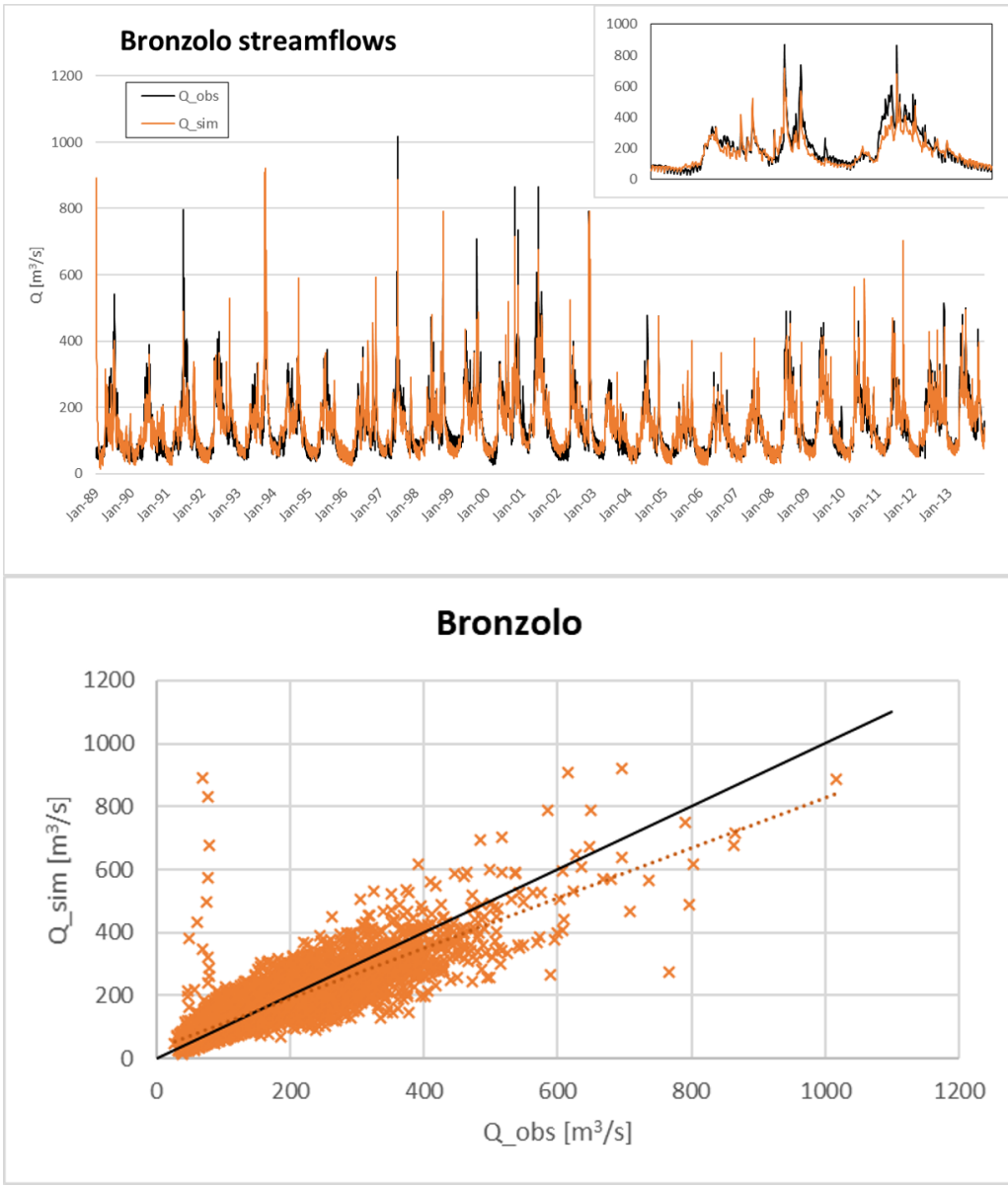

Figure 5.1 *Observed and simulated streamflows at the Bronzolo gauging station; the inset shows the streamflows for years 2002-2004. The continuous line in the scatterplot marks the 1:1 correspondence, while the dashed line represent the set trend.*

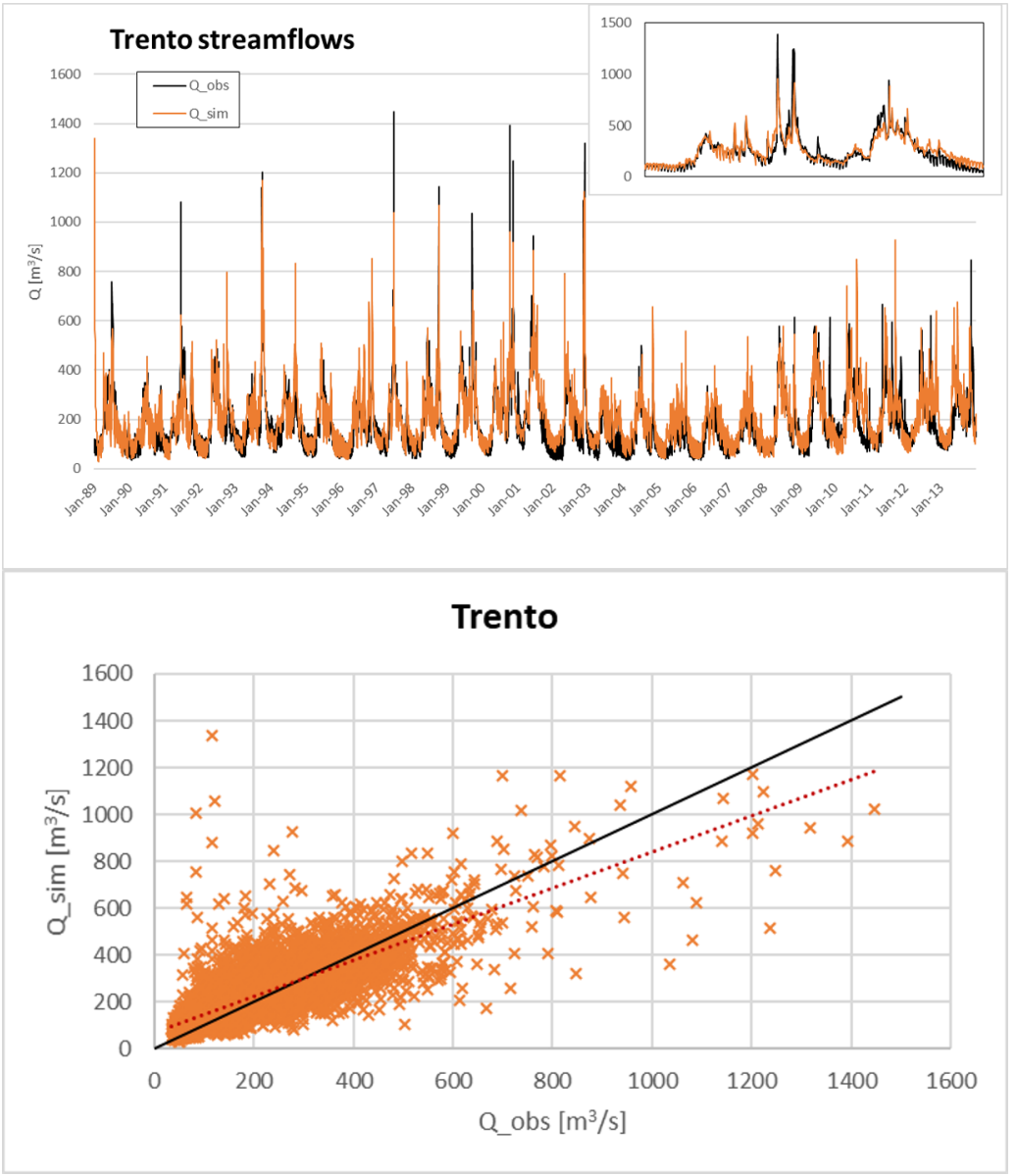

Figure 5.2 *Observed and simulated streamflows at the Trento gauging station; the inset shows the streamflows for years 2002-2004. The continuous line in the scatterplot marks the 1:1 correspondence, while the dashed line represent the set trend.*

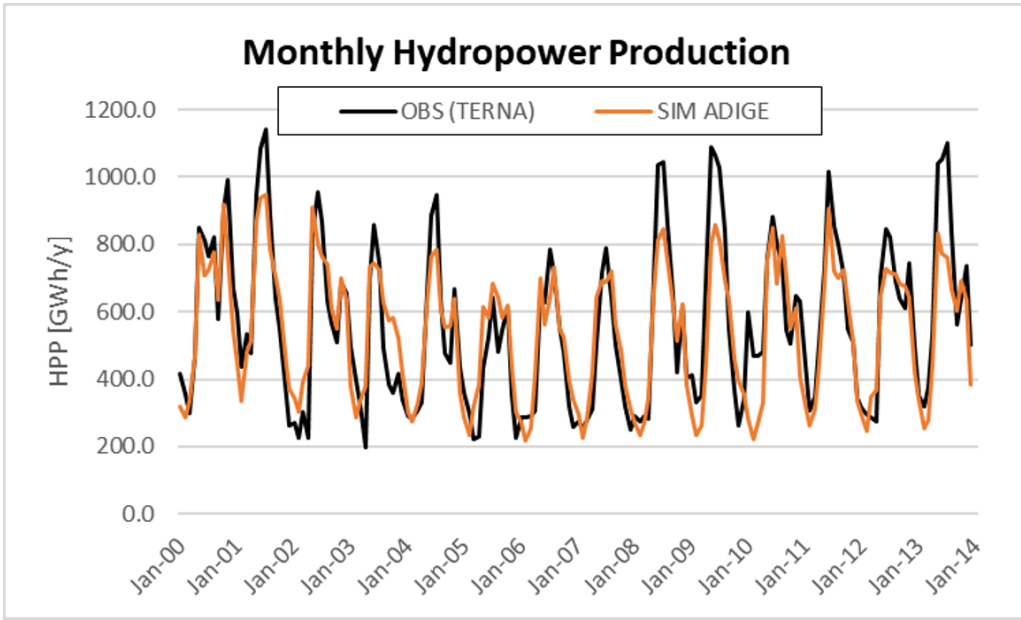

Figure 5.3 *Aggregate monthly hydropower production over the Adige catchment.*

5.3 Effects of the deterioration of the input information

It is well known that anthropogenic interventions cause profound alteration of numerous physical and hydrological processes in the affected reaches (Nazemi and Wheater, 2015a,b). The activity of hydraulic infrastructures such as dams and diversion channels, for instance, alters streamflows in terms of both timing and magnitude. Furthermore, a proper representation of hydropower systems is crucial when developing hydropower production predictive tools. In this section, we investigated to what extent an unrealistically simplified modelling of human system might affect model performances. Firstly, we investigated the incidence on hydropower production of simplifications in hydropower system geometry, neglecting intermediate water intakes where it was possible, reducing each system to a dam-plant one. Secondly, we replaced our hydropower production schedule with a simpler one that finds frequent application in literature, where water is always turbined at the maximum plant capacity: we compared effects on hydropower production and on macroscopic reservoir dynamics (i.e. stored volume time series) between this approach and ours. Finally, we maintained the aforementioned hydropower production schedule, and assumed a biased knowledge of the plant capacity, in order to assess its effects on hydropower production, putting it in relationship with other reservoir characteristics by means of a clustering analysis.

5.3.1 Effect of flaws in artificial network geometry

Many works usually refer to the World Register of Dams (https://www.icold-cigb.org), to the USACE register (nid.usace.army.mil) or to other national or continental dam registers to gather geometry information on hydropower reservoirs (see for instance Boehlert et al. (2016); Turner et al. (2017); Zhao et al. (2016)). Other works assume that a direct link exists between the intake located in the reservoir and the hydropower plant (see Ali et al., 2018; Bosona and Gebresenbet, 2010). However, it should be noted that the aforementioned global

dam datasets rarely contain detailed information on penstock capacity or on additional intakes that might be present between the dam and the hydropower plant; in fact, these registers provide information on reservoir geometry, storage volume, dam height and spillway capacity, as well as information on the downstream plant mean annual production: therefore, the maximum discharge capacity of the hydropower system could in principle be computed backwards, but this value together with any additional downstream characteristics of each system remain substantially uncertain. Information on maximum turbine capacity can sometimes be provided by the Global Energy Observatory database (http://globalenergyobservatory.org), however information coverage varies significantly across the world (e.g., for Italy only 5 hydropower plants are listed, while at least 260 large hydropower plants exist in Northern Italy), and information for each dam is not certified, nor necessarily exhaustive. Despite being possibly correct in some cases, making the assumption that no other contributions to hydropower production exist between reservoir and hydropower plant, hence relying solely on reservoir management models to reproduce hydropower production leads to incorrect estimations when more complex geometries are involved. In our case study, five reservoir hydropower systems (out of 22 total) had intermediate water intakes between the reservoir and the hydropower plant. To test their significance, we simplified these systems excluding any intermediate water intake, considering discharge from the reservoir as the only contribution to the hydropower plant. Results obtained under this hypothesis are shown in Table 5.2.

As it can be seen from Table 5.2, neglecting intermediate water intakes basically leads to neglecting effectively contributing drainage area: a rather obvious direct relationship exists between the reduction of the drainage area contributing to a specific hydropower plant, and the reduction in hydropower production: this caused underestimations up to 48% in the case of the Sarentino power plant. It is therefore clear that the best possible level of detail needs to be sought when implementing complex hydropower systems, as simplifications in system geometry showed direct consequences on the model's predictive

Table 5.2 *Incidence of the reduction of catchment area due to the use of simplified geometry in terms of mean annual production, investigated in five catchments with complex geometry.*

Power Plant	Area $[km^2]$	Area reduction [%]	Baseline HPP [GWh/y]	HPP variation [%]
Cogolo	88.0	22	116	17
Glorenza	217.9	34	291	18
Naturno	124.1	40	335	32
Sarentino	180.6	46	63	48
Santa Valpurga	23.5	35	52	46

capabilities.

5.3.2 Simplified reservoir operation scheme

Hydropower reservoir operating rules often represent a difficult step in hydropower production modelling, as they are kept secret by the dam operating companies. A simplification that can be commonly found in literature is to assume that the reservoir always turbines water at its maximum capacity (see Ng et al. (2017) as well as the already cited works from Turner et al. (2017); Wagner et al. (2016)); this means that monthly variability, according to the overall hydropower production, is no longer imposed to the single hydropower system, which operates at its maximum capacity under the constraint that storage cannot be smaller than the minimum storage. When the minimum storage is reached production is disactivated until the storage recovers to a value that allows to operate again the system at its maximum capacity. Although this kind of simplification might still perform well in terms of long term water balance, it might lead to biased predictions of the timing of the releases downstream of the power plants, as well as to wrong estimation of hydropower production, if the system constraints are based on wrong or missing information (as stated in the previous section, outlet capacity is not always available in global dams registers).The expected result in this approach was that discrepancies between the mean inflow in the reservoir and the enforced release scheme would have led to a loss of geodetic jump if the discharge was higher than the average

inflow, or to water spilling if it was lower. In either case, we expected a reduction of hydropower production either due to geodetic head loss or to lower total turbined water volume. As it can be seen from the example plot in Figure 5.4, reservoir Gioveretto behave very differently with an operation scheme set at a constant discharge equal to its maximum outlet capacity, as opposed to the so-denominated TERNA rule (the one adopted in this work), which is inferred accounting for flow seasonality and reservoir specifics: in fact, the reservoir suffered a significant reduction of the average water stage, due to the fact that the operation scheme does not follow neither the seasonality of the inflows nor their amount. Always turbining at maximum systems capacity leads to similar turbined volumes between the two approaches, the only difference being in the spilled volumes, which are often negligible in common operations and obviously even lower when turbining at maximum capacity. This notwithstanding, the loss in reservoir geodetic head caused by continued production at maximum capacity results in a loss of hydropower production. As we expected, this approach caused some losses in hydropower production, resulting in a decrease of modelled hydropower production: while our approach achieved a -4.7% error with respect to historical observations, this approach showed a worse performance , achieving a -9.8% discrepancy (reservoir hydropower lost around 5.6% of their modelled production, as recalled in Table 5.3). Another aspect that should be kept in mind is the fact that, despite potentially being able to guess the long-time estimates for hydropower production with low bias, this kind of approach misses completely the timing of hydropower production. Although not being relevant in many hydropower production studies, timing of discharges plays a key role in assessing the impacts of hydropeaking on the downstream biota (Kiesel et al., 2019; Poff et al., 2015), and efforts should be devoted to this aim, in order to have a more complete understanding of the impacts of hydropower systems on a river catchment.

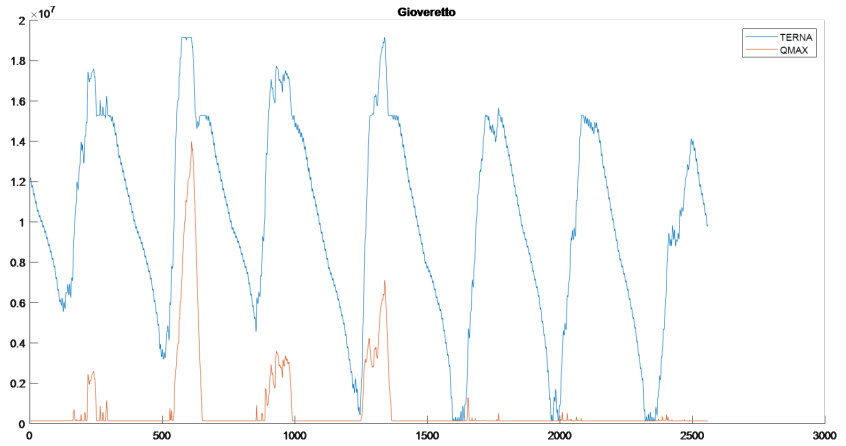

Figure 5.4 *Stored volume time series for the Gioveretto reservoir over the 2000-2006 period. The QMAX discharge scheme causes a decrease in the average water stage inside the reservoir, as opposed to the TERNA scheme which accounts for expected inflow and seasonality.*

5.3.3 Incorrect assumptions or missing knowledge on turbined flows

Secondly, we further investigated the Q_{MAX} approach detailed in the previous Section, by testing the effects of incorrect estimation of the turbined flows; in fact, most hydropower plants can operate each turbine independently, according to the available water inflow. Since the maximum system capacity refers to all the turbines being operated simultaneously, assuming that a constant flow is always turbined in a plant might incur in both overestimation and underestimation bias. For this reason, the (constant) turbined flow value enforced to each reservoir was modified by [-80%, -50%, +50%]: these values were arbitrary, and were aimed at investigating the effects of both overestimation and underestimation of the turbined flows. The expected results were the same as in the previous approach (i.e., a reduced hydropower production either due to head loss or to lower turbined water volume), but this time quantitatively emphasizing impacts of overestimation and underestimation of the constant flow to be turbined. The effects on modelled hydropower production at the

Table 5.3 *Variation in mean annual hydropower production achieved in different scenarios: the reference scenario is represented by our simulation (reservoir release scheme detailed in Section 2.1.2.5), and it is compared with the production obtained adopting a constant reservoir operation scheme equal to system capacity (i.e., Q_{MAX}) modulated by a constant parameter (detailed in Section 5.3.2 and 5.3.3). The variation is computed both in terms of overall hydropower production over the whole catchment and restricted to the subset of reservoir hydropower systems.*

	$0.2Q_{MAX}$	$0.5Q_{MAX}$	Q_{MAX}	$1.5Q_{MAX}$
Overall HPP	−22.7%	−6.7%	−3.1%	−2.5%
Reservoir HPP	−44.4%	−13.4%	−5.6%	−3.9%

catchment scale are synthesized in Table 5.3: the results confirmed our expectations and in fact a decrease in hydropower production was observed in all four cases. Furthermore, our results suggests that underestimating the turbined flows implies severe underestimation of hydropower production compared to turbined flow overestimations, which only affect hydropower production marginally.

A k-means clustering analysis (described in Section 3.5) was performed on the sample constituted by all 30 reservoir hydropower systems operated with the constant turbined flows equal to 0.2, 0.5, 1 and 1.5 times the outlet capacity (120 points total). The analysis compared normalized indicators for geodetic head incidence (H, defined in Equation 3.2), variation in hydropower production (HPP, defined in Equation 3.3), and ratio between average turbined flow and average inflow to the reservoir (Q, defined in Equation 3.4). The results are summarized in Figure 5.5.

The three clusters resulting from the analysis represent three typical situations. The first cluster (blue) gathers those cases in which the discharge requested by the reservoir operation rule is roughly equal to the average inflow to the reservoir (Q=1), or in which the reservoir head has limited incidence on the hydraulic jump of the system (H«20%): in both cases, losses in hydropower production are very limited (average HPP for this cluster = -3.22%). The sec-

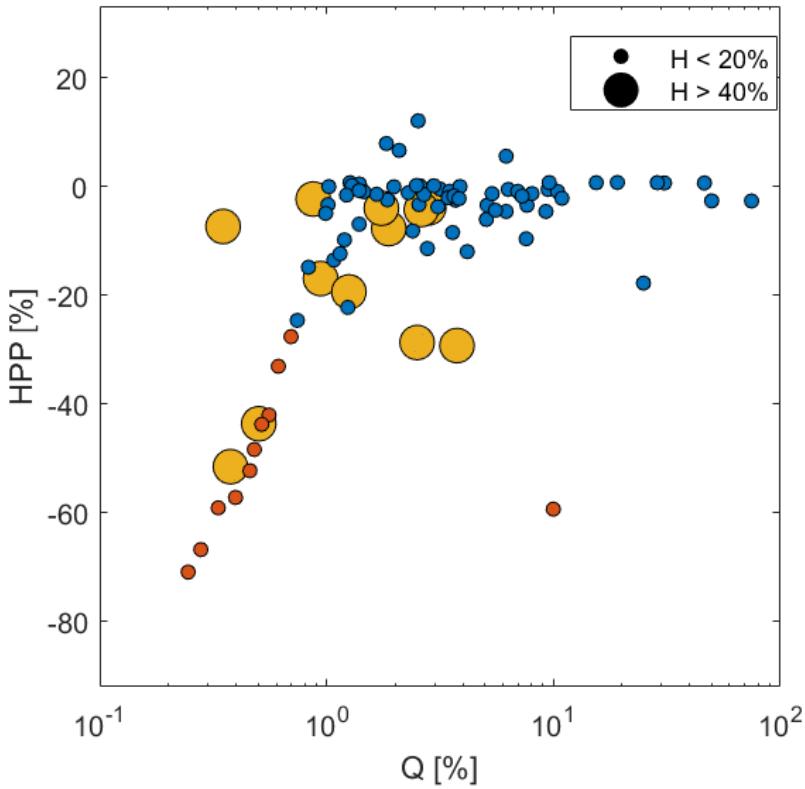

Figure 5.5 *Clustering analysis between normalized indicators of reservoir head, discharge and hydropower production: when the turbined flow is higher than the inflow and the reservoir head has significant incidence on the overall system head, minor losses in hydropower production can be expected (yellow cluster). When the turbined flow is lower than the average inflow, major losses can be expected (red cluster). The other cases include turbined flow slightly higher than average inflow and/or small incidence of the reservoir head compared to system head: in both cases, losses are negligible (blue cluster).*

ond cluster (yellow) only comprises reservoirs in which the reservoir head has considerable incidence on the hydraulic jump of the system (H > 40%, this can be visually noticed from the size of the markers): in this cluster, as soon as Q gets greater than 1, the reservoir faces losses in average head as it is forced to operate at its minimum level, resulting in significant HPP loss (average HPP = -18.23%). Finally, a third cluster gathers the majority of the situations in which

Q < 1, meaning that the requested discharge to be turbined is lower than the available inflow: in this way, a lower volume of water is used for hydropower overall, resulting in serious losses in terms of HPP (average HPP = -50.91%).

It can also be noticed that some outliers are present in Figure 5.5, being them the cases resulting in an increased hydropower production (HPP > 0) despite the simplification of the reservoir operation rules. This behavior can be explained splitting the outliers into two opposite categories: the reservoirs exploiting Q>1 to increase their production, and those achieving increases in hydropower production while Q<1 (in fact, the highest hydropower production should be obtained when Q=1, in which case the system is able to turbine all the incoming flow at optimal head). In the first category, the reservoir operation scheme that was applied to the reservoir during the reference simulation prescribed a turbined flow lower than the average inflow: therefore, the reservoir is operating 'often full', spilling water many times; as a result, when a higher discharge is enforced, the reservoir is still able to meet the demand and to achieve a higher hydropower production. On the other hand, and for opposite reasons, there are reservoirs that operate 'often empty', working at their minimum stage: in these cases, when a lower discharge is enforced, the reservoir is able to raise its average stage while turbining the same water volume overall (limited by inflow), hence increasing its hydropower production.

5.4 Conclusions

The analyses presented in this Chapter highlighted the positive performance of HYPERstreamHS, both in terms of hydrological and hydropower production modelling, finding that the explicit representation of Human System improves the performance of the hydrological model, and validating modelled hydropower production at the catchment scale against monthly observations, achieving satisfactory results. Further tests tried to deteriorate the input information to the model, following some assumptions or simplified approaches that are commonly made when dealing with reservoir operation modelling. The

analyses showed that such assumptions are mostly prone to errors, in particular if further uses of the model's results are planned like e.g. ecological impact assessment studies.

A detailed implementation of Human Systems should be therefore sought after in order to guarantee reliable estimations of streamflow alterations and hydropower production.

CHAPTER 6

PERSPECTIVE WORK

In this final chapter, the HYPERstreamHS model was applied to five large catchments in the Western Italian Alps. The aim of this section is to validate the hydropower production model using the COSMO dataset as meteorological input, as a first step towards the application of the HYPERstreamHS framework over the Italian Alpine Region.

6.1 Model setup

In this Chapter a second application of the HYPERstreamhS framework will be presented. This simulation had the main objective of validating the modelling framework on a second study area (as explained in Section 3.3, complete characterization of HS nodes is inherently time consuming, therefore new catchments can be tested only as soon their implementation is complete). This contributes to the overall goal of our activity, which is the application of HYPERstreamHS on the Italian Alpine Region.

As anticipated in Section 3.4, this analysis will focus on five catchments located in the Western Alps: namely, the Dora Baltea, Orco, Stura di Lanzo, Dora Riparia and Pellice river catchments. Since the hydrologic regime of Dora Baltea differs rather strongly from that of the other four catchments, and given the noticeable discrepancies in the morphology of the upper and lower sides of this study area, we decided to split this domain in two parts, as it was already illustrated in Section 3.4, in order to improve the spatial reliability of the parameters of the hydrological model (explained in Section 2.1.1.4). This resulted in performing two different calibrations of the model as well as the corresponding forward simulation, so that each set could be simulated with the appropriate hydrological parameters. The two resulting sub-domains and their conceptual models are described in detail in Section 3.4. The simulations were performed on the 1995-2008 time window, at a hourly time step. As anticipated, the COSMO dataset was used as meteorological input forcing (see Section 3.2). The same configuration of the parallelization scheme adopted in the previous Chapter was used (i.e. 2-masters, 8 slaves for a total of 16 processors used), to minimize calibration time; likewise, the PSO algorithm aimed at maximizing the NSE index at the calibration nodes was adopted for both calibrations.

The calibration was performed over the 1995-2008 time window, adopting the PSO algorithm with a NSE averaged between calibration sites as its objective functions, following the same logic explained in Section 5.1; we selected stream gauging stations located at the end of undisturbed (i.e. by hydropower

activities) mountainous sub-catchments as calibration nodes. Two nodes were chosen for the calibration of the hydrological model in each sub-domain, to ensure spatial reliability of the resulting parametrizations (Zhang et al., 2008): after investigating the available streamflow observations and the degree of completeness of each time serie, we chose the stream gauging stations at Gressoney and Cogne for the calibration of the hydrological model in the Dora Baltea catchment (node location shown in Figure 6.1), and those located at Beulard and Germagnano for calibrating the hydrological model in the second sub-domain (node location shown in Figure 6.2). Finally, NSE index at several down-stream stations was computed to assess the hydrological performance of the model. The gauging stations that were used for validation were Tavagnasco (Dora Baltea, Figure 6.1), and S.Benigno (Orco), Torino (one gauging station for Dora Riparia and one for Sturadi Lanzo) and Villafranca (Pellice), all four shown in Figure 6.2. The following Sections will illustrate the results on each one of the two sub-domains separately, for sake of clarity.

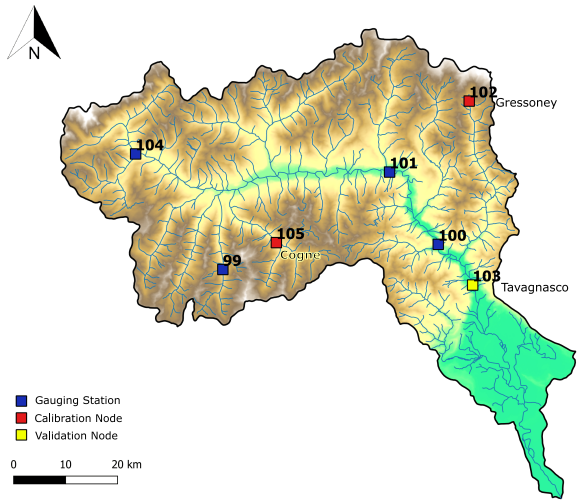

Figure 6.1 *Location of the relevant stream gauging stations in the Dora Baltea catchment, including those adopted as calibration (red) and validation nodes (yellow).*

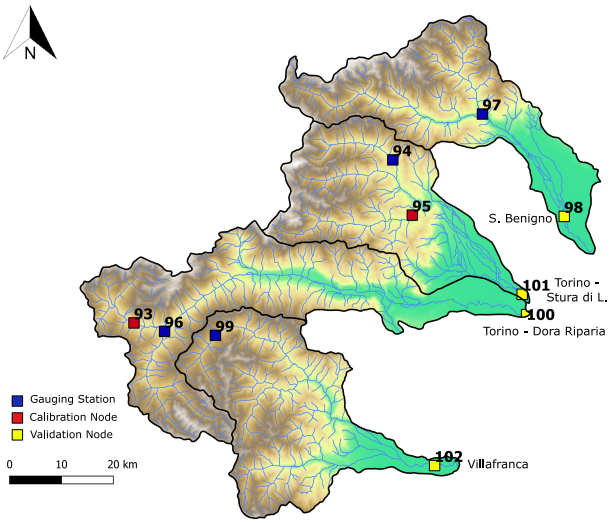

Figure 6.2 *Location of the relevant stream gauging stations in the Orco, Stura di Lanzo, Dora Riparia and Pellice catchments, including those adopted as calibration (red) and validation nodes (yellow).*

6.2 Dora Baltea catchment

The hydrological performance of HYPERstreamHS in the Dora Baltea catchment was measured evaluating the NSE values computed at the Tavagnasco station. The NSE index achieved by the simulations was 0.408: according to Moriasi et al. (2007), a threshold for good performance in hydrological applications can be set at NSE = 0.5, thus making the hydrological performance almost satisfactory. The NSE achieved during calibration and validation are summarised in Table 6.1.

A comparison between observed and simulated streamflows is shown in Figure 6.3: as it can be seen, streamflows are often overestimated. This result is possibly due to having calibrated the hydrological model parameters in upstream nodes of the catchment, which most likely have different hydrological properties compared to those found at the Tavagnasco section.

Hydropower production was validated at the aggregate catchment and monthly scale, following the procedure described in 3.3, and the result is vi-

Table 6.1 *NSE values obtained during multisite calibration and during validation in the Dora Baltea catchment. Numeric indexes refer to nodes depicted in Figure 6.1.*

efficiency	NSE_{cal} multisite$_{102,105}$	NSE_{val} N_{103}
NSE	0.615	0.408

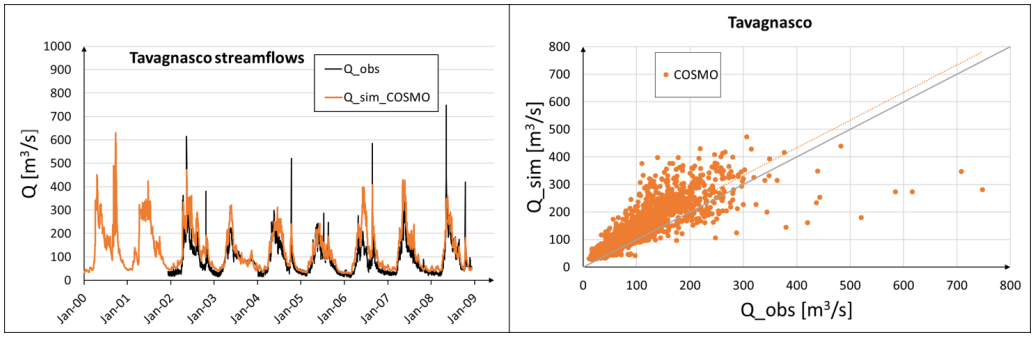

Figure 6.3 *Observed and simulated streamflows at the Tavagnasco gauging station. The continuous line in the scatterplot marks the 1:1 correspondence, while the dashed line represents the set trend.*

sually displayed in Figure 6.4. While the observed mean annual hydropower production is 2886 GWh, the predicted value was 3768 GWh which overestimates the observed value by 30.6%. This result could also be foreseen, given that this model calibration tends to overestimate streamflows and given that few reservoir systems are present in this catchment, hence allowing for little regulation of the incoming flows, that are therefore turbined whenever available. From a visual inspection of Figure 6.4 it can be noticed that overestimation of hydropower production is recurrent, with an exception in the months from January to May every year, suggesting that the excessive flows might possibly be due to flawed estimation of snow melting.

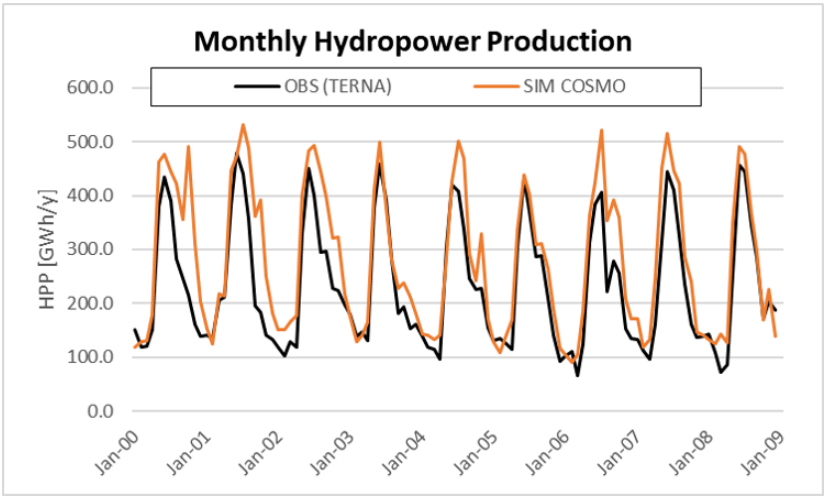

Figure 6.4 *Aggregate monthly hydropower production over the Dora Baltea catchment.*

6.3 Orco, Stura di Lanzo, Dora Riparia and Pellice catchments

The resulting NSE values computed at the S. Benigno, Torino and Villafranca gauging stations, obtained from the simulations are summarized in Table 6.2.

Table 6.2 *NSE values computed at the S. Benigno, Torino and Villafranca gauging stations. Numeric indexes refer to nodes depicted in Figure 6.2.*

efficiency	NSE_{cal}	NSE_{val}			
	$\text{multisite}_{93,95}$	N_{98}	N_{100}	N_{101}	N_{102}
NSE	0.601	0.591	0.245	0.159	0.001

Multisite calibration of the hydrological model yielded satisfactory performance, ensuring spatial reliability of the hydrological paramenters (NSE>0.6); streamflows computed at the two calibration nodes are displayed in Figure 6.5. However, once we consider validation performance, only node 98 (S. Benigno station) exhibits a satisfactory behavior, node 100 has a mediocre performance, while the performance in nodes 101 and 102 is clearly not satisfactory. It should be noted, however, that all validation nodes are located downstream, and that

their streamflow signals are disturbed by the presence of water diversions or restitutions related to hydropower; therefore, the biased prediction of streamflows might be due to poor representation of Human Systems. Indeed, our approach is general and might not suit perfectly every hydropower system. As opposed to the relatively good results achieved during calibration, an analysis of the plots shown in Figure 6.6 shows that the model tends to largely overestimate low flows and to underestimate high flows, amplifying a behavior that was already visible at the calibration nodes. A preliminary calibration test conducted adopting the four downstream stations (nodes 98, 100, 101 and 102) as calibration nodes showed that good NSE indexes can be achieved in these stations, exhibiting NSE values always larger than 0.6 both in single-site and multi-site calibration. However, as we expected, this kind of calibration largely underestimated upstream flows, dramatically reducing modelled hydropower production, achieving a variation of -65% with respect to observed hydropower. For this reason, we eventually maintained the upstream-nodes calibration in order to improve the representation of hydropower production.

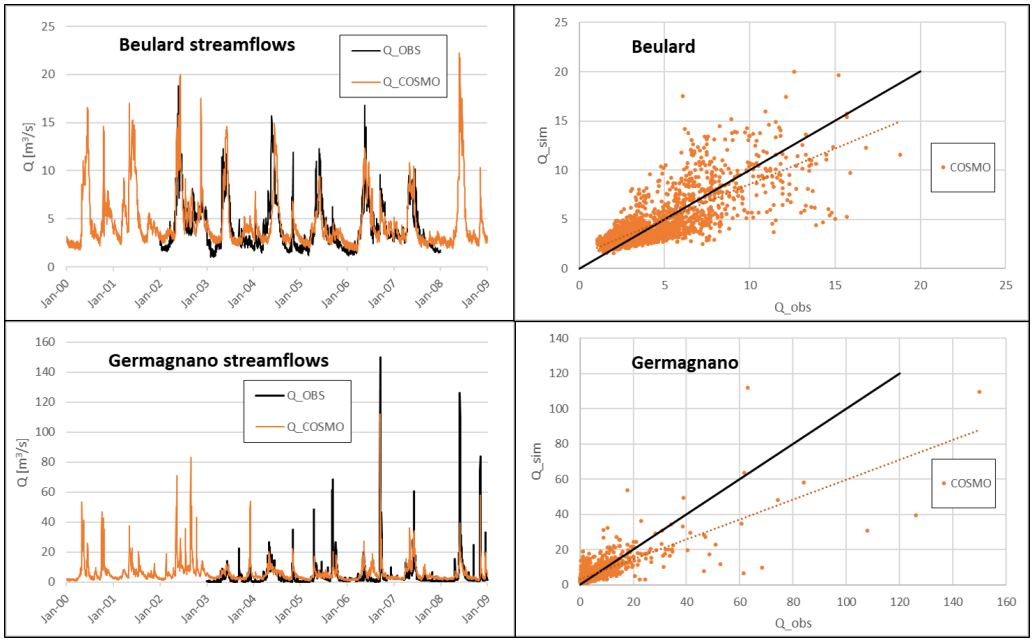

Figure 6.5 *Observed and simulated streamflows at the calibration nodes of Germagnano and Beulard gauging stations. The continuous line in the scatterplot marks the 1:1 correspondence, while the dashed line represents the set trend.*

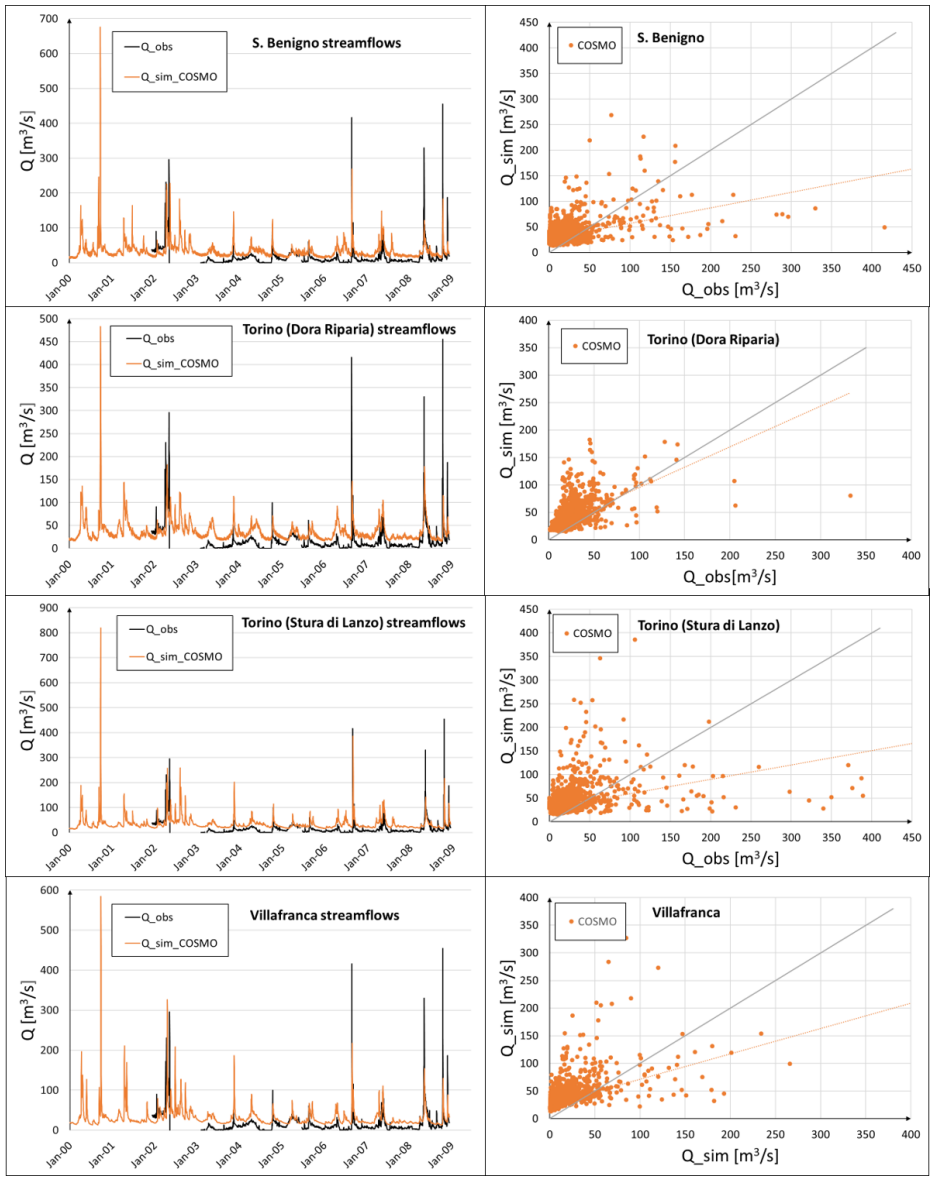

Figure 6.6 *Observed and simulated streamflows at the validation nodes of S. Benigno, Torino and Villafranca gauging stations. The continuous line in the scatterplots marks the 1:1 correspondence, while the dashed lines represent the set trend.*

Hydropower production was validated aggregating data from the four catchments and at the monthly scale, following the procedure described in 3.3: the result is displayed in Figure 6.7. While the observed mean annual hydropower production is 1610 GWh, the predicted value was 1646 GWh (+2.3%). From a visual inspection of Figure 6.7 we can see a general agreement between the observations and the hydropower production, with the exception of few low-peak months. It is worth pointing out that the observations themeselves exhibit very little regularity: this is due to the fact that most of the upstream water bodies in this area are mountain creeks which rather often face droughts or floods. In these situations, multiple choices can be taken by plant operators, depending on the physical condition of the streams: such complex decision making can hardly be framed analitically, therefore in cases like this we might have to accept some loss of accuracy.

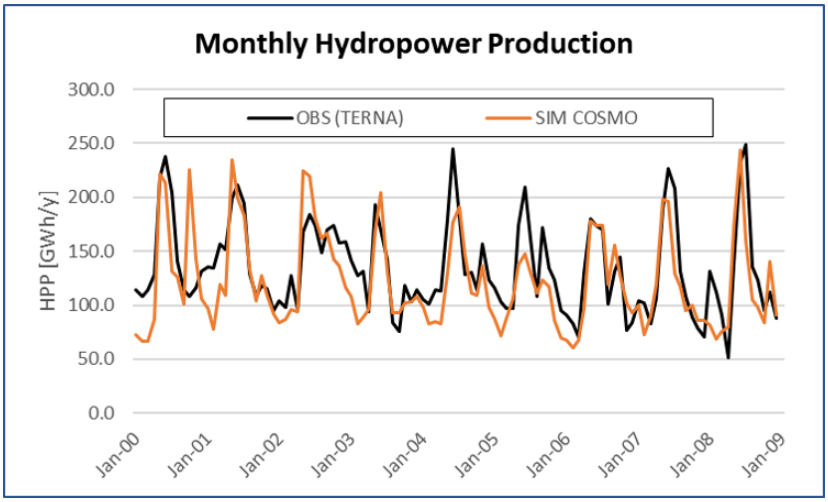

Figure 6.7 *Aggregate monthly hydropower production over the four catchments under analysis.*

6.4 Conclusions

In this Chapter we applied HYPERstreamHS on five catchments in the Western Alps with the objective of validating the modelling framework in terms of hydrological- and hydropower production modelling. A multi-site calibration

of the hydrological model was performed in the two domains of study, calibrating the model in upstream, undisturbed catchments, achieving satisfactory results (multisite NSE > 0.5 in all cases). However, three validation nodes located downstream of the corresponding sub-catchments did not achieve satisfactory performance, suggesting that the alterations to the natural streamflow due to hydropower weren't modelled properly due to the difficulty of collecting detailed system-specific information. Hydropower production was compared with historical observations on the two sub-domains, achieving an error of +30% in the Dora Baltea catchment and a discrepancy of +2.3% in the second sub-domain, with respect to the observed mean annual production; as it could be expected, some flaws in streamflow modelling also affected the timing of hydropower production modelling.

This Chapter presented the first application of the HYPERstreamHS framework in the perspective of completing its modelling setup over the entire Italian Alpine Region. As soon as more catchments will be fully characterized in terms of hydropower systems, this same framework will be applied to them. Once the model setup will be complete, it will serve as stepping stone for several scenario analyses.

CHAPTER 7

CONCLUSIONS

This Chapter draws conclusions on the present work, and offers some perspective on its future developments, either planned or potential.

7.1 Concluding remarks and perspective work

This work revolved around the development and implementation of a suitable modelling framework to perform analyses at multiple scales, and at a high temporal resolution, explicitly simulating hydropower systems in order to be able to model hydropower production together with the hydrological cycle, with the ultimate goal of applying the framework to the Italian Alpine Region.

The task presented multiple challenges: first of all, most hydrological models include steps that must be executed serially: this hinders the models' ability to fully exploit the available computational resources, as well as requiring the simultaneous allocation of large segments of memory; therefore, complex hydrological simulations represent a computationally intensive task. The second challenge is represented by how the interactions between the natural hydrological system and anthropogenic water uses are modelled: indeed, most times a trade-off exists between the level of detail embedded in such models and the extension of the domain on which such approach is applied, due to the bottleneck created by limited or even secret information concerning these uses. Thirdly, we found that few studies on hydropower production devote their attention on the validation of the model, focusing their analyses on different scenarios compared to a (synthetic) one. This problem is, in all likelihood, due to similar reasons i.e. to the very little amount of information freely available for scientific research.

We aimed to contribute to the above challenges and topic with the development of HYPERstreamHS, a hydrological model that explicitly models alterations due to Human Systems such as reservoirs, intakes, power plants, etc. when simulating natural streamflows, and is also able to exploit HPC resources by mean of a dual-layer MPI implementation. Indeed, a scalability analysis performed on multiple combinations of workload subdivision allowed to assess the optimal subdivision between the two parallelization layers, granting HYPERstreamHS a quasi-ideal speedup, up to 64 processors used. HYPERstreamHS was also embedded with explicit modules for Human Systems, which were

developed and refined exclusively basing them on information that is publicly available in Italy. In order to fully inform the model, an in-depth search is conducted for each case-study, in order to fill in a highly detailed dataset for Human Systems' characteristics.

The model was firstly applied to the Adige catchment (Eastern Italian Alps), achieving very good results both in terms of hydrological and hydropower production modelling, and showing that the inclusion of Human System improved the predictions of the hydrological model. Modelled hydropower production was also validated at the catchment scale against monthly observations, achieving satisfactory results. Further analyses showed that many common simplificative assumptions come at a cost and are mostly prone to errors, especially in terms of timing and magnitude of the releases from hydropower systems, which in turn are very relevant quantity in ecosystem impact assessments.

A second application of HYPERstreamHS was performed over 5 catchments in the Western Alps, adopting the general framework that we plan on applying to every other catchment in the Italian Alpine Region as soon as their datasets are ready to be implemented. The model succesfully reproduced hydropower production, despite showing some flaws in reproducing the downstream hydrological behavior, possibly due to the spatial variability of the hydrological properties of the catchment.

The perspective activities for this work include the validation on the remaining portion of the Italian Alpine Region of the HYPERstreamHS framework, hence including the completion of the Human Systems input dataset. Once the modelling setup is completed and validated, it will provide stepping stone for analyses that can range from climate change impact assessments, to scenario analyses comparing the effects of several reservoir operating rules and environmental policies, to multi-objective optimization studies.

A.1 Natural Hydrological conceptual model

In this Appendix, the vertical water flux generation module adopted in HYPERstremHS model is presented, together with the main concepts of HYPERstream routing scheme (Piccolroaz et al., 2016).

A.1.1 Computational grid

The spatial domain is partitioned into M macrocells of equal shape and size (Figure 2.1b). Furthermore, N nodes are identified, which correspond to the locations where streamflow is computed (Figure 2.1a). Macrocells can be defined such that the hydrological model shares the same grid of an overlaying climate model or of a gridded dataset providing the input meteorological forcing. The nodes are arbitrarily distributed along the river network, and typically are located in correspondence of existing gauging stations where streamflow observations are available (needed for model calibration and validation), or in the presence of infrastructures that need to be simulated by human system module.

A one-time and offline pre-processing step is run to prepare the geometrical information needed to implement the streamflow routing scheme. The DEM is analyzed in order to extract the river network and the drainage characteristics of the study area, and to derive the corresponding geomorphological width functions for each macrocell-node pair (see Figure 2.1b). Other properties useful for the evaluation of the water fluxes (e.g., average elevation, soil use and type, crop coefficient etc.) are computed for each macrocell based on the analysis of the available DEM and land-use/land-cover spatial maps. A detailed example of macrocell-discretization and width functions derivations can be found in Piccolroaz et al. (2016).

A.1.2 Vertical water flux module

The vertical water flux module adopted in HYPERstreamHS employs the formulation proposed by Laiti et al. (2018). It relies on the coupling of the con-

tinuous soil-moisture accounting scheme for surface flow generation based on the SCS-CN (Michel et al., 2005) with a non-linear bucket model for soil moisture depletion (Majone et al., 2010), and a linear reservoir model to simulate the base-flow component. In addition, a simple degree-day model is used for the simulation of snow dynamics while Hargreaves and Samani (1982) formulation is employed for the computation of potential evapotranspiration (ET_p). A schematic of the water flux generation module is presented in Figure 2.1a, while each component is presented in details in the ensuing paragraphs. Calibration parameters are shown in bold.

The degree-day model for snow accumulation and melting dynamics is based on the following water balance equation (e.g., Hock, 2003; Majone et al., 2010; Rango and Martinec, 1995):

$$\frac{dh_s}{dt} = p_s - p_m, \tag{1}$$

where h_s $[L]$ is the snowpack water equivalent, p_s $[LT^{-1}]$ is the solid precipitation intensity, and p_m $[LT^{-1}]$ is the snowmelt intensity. p_s and p_m are quantified according to the following equations based on air temperature thresholds:

$$p_s = \begin{cases} p, & T_a \leq \mathbf{T_s} \\ 0, & T_a > \mathbf{T_s} \end{cases} \tag{2}$$

$$p_m = \begin{cases} 0, & T_a \leq \mathbf{T_m} \\ \mathbf{c_m}(T_a - \mathbf{T_m}), & T_a > \mathbf{T_m} \end{cases} \tag{3}$$

where, T_a $[^\circ C]$ is the air temperature, T_s $[^\circ C]$ is the threshold temperature below which precipitation is assumed as solid, T_m $[^\circ C]$ is the threshold temperature above which the snowpack melts, and c_m $[L\ T^{-1}\ ^\circ C^{-1}]$ is the melting factor providing the amount of snow melted per unit of time. Notice that when $T_s < T_a \leq T_m$ precipitation is liquid, but the energy input to the snowpack is

not sufficient for triggering melting. The effective liquid precipitation p_e $[LT^{-1}]$ entering the soil can be then computed as follows:

$$p_e = \begin{cases} 0, & T_a \leq \mathbf{T_s} \\ p, & \mathbf{T_s} < T_a \leq \mathbf{T_m} \\ p + p_m, & T_a > \mathbf{T_m} \end{cases}$$

The degree-day approach used here requires mean daily air temperature T_a as input, thus provides mean daily values of p_m. If the time step integration of the HYPERstreamHS model is less than one day, the melt water contribution is evenly distributed during the day.

The soil moisture accounting accounting scheme for surface flow generation is fed by effective rainfall p_e, and is governed by the following non-linear water balance equation:

$$\frac{dSM}{dt} = p_e - q_r - q_p - ET_r\,, \tag{4}$$

where SM $[L]$ is the soil moisture, q_r $[LT^{-1}]$ is the surface runoff rate, q_p $[LT^{-1}]$ is the leakage flux (i.e., the water flux from the top soil layer towards groundwater), and $ET_r[LT^{-1}]$ is the real evapotranspiration. The surface runoff rate q_r is evaluated according to the procedure proposed by Michel et al. (2005), which is an extension of the well-known SCS-CN approach (U.S. Soil Conservation Service, 1964) accounting for a time varying soil moisture in the active soil. In particular, q_r is evaluated as follows:

$$q_r = \begin{cases} p_e \dfrac{SM - S_a}{S^*}\left(2 - \dfrac{SM - S_a}{S^*}\right), & SM \geq S_a \\ 0, & SM < S_a \end{cases}$$

where S^* $[L]$ is the maximum potential soil infiltration, and S_a $[L]$ is the threshold above which runoff is generated. S^* is given by the product of the

maximum potential infiltration estimated from the land use and lithological characteristics of the soil (S [L]) and a scaling coefficient c_s [-], such that:

$$S^* = \mathbf{c_s} S. \tag{5}$$

This correction allows to account for possible uncertainties in the identification of S. S_a is defined as the soil moisture level at the beginning of a precipitation event plus the initial abstraction, and is assumed proportional to S^* through the following relationship:

$$S_a = \mathbf{c_a} S, \tag{6}$$

where c_a [-] is a scaling coefficient. We notice that $p_e - q_r$ is the infiltration rate into the soil layer and that its saturation level is given by S^* plus S_a.

Daily reference evapotranspiration ET_0 [LT^{-1}] is estimated through the equation proposed by Hargreaves and Samani (1982), based on mean, minimum, and maximum daily air temperature T_a. Following Allen et al. (1998), ET_0 is multiplied by a monthly varying crop coefficient K_c [-] in order to estimate potential evapotranspiration ET_p, thus accounting for the presence of specific crop or natural vegetation and their seasonal vegetative conditions:

$$ET_p = K_c 0.408 \left[0.0023 R_a \left(T_a + 17.8\right) \sqrt{T_a^{max} - T_a^{min}} \right], \tag{7}$$

where R_a is the extraterrestrial radiation [$MJm^{-2}d^{-1}$]. Finally, real evapotranspiration ET_r is computed taking into account that evapotranspiration reaches its potential (upper) limit only when soil moisture is larger than the field capacity values SM_{fc} [-], and that ET_r tends to zero as SM approaches its residual limit SM_r:

$$ET_r = \begin{cases} 0, & SM \leq SM_r \\ ET_p \dfrac{SM - SM_r}{SM_{fc} - SM_r)} & SM_r < SM \leq SM_{fc} \\ ET_p, & SM > SM_{fc} \end{cases}$$

where

$$SM_r = (S^* + S_a)\mathbf{c_r},$$
$$SM_{fc} = (S^* + S_a)\mathbf{c_{fc}},$$

and c_{fc} and c_r are calibration coefficients smaller than one. In particular, for values of SM between SM_r and SM_{fc}, ET_r is assumed to vary linearly from zero to ET_p. Similar to the snowmelting, ET_r is evaluated as daily average, and if the computational time step of HYPERstreamHS is smaller than one day, ET_r is evenly distributed during the day.

The leakage flux from the active soil q_p is evaluated through the following exponential law

$$q_p = \mathbf{q_{ref}} \left[e^{\left(\frac{SM - SM_r}{\mu} \right)} - 1 \right], \tag{8}$$

where q_{ref} $[LT^{-1}]$ and μ $[L]$ are calibration parameters controlling the maximum and rate of variation of the leakage flux, respectively. We notice that both q_p and ET_r tends to zero as SM approaches SM_r, thus avoiding SM to drop below its lower physical bound SM_r in absence of infiltration (i.e., when $p_e - q_r = 0$). Similar exponential relationships for storage-discharge dynamics coupled with the surface runoff model by Michel et al. (2005) have been successfully applied in previous applications conducted in Alpine and Mediterranean catchments (Bellin et al., 2016; Majone et al., 2012, 2016; Piccolroaz et al., 2015).

The leakage flux q_p is then divided into two components through a partition parameter α. The first component contributes to the runoff as interflow q_i $[LT^{-1}]$, whilst the latter constitutes deep percolation to groundwater q_{dp} $[LT^{-1}]$:

$$q_i = q_p \alpha ,$$
$$q_{dp} = q_p (1-\alpha) .$$

Finally, q_{dp} feeds a linear reservoir model described by the following continuity equation:

$$\mathbf{k} \frac{dq_b}{dt} = q_{dp} - q_b , \tag{9}$$

where q_b $[LT^{-1}]$ is the baseflow contributing to the streamflow, and k is a calibration parameter.

The vertical water flux generation model described above is applied for all macrocells separately, using as input the meteorological forcing pertaining to each of them. At each macrocell, the total runoff per unit area q_s $[LT^{-1}]$ is evaluated by summing together the surface runoff rate q_r, the interflow q_i, and the baseflow contribution q_b.

A.1.3 Routing algorithm

Following Piccolroaz et al. (2016), the streamflow $Q_k^{(i)}(t)$ $[L^3T^{-1}]$ generated by macrocell i and contributing to the node k at time t reads as follow:

$$Q_k^{(i)}(t) = A_k^{(i)} \int_0^t q_s^{(i)}(t-\tau) f_k^{(i)}(\tau) d\tau = A_k^{(i)} \left(q_s^{(i)}(t) * f_k^{(i)}(t) \right) , \tag{10}$$

where $A_k^{(i)}$ $[L^2]$ is the fraction (area) of macrocell i contributing to node k, $q_s^{(i)}$ $[LT^{-1}]$ is the vertical water flux per unit area produced by the macrocell i, $f_k^{(i)}$ is the pdf of the travel times of macrocell i relative to node k obtained by

rescaling the width function (built in the pre-processing step) by the stream velocity, and the asterisk denotes convolution. In doing this, it is assumed that $q_s^{(i)}$ is constant through the macrocell and is evaluated according to the vertical flux generation module above described.

The total streamflow at node k ($Q_k(t)$) is computed as the sum of the contribution of each macrocell to that node, plus the streamflow transferred from the nodes upstream of k:

$$Q_k(t) = \sum_{i=1}^{M_k^{con}} Q_k^{(i)}(t) + \sum_{j=1}^{N_k^{up}} Q_j(t-\tau_{jk}), \tag{11}$$

where $\tau_{jk} = D_{jk}/V_c$ $[T]$ is the travel time from node j, located upstream of k, to node k, D_{jk} $[L]$ is the distance between the two nodes, V_c $[LT^{-1}]$ is the stream velocity, M_k^{con} is the number of macrocells contributing to node k, and N_k^{up} is the number of nodes upstream of k.

A.1.4 Model's parameters

A total of 12 model parameters is used, 11 pertaining to the vertical water flux generation module and 1 to the HYPERstream routing scheme. Parameters of vertical water flux module are assumed as spatially uniform, with the spatial heterogeneity of hydrological processes being delegated to the different values of S and K_c assigned to the different macrocells. Such values are derived from available infiltration capacity and soil use maps, and are computed as weighted averages of the values at each DTM cell contained in a given macrocell. Routing scheme requires the definition of a single parameter, the stream velocity V_c, which is assumed constant, thus making the model linear and easily parallelizable. The list of the 12 calibration parameters, with their units and range of variation is presented in Table .1.

Table .1 *List of the calibration parameters with their range of variation. T_s and T_m: temperature thresholds for snow precipitation and snow melting; c_m: snow melting factor; c_s and c_a: parameters of the rainfall excess model; q_{ref} and μ: parameters of the nonlinear reservoir mimicking the dynamics of the unsaturated zone; c_{fc} and c_r: coefficients for field capacity and residual soil moisture; k: mean residence time of the baseflow linear reservoir; : α partition coefficient for leakage flux; V_c: stream velocity.*

Parameters	Range of variation	Unit
T_s	$-2 \div 6$	$[^\circ C]$
T_m	$-2 \div 6$	$[^\circ C]$
c_m	$0 \div 10$	$[mm^\circ C^{-1} d^{-1}]$
c_s	$0.1 \div 10$	-
c_a	$0.01 \div 1$	-
q_{ref}	$10^{-7} \div 10^{-3}$	$[mm\ s^{-1}]$
μ	$0.5 \div 300$	$[mm]$
c_{fc}	$0 \div 1$	-
c_r	$0 \div 0.25$	-
k	$200 \div 1000$	$[day]$
α	$0 \div 1$	-
V_c	$0.2 \div 4$	$[m\ s^{-1}]$

RESEARCH OUTPUTS AND RELEVANT WORKS

The work presented in this thesis produced the following scientific research outputs:

B.2 Articles

Avesani, D., Galletti, A., Piccolroaz, S., Bellin, A., Majone, B. A Dual layer MPI continuous large-scale hydrological model including Human Systems, Environmental Modelling & Software, **SUBMITTED**;

Galletti, A., Avesani, D., Bellin, A., Majone, B. Detailed simulation of storage hydropower systems in a large Alpine watershed, in preparation for Water Resources Research.

C.3 MS Theses supervision

Analysis of the correlation between hydropower production, observed streamflows and electricity price in the Italian Alps Region (original title: "Influenza dei fattori idrologici e di mercato sulla produzione idrolettrica nell'Arco Alpino Italiano", author: Stefano Flaim);

Setup and validation of HYPERstreamHS on a large catchment in the Western Alps (original title: "Simulazione della produzione idroelettrica in cinque bacini delle Alpi Ociidentali", author: Sergio Cimoli);

Investigation of the performance of several Machine Learning techniques in reproducing anthropogenic streamflow alterations (original title: "Applicazione delle tecniche di intelligenza artificiale nella previsione della portata nei bacini

con deflussi alterati dall'uso idroelettrico", author: Gregorio Ortombina).

D.4 Posters and Oral presentation

Poster: Galletti A., Todaro A., Bellin A., Majone B. (2017), "Hydropower Generation in the Italian Alpine Region", EoCoE F2F meeting, Toulouse (France), 29-30 November 2017;

Presentation: Galletti A., Todaro A., Bellin A., Majone B. (2018), "Modelling hydropower production in the Italian Alpine region: statistical vs physically-based approach", EoCoE Project final conference, Nicosia (Cyprus), 17-18 September 2018;

Poster: Galletti A., Avesani, D., Bellin A., Majone B. (2019), "Detailed simulation of storage hydropower in a large alpine watershed", EGU meeting, Wien (Austria), 7-12 April 2019;

Poster: Avesani, D., Galletti A., Bellin A., Majone B. (2019), "HYPERstreamHS: a dual-layer MPI continuous large-scale hydrological model", SII meeting, Bologna (Italy), 17 September 2019;

Poster: Galletti A., Avesani D., Bellin A., Majone B., (2019) "Detailed simulation of storage hydropower in a mesoscale catchment: modelling approach and data requirements", AGU meeting, S. Francisco (California), 9-13 December 2019.

BIBLIOGRAPHY

Akpinar, A., 2013.
The contribution of hydropower in meeting electric energy needs: The case of turkey.
Renewable Energy 51, 206 – 219.
URL: http://www.sciencedirect.com/science/article/pii/S0960148112006209, doi:https://doi.org/10.1016/j.renene.2012.09.049.

Ali, S., Aadhar, S., Shah, H., Mishra, V., 2018.
Projected increase in hydropower production in india under climate change.
Scientific Reports 8, 12450.
doi:10.1038/s41598-018-30489-4.

Allen, R., Allen, R., Food, of the United Nations, A.O., 1998.
Crop evapotranspiration: guidelines for computing crop water requirements.
Number nos. 56-57 in FAO irrigation and drainage paper, Food and Agriculture Organization of the United Nations.
URL: https://books.google.it/books?id=42hRAAAAMAAJ.

Amdahl, G.M., 1967.
Validity of the single processor approach to achieving large scale computing capabilities, in: Proceedings of the April 18-20, 1967, Spring Joint Computer Conference, ACM, New York, NY, USA. pp. 483–485.
URL: http://doi.acm.org/10.1145/1465482.1465560, doi:10.1145/1465482.1465560.

Amjath-Babu, T., Sharma, B., Brouwer, R., Rasul, G., Wahid, S.M., Neupane, N., Bhattarai, U., Sieber, S., 2019.

Integrated modelling of the impacts of hydropower projects on the water-food-energy nexus in a transboundary himalayan river basin.
Applied Energy 239, 494 – 503.
URL: http://www.sciencedirect.com/science/article/pii/S030626191930128X, doi:https://doi.org/10.1016/j.apenergy.2019.01.147.

Anand, J., Gosain, A., Khosa, R., 2018.
Optimisation of multipurpose reservoir operation by coupling soil and water assessment tool (swat) and genetic algorithm for optimal operating policy (case study: Ganga river basin).
Sustainability 10, 1–20.
doi:10.3390/su10051660.

Ashraf, F., Torabi Haghighi, A., Riml, J., Alfredsen, K., Koskela, J., Klöve, B., Marttila, H., 2018.
Changes in short term river flow regulation and hydropeaking in nordic rivers.
Scientific Reports 8.
doi:10.1038/s41598-018-35406-3.

Barton, J.P., Infield, D.G., 2004.
Energy storage and its use with intermittent renewable energy.
IEEE Transactions on Energy Conversion 19, 441–448.
doi:10.1109/TEC.2003.822305.

Bavay, M., Grunewald, T., Lehning, M., 2013.
Response of snow cover and runoff to climate change in high alpine catchments of eastern switzerland.
Advances in Water Resources 55, 4 – 16.
URL: http://www.sciencedirect.com/science/article/pii/S0309170812003193, doi:https://doi.org/10.1016/j.advwatres.2012.12.009. snow-Atmosphere Interactions and Hydrological Consequences.

Beheshti, M., Heidari, A., Saghafian, B., 2019.
Susceptibility of hydropower generation to climate change: Karun iii dam case study.
Water 11, 1025.
doi:10.3390/w11051025.

Bellin, A., Majone, B., Cainelli, O., Alberici, D., Villa, F., 2016.
A continuous coupled hydrological and water resources management model.
Environmental Modelling & Software 75, 176 – 192.
URL: http://www.sciencedirect.com/science/article/pii/S1364815215300712, doi:https://doi.org/10.1016/j.envsoft.2015.10.013.

Beniston, M., 2012.
Impacts of climatic change on water and associated economic activities in the swiss alps.
Journal of Hydrology 412-413, 291–296.
URL: https://archive-ouverte.unige.ch/unige:18512. iD: unige:18512.

Beven, K., Binley, A., 1992.
The future of distributed models: Model calibration and uncertainty prediction.
Hydrological Processes 6, 279–298.
URL: https://onlinelibrary.wiley.com/doi/abs/10.1002/hyp.3360060305, doi:10.1002/hyp.3360060305, arXiv:https://onlinelibrary.wiley.com/doi/pdf/10.1002/hyp.

Boehlert, B., Strzepek, K.M., Gebretsadik, Y., Swanson, R., McCluskey, A., Neumann, J.E., McFarland, J., Martinich, J., 2016.
Climate change impacts and greenhouse gas mitigation effects on u.s. hydropower generation.
Applied Energy 183, 1511 – 1519.

URL: http://www.sciencedirect.com/science/article/pii/S0306261916313563, doi:https://doi.org/10.1016/j.apenergy.2016.09.054.

Bollmeyer, C., Keller, J.D., Ohlwein, C., Wahl, S., Crewell, S., Friederichs, P., Hense, A., Keune, J., Kneifel, S., Pscheidt, I., Redl, S., Steinke, S., 2015.
Towards a high-resolution regional reanalysis for the european cordex domain.
Quarterly Journal of the Royal Meteorological Society 141, 1–15.
URL: https://rmets.onlinelibrary.wiley.com/doi/abs/10.1002/qj.2486, doi:10.1002/qj.2486, arXiv:https://rmets.onlinelibrary.wiley.com/doi/pdf/10.1002/qj

Bombelli, G.M., Soncini, A., Bianchi, A., Bocchiola, D., 2019.
Potentially modified hydropower production under climate change in the italian alps.
Hydrological Processes 33, 2355–2372.
URL: https://onlinelibrary.wiley.com/doi/abs/10.1002/hyp.13473, doi:10.1002/hyp.13473, arXiv:https://onlinelibrary.wiley.com/doi/pdf/10.1002/hyp.1347

Bonnema, M., Hossain, F., 2017.
Inferring reservoir operating patterns across the mekong basin using only space observations.
Water Resources Research 53, 3791–3810.
URL: https://agupubs.onlinelibrary.wiley.com/doi/abs/10.1002/2016WR019978, doi:10.1002/2016WR019978, arXiv:https://agupubs.onlinelibrary.wiley.com/doi/pdf/10.1002/

Bosona, T., Gebresenbet, G., 2010.
Modeling hydropower plant system to improve its reservoir operation.
International Journal of Water Resources and Environmental Engineering 2, 88–95.

Brunetti, M., Lentini, G., Maugeri, M., Nanni, T., Auer, I., Bohm, R., Schoner, W., 2009.
Climate variability and change in the greater alpine region over the last two centuries based on multi,Äêvariable analysis.
International Journal of Climatology 29, 2197 – 2225.
doi:10.1002/joc.1857.

Carvajal, P., Anandarajah, G., Mulugetta, Y., Dessens, O., 2017.
Assessing uncertainty of climate change impacts on long-term hydropower generation using the cmip5 ensemble,Äîthe case of ecuador.
Climatic Change doi:10.1007/s10584-017-2055-4.

Castagna, M., Bellin, A., 2009.
A bayesian approach for inversion of hydraulic tomographic data.
Water Resources Research 45.
URL: https://agupubs.onlinelibrary.wiley.com/doi/abs/10.1029/2008WR007078, doi:10.1029/2008WR007078, arXiv:https://agupubs.onlinelibrary.wiley.com/doi/pdf/10.1

Clark, M., Fan, Y., Lawrence, D., Adam, J., Bolster, D., Gochis, D., Hooper, R., Kumar, M., Leung, L., Mackay, D., Maxwell, R., Shen, C., Swenson, S., Zeng, X., 2015.
Improving the representation of hydrologic processes in earth system models.
Water Resources Research 51, 5929–5956.
doi:10.1002/2015WR017096.

Clark, M., Wilby, R., Gutmann, E., Vano, J., Gangopadhyay, S., Wood, A., Fowler, H., Prudhomme, C., Arnold, J., Brekke, L., 2016.
Characterizing uncertainty of the hydrologic impacts of climate change.
Current Climate Change Reports 2.
doi:10.1007/s40641-016-0034-x.

Dagum, L., Menon, R., 1998.
Openmp: an industry standard api for shared-memory programming.
Computational Science & Engineering, IEEE 5, 46–55.

Dang, T., Chowdhury, A.K., Galelli, S., 2020.
On the representation of water reservoir storage and operations in large-scale hydrological models: implications on model parameterization and climate change impact assessments.
Hydrology and Earth System Sciences 24, 397–416.
doi:10.5194/hess-24-397-2020.

Destouni, G., Asokan, S.M., Jarsj ö, J., 2010.
Inland hydro-climatic interaction: Effects of human water use on regional climate.
Geophysical Research Letters 37.
URL: https://agupubs.onlinelibrary.wiley.com/doi/abs/10.1029/2010GL044153, doi:10.1029/2010GL044153, arXiv:https://agupubs.onlinelibrary.wiley.com/doi/pdf/10.1029/

Destouni, G., Jaramillo, F., Prieto, C., 2013.
Hydroclimatic shifts driven by human water use for food and energy production.
Nature Climate Change 3, 213 – 217.
doi:10.1038/nclimate1719.

Fatichi, S., Rimkus, S., Burlando, P., Bordoy, R., Molnar, P., 2015.
High-resolution distributed analysis of climate and anthropogenic changes on the hydrology of an alpine catchment.
Journal of Hydrology 525, 362–382.
doi:10.1016/j.jhydrol.2015.03.036.

Finger, D., Heinrich, G., Gobiet, A., Bauder, A., 2012.
Projections of future water resources and their uncertainty in a glacierized catchment in the swiss alps and the subsequent effects on hydropower production during the 21st century.
Water Resources Research 48.

URL: https://agupubs.onlinelibrary.wiley.com/doi/abs/10.1029/2011WR010733, doi:10.1029/2011WR010733, arXiv:https://agupubs.onlinelibrary.wiley.com/doi/pdf/10.1

Gobiet, A., Kotlarski, S., Beniston, M., Heinrich, G., Rajczak, J., Stoffel, M., 2014.
21st century climate change in the european alps,Äîa review.
Science of The Total Environment 493, 1138 – 1151.
URL: http://www.sciencedirect.com/science/article/pii/S0048969713008188, doi:https://doi.org/10.1016/j.scitotenv.2013.07.050.

Gregory, K., 2006.
The human role in changing river channels.
Geomorphology 79, 172 – 191.
URL: http://www.sciencedirect.com/science/article/pii/S0169555X06002509, doi:https://doi.org/10.1016/j.geomorph.2006.06.018. 37th Binghamton Geomorphology Symposium.

Gropp, W., Lusk, E., Doss, N., Skjellum, A., 1996.
A high-performance, portable implementation of the mpi message passing interface standard.
Parallel Computing 22, 789 – 828.
URL: http://www.sciencedirect.com/science/article/pii/0167819196000245, doi:https://doi.org/10.1016/0167-8191(96)00024-5.

Guo, X., Hu, T., Wu, C., Zhang, T., Lv, Y., 2013.
Multi-objective optimization of the proposed multi-reservoir operating policy using improved nspso.
Water Resources Management 27.
doi:10.1007/s11269-013-0280-9.

Gupta, H.V., Kling, H., Yilmaz, K.K., Martinez, G.F., 2009.

Decomposition of the mean squared error and nse performance criteria: Implications for improving hydrological modelling.
Journal of Hydrology 377, 80 – 91.
URL: http://www.sciencedirect.com/science/article/pii/S0022169409004843, doi:https://doi.org/10.1016/j.jhydrol.2009.08.003.

Hargreaves, G., Samani, Z., 1982.
Estimating potential evapotranspiration.
Journal of the Irrigation & Drainage Division - ASCE 108, 225–230.

Hock, R., 2003.
Temperature index melt modelling in mountain areas.
Journal of Hydrology 282, 104 – 115.
URL: http://www.sciencedirect.com/science/article/pii/S0022169403002579, doi:https://doi.org/10.1016/S0022-1694(03)00257-9. mountain Hydrology and Water Resources.

Hwang, H.T., Park, Y.J., Frey, S.K., Callaghan, M.V., Berg, S.J., Lapen, D.R., Sudicky, E.A., 2019.
Efficient numerical incorporation of water management operations in integrated hydrosystem models: Application to tile drainage and reservoir operating systems.
Journal of Hydrology 575, 1253 – 1266.
URL: http://www.sciencedirect.com/science/article/pii/S0022169419303270, doi:https://doi.org/10.1016/j.jhydrol.2019.03.098.

IEA, .
International energy agency report on renewable energies.
https://www.iea.org/renewables2018/.
Accessed: 2019-Aug-02.

Jabbari, A., Nazemi, A., 2019.

Alterations in canadian hydropower production potential due to continuation of historical trends in climate variables.
Resources 8, 163.
doi:10.3390/resources8040163.

Jasper, K., Calanca, P., Gyalistras, D., 2004.
Differential impacts of climate change on the hydrology of two alpine river basins.
Climate Research 26, 113–129.
doi:10.3354/cr026113.

Kan, G., He, X., Ding, L., Li, J., Hong, Y., Zuo, D., Ren, M., Lei, T., Liang, K., 2018.
Fast hydrological model calibration based on the heterogeneous parallel computing accelerated shuffled complex evolution method.
Engineering Optimization 50, 106–119.
URL: https://doi.org/10.1080/0305215X.2017.1303053, doi:10.1080/0305215X.2017.1303053, arXiv:https://doi.org/10.1080/0305215X.2017.1303053.

Keiler, M., Knight, J., Harrison, S., 2010.
Climate change and geomorphological hazards in the eastern european alps.
Philosophical Transactions of the Royal Society A: Mathematical, Physical and Engineering Sciences 368, 2461–2479.
URL: https://royalsocietypublishing.org/doi/abs/10.1098/rsta.2010.0047, doi:10.1098/rsta.2010.0047, arXiv:https://royalsocietypublishing.org/doi/pdf/10.1098/r

Kennedy, J., Eberhart, R., 1995.
Particle swarm optimization, in: Proceedings of ICNN'95 - International Conference on Neural Networks, pp. 1942–1948 vol.4.
doi:10.1109/ICNN.1995.488968.

Kiesel, J., Gericke, A., Rathjens, H., Wetzig, A., Kakouei, K., J ahnig, S.C., Fohrer, N., 2019.

Climate change impacts on ecologically relevant hydrological indicators in three catchments in three european ecoregions.
Ecological Engineering 127, 404 – 416.
URL: http://www.sciencedirect.com/science/article/pii/S092585741830466X, doi:https://doi.org/10.1016/j.ecoleng.2018.12.019.

Knutti, R., 2010.
The end of model democracy?, pp. 395–404.
doi:10.1007/s10584-010-9800-2.

Koch, F., Reiter, A., Bach, H., 2016.
Effects of climate change on hydropower generation and reservoir management.
pp. 593–599.
doi:10.1007/978-3-662-48494-4_68.

Kotlarski, S., Keuler, K., Christensen, O.B., Colette, A., Déqué, M., Gobiet, A., Goergen, K., Jacob, D., Lüthi, D., van Meijgaard, E., Nikulin, G., Schär, C., Teichmann, C., Vautard, R., Warrach-Sagi, K., Wulfmeyer, V., 2014.
Regional climate modeling on european scales: a joint standard evaluation of the euro-cordex rcm ensemble.
Geoscientific Model Development 7, 1297–1333.
URL: https://www.geosci-model-dev.net/7/1297/2014/, doi:10.5194/gmd-7-1297-2014.

Kundzewicz, Z., Mata, L., Arnell, N., Doell, P., Kabat, P., Jiménez, B., Miller, K., Oki, T., Şen, Z., Shiklomanov, I., 2007.
Freshwater Resources and their Management.
pp. 173–210.

Lai, C., Shi, X., Huang, M., 2018.
Efficient utilization of multi-core processors and many-core co-processors on supercomputer beacon for scalable geocomputation and geo-simulation over big earth data.

Big Earth Data 2, 65–85.
doi:10.1080/20964471.2018.1434265.

Laiti, L., Mallucci, S., Piccolroaz, S., Bellin, A., Zardi, D., Fiori, A., Nikulin, G., Majone, B., 2018.
Testing the hydrological coherence of high-resolution gridded precipitation and temperature data sets.
Water Resources Research 54, 1999–2016.
doi:10.1002/2017WR021633.

Lazzaro, M.D., 2009.
Regional analysis of storm hydrographs in the rescaled width function framework.
Journal of Hydrology 373, 352 – 365.
doi:https://doi.org/10.1016/j.jhydrol.2009.04.027.

Le, P.V., Kumar, P., Valocchi, A.J., Dang, H.V., 2015.
Gpu-based high-performance computing for integrated surface,Äìsubsurface flow modeling.
Environmental Modelling & Software 73, 1 – 13.
URL: http://www.sciencedirect.com/science/article/pii/S1364815215300207, doi:https://doi.org/10.1016/j.envsoft.2015.07.015.

Lehner, B., Czisch, G., Vassolo, S., 2005.
The impact of global change on the hydropower potential of europe: a model-based analysis.
Energy Policy 33, 839 – 855.
URL: http://www.sciencedirect.com/science/article/pii/S0301421503003112, doi:https://doi.org/10.1016/j.enpol.2003.10.018.

Li, T., Wang, G., Chen, J., Wang, H., 2011.
Dynamic parallelization of hydrological model simulations.
Environmental Modelling & Software 26, 1736 – 1746.

URL: http://www.sciencedirect.com/science/article/pii/S1364815211001769, doi:https://doi.org/10.1016/j.envsoft.2011.07.015.

Liu, J., Zhu, A.X., Qin, C.Z., 2013.
Estimation of theoretical maximum speedup ratio for parallel computing of grid-based distributed hydrological models.
Computers & Geosciences 60, 58 – 62.
URL: http://www.sciencedirect.com/science/article/pii/S0098300413001568, doi:https://doi.org/10.1016/j.cageo.2013.04.030.

Liu, J., Zhu, A.X., Qin, C.Z., Wu, H., Jiang, J., 2016.
A two-level parallelization method for distributed hydrological models.
Environmental Modelling & Software 80, 175 – 184.
URL: http://www.sciencedirect.com/science/article/pii/S1364815216300524, doi:https://doi.org/10.1016/j.envsoft.2016.02.032.

Liu, Y., Gupta, H.V., 2007.
Uncertainty in hydrologic modeling: Toward an integrated data assimilation framework.
Water Resources Research 43.
URL: https://agupubs.onlinelibrary.wiley.com/doi/abs/10.1029/2006WR005756, doi:10.1029/2006WR005756, arXiv:https://agupubs.onlinelibrary.wiley.com/doi/pdf/10.1029/

Lloyd, S., 1982.
Least squares quantization in pcm.
IEEE Transactions on Information Theory 28, 129–137.
doi:10.1109/TIT.1982.1056489.

Madsen, H., 2000.
Automatic calibration of a conceptual rainfall-runoff model using multiple objectives.

Journal of Hydrology 235, 276 – 288.
URL: http://www.sciencedirect.com/science/article/pii/S0022169400002791, doi:https://doi.org/10.1016/S0022-1694(00)00279-1.

Majone, B., Bertagnoli, A., Bellin, A., 2010.
A non-linear runoff generation model in small alpine catchments.
Journal of Hydrology 385, 300 – 312.
URL: http://www.sciencedirect.com/science/article/pii/S0022169410001228, doi:https://doi.org/10.1016/j.jhydrol.2010.02.033.

Majone, B., Bovolo, C.I., Bellin, A., Blenkinsop, S., Fowler, H.J., 2012.
Modeling the impacts of future climate change on water resources for the gállego river basin (spain).
Water Resources Research 48.
URL: https://agupubs.onlinelibrary.wiley.com/doi/abs/10.1029/2011WR010985, doi:10.1029/2011WR010985, arXiv:https://agupubs.onlinelibrary.wiley.com/doi/pdf/10.1

Majone, B., Villa, F., Deidda, R., Bellin, A., 2016.
Impact of climate change and water use policies on hydropower potential in the south-eastern alpine region.
Science of The Total Environment 543, 965 – 980.
URL: http://www.sciencedirect.com/science/article/pii/S004896971530067X, doi:https://doi.org/10.1016/j.scitotenv.2015.05.009. special Issue on Climate Change, Water and Security in the Mediterranean.

Mallucci, S., Majone, B., Bellin, A., 2019.
Detection and attribution of hydrological changes in a large alpine river basin.
Journal of Hydrology 575, 1214 – 1229.

URL: http://www.sciencedirect.com/science/article/pii/S0022169419305712, doi:https://doi.org/10.1016/j.jhydrol.2019.06.020.

McKay, M.D., Beckman, R.J., Conover, W.J., 1979.
A comparison of three methods for selecting values of input variables in the analysis of output from a computer code.
Technometrics 21, 239–245.
URL: http://www.jstor.org/stable/1268522.

Meissner, S., Relier, A., 2005.
Sustainable Management of Alpine Water Potentials.
Institut de Geographie Alpine.
URL: https://www.persee.fr/doc/rga_0035-1121_2005_num_93_3_2353, doi:10.3406/rga.2005.2353.

Michel, C., Andréassian, V., Perrin, C., 2005.
Soil conservation service curve number method: How to mend a wrong soil moisture accounting procedure?
Water Resources Research 41.
doi:10.1029/2004WR003191.

Montanari, A., Shoemaker, C.A., van de Giesen, N., 2009.
Introduction to special section on uncertainty assessment in surface and subsurface hydrology: An overview of issues and challenges.
Water Resources Research 45.
URL: https://agupubs.onlinelibrary.wiley.com/doi/abs/10.1029/2009WR008471, doi:10.1029/2009WR008471, arXiv:https://agupubs.onlinelibrary.wiley.com/doi/pdf/10.1029/

Moriasi, D., Arnold, J., Van Liew, M., Bingner, R., Harmel, R., Veith, T., 2007.
Model evaluation guidelines for systematic quantification of accuracy in watershed simulations.
Transactions of the ASABE 50.
doi:10.13031/2013.23153.

MPI Forum, M.P., 1994.
MPI: A Message-Passing Interface Standard.
Technical Report. Knoxville, TN, USA.

Musiał, G., D»©bski, L., Jeziorek-Knioła, D., GołaÃßb, K., 2008.
A self-scheduling scheme for parallel processing in heterogeneous environment: Simulations of the monte carlo type, in: Wyrzykowski, R., Dongarra, J., Karczewski, K., Wasniewski, J. (Eds.), Parallel Processing and Applied Mathematics, Springer Berlin Heidelberg, Berlin, Heidelberg. pp. 429–438.

Nash, J., Sutcliffe, J., 1970.
River flow forecasting through conceptual models part i - a discussion of principles.
Journal of Hydrology 10, 282 – 290.
URL: http://www.sciencedirect.com/science/article/pii/0022169470902556, doi:https://doi.org/10.1016/0022-1694(70)90255-6.

Nazemi, A., Wheater, H.S., 2015a.
On inclusion of water resource management in earth system models - part 2: Representation of water supply and allocation and opportunities for improved modeling.
Hydrology and Earth System Sciences 19, 63–90.
URL: https://www.hydrol-earth-syst-sci.net/19/63/2015/, doi:10.5194/hess-19-63-2015.

Nazemi, A., Wheater, H.S., 2015b.
On inclusion of water resource management in earth system models; part 1: Problem definition and representation of water demand.
Hydrology and Earth System Sciences 19, 33–61.
URL: https://www.hydrol-earth-syst-sci.net/19/33/2015/, doi:10.5194/hess-19-33-2015.

Ng, J.Y., Turner, S.W.D., Galelli, S., 2017.
Influence of el niño southern oscillation on global hydropower production.

Environmental Research Letters 12, 034010.
URL: https://doi.org/10.1088%2F1748-9326%2Faa5ef8, doi:10.1088/1748-9326/aa5ef8.

Ortega, L., Rueda, A., 2010.
Parallel drainage network computation on cuda.
Computers & Geosciences 36, 171 – 178.
URL: http://www.sciencedirect.com/science/article/pii/S0098300409002970, doi:https://doi.org/10.1016/j.cageo.2009.07.005.

Oyerinde, G., Wisser, D., Hountondji, F., Odofin, A., Lawin, A., Afouda, A., Diekkr uger, B., 2016.
Quantifying uncertainties in modeling climate change impacts on hydropower production.
Climate 4, 34.
doi:10.3390/cli4030034.

de Paiva, R.C.D., Buarque, D.C., Collischonn, W., Bonnet, M.P., Frappart, F., Calmant, S., Bulhões Mendes, C.A., 2013.
Large-scale hydrologic and hydrodynamic modeling of the amazon river basin.
Water Resources Research 49, 1226–1243.
URL: https://agupubs.onlinelibrary.wiley.com/doi/abs/10.1002/wrcr.20067, doi:10.1002/wrcr.20067, arXiv:https://agupubs.onlinelibrary.wiley.com/doi/pdf/10.1002/

Panday, S., Huyakorn, P.S., 2004.
A fully coupled physically-based spatially-distributed model for evaluating surface/subsurface flow.
Advances in Water Resources 27, 361 – 382.
URL: http://www.sciencedirect.com/science/article/pii/S030917080400017X, doi:https://doi.org/10.1016/j.advwatres.2004.02.016. a Tribute to George F. Pinder.

Piccolroaz, S., Di Lazzaro, M., Zarlenga, A., Majone, B., Bellin, A., Fiori, A., 2016.
Hyperstream: a multi-scale framework for streamflow routing in large-scale hydrological model.
Hydrology and Earth System Sciences 20, 2047–2061.
URL: https://www.hydrol-earth-syst-sci.net/20/2047/2016/, doi:10.5194/hess-20-2047-2016.

Piccolroaz, S., Majone, B., Palmieri, F., Cassiani, G., Bellin, A., 2015.
On the use of spatially distributed, time-lapse microgravity surveys to inform hydrological modeling.
Water Resources Research 51, 7270–7288.
doi:10.1002/2015WR016994.

Pilgrim, D.H., 1977.
Isochrones of travel time and distribution of flood storage from a tracer study on a small watershed.
Water Resources Research 13, 587–595.
doi:10.1029/WR013i003p00587.

Pitman, W.V., 1973.
A mathematical model for generating monthly river flows from meteorological data in South Africa.
Technical Report 2/73. Johannesburg : University of the Witwatersrand, Dept. of Civil Engineering.

Poff, N., Brown, C., Grantham, T.T., Mendoza, G., Dominique, K., Haasnoot, M., Baeza, A., Spence, C., Wilby, R., Palmer, M., Matthews, J., 2015.
Sustainable water management under future uncertainty with eco-engineering decision scaling.
Nature Climate Change doi:10.1038/NCLIMATE2765.

Qin, C.Z., Zhan, L., 2012.
Parallelizing flow-accumulation calculations on graphics processing units-from iterative dem preprocessing algorithm to recursive multiple-flow-direction algorithm.

Computers & Geosciences 43, 7 – 16.
URL: http://www.sciencedirect.com/science/article/pii/S0098300412000787, doi:https://doi.org/10.1016/j.cageo.2012.02.022.

Qin, P., Xu, H., Liu, M., Du, L., Xiao, C., Liu, L., Tarroja, B., 2020.
Climate change impacts on three gorges reservoir impoundment and hydropower generation.
Journal of Hydrology 580, 123922.
URL: http://www.sciencedirect.com/science/article/pii/S0022169419306420, doi:https://doi.org/10.1016/j.jhydrol.2019.123922.

Rango, A., Martinec, J., 1995.
Revisiting the degree-day method for snowmelt computations1.
JAWRA Journal of the American Water Resources Association 31, 657–669.
doi:10.1111/j.1752-1688.1995.tb03392.x.

Refsgaard, J.C., Højberg, A.L., Møller, I., Hansen, M., Søndergaard, V., 2010.
Groundwater modeling in integrated water resources management,Äîvisions for 2020.
Groundwater 48, 633–648.
URL: https://ngwa.onlinelibrary.wiley.com/doi/abs/10.1111/j.1745-6584.2009.00634.x, doi:10.1111/j.1745-6584.2009.00634.x, arXiv:https://ngwa.onlinelibrary.wiley.com/doi/pdf/10.1111/j.1

Rinaldo, A., Marani, A., Rigon, R., 1991.
Geomorphological dispersion.
Water Resources Research 27, 513–525.
doi:10.1029/90WR02501.

Robinson, J., Rahmat-Samii, Y., 2004.
Particle swarm optimization in electromagnetics.
IEEE Transactions on Antennas and Propagation 52, 397–407.

doi:10.1109/TAP.2004.823969.

Rodríguez-Iturbe, I., Rinaldo, A., 1997.
Fractal River Basins –- chance and self-organization.
Cambridge University Press, Cambridge.

Rojas, R., Velleux, M., Julien, P.Y., Johnson, B.E., 2008.
Grid scale effects on watershed soil erosion models.
Journal of Hydrologic Engineering 13, 793–802.
doi:10.1061/(ASCE)1084-0699(2008)13:9(793).

Rouholahnejad, E., Abbaspour, K., Vejdani, M., Srinivasan, R., Schulin, R., Lehmann, A., 2012.
A parallelization framework for calibration of hydrological models.
Environmental Modelling & Software 31, 28 – 36.
URL: http://www.sciencedirect.com/science/article/pii/S1364815211002829, doi:https://doi.org/10.1016/j.envsoft.2011.12.001.

Rueda, A.J., Noguera, J.M., Luque, A., 2016.
A comparison of native gpu computing versus openacc for implementing flow-routing algorithms in hydrological applications.
Computers & Geosciences 87, 91 – 100.
URL: http://www.sciencedirect.com/science/article/pii/S0098300415300959, doi:https://doi.org/10.1016/j.cageo.2015.12.004.

Schaefli, B., Hingray, B., Musy, A., 2007.
Climate change and hydropower production in the swiss alps: quantification of potential impacts and related modelling uncertainties.
Hydrology and Earth System Sciences 11, 1191–1205.
URL: https://www.hydrol-earth-syst-sci.net/11/1191/2007/, doi:10.5194/hess-11-1191-2007.

Scipión, D.E., Mott, R., Lehning, M., Schneebeli, M., Berne, A., 2013.

Seasonal small-scale spatial variability in alpine snowfall and snow accumulation.
Water Resources Research 49, 1446–1457.
URL: https://agupubs.onlinelibrary.wiley.com/doi/abs/10.1002/wrcr.20135, doi:10.1002/wrcr.20135, arXiv:https://agupubs.onlinelibrary.wiley.com/doi/pdf/10.1002/

Shin, S., Pokhrel, Y., Miguez-Macho, G., 2019.
High-resolution modeling of reservoir release and storage dynamics at the continental scale.
Water Resources Research 55, 787–810.
URL: https://agupubs.onlinelibrary.wiley.com/doi/abs/10.1029/2018WR023025, doi:10.1029/2018WR023025, arXiv:https://agupubs.onlinelibrary.wiley.com/doi/pdf/10.1029/

Shrestha, S., Khatiwada, M., Babel, M., Parajuli, K., 2014.
Impact of climate change on river flow and hydropower production in kulekhani hydropower project of nepal.
Environmental Processes 1.
doi:10.1007/s40710-014-0020-z.

Sperna Weiland, F., Vrugt, J., Beek, R., Weerts, A., Bierkens, M., 2015.
Significant uncertainty in global scale hydrological modeling from precipitation data errors.
Journal of Hydrology 529.
doi:10.1016/j.jhydrol.2015.08.061.

Tarboton, D.G., Bras, R.L., Rodriguez-Iturbe, I., 1991.
On the extraction of channel networks from digital elevation data.
Hydrological Processes 5, 81–100.
doi:10.1002/hyp.3360050107.

TERNA, 2015.
Statistic reports on electricity consumption.

https://www.terna.it/it/sistema-elettrico/statistiche/pubblicazioni-statistiche.

Todaro, A., 2020.
Improved representation of hydrological processes in a mesoscale alpine watershed: climating forcing issue and hydrological benchmarking.
Master's thesis. University of Trento.

Todd, M.C., Taylor, R.G., Osborn, T.J., Kingston, D.G., Arnell, N.W., Gosling, S.N., 2011.
Uncertainty in climate change impacts on basin-scale freshwater resources ,Äì preface to the special issue: the quest-gsi methodology and synthesis of results.
Hydrology and Earth System Sciences 15, 1035–1046.
URL: https://www.hydrol-earth-syst-sci.net/15/1035/2011/, doi:10.5194/hess-15-1035-2011.

Tristram, D., Hughes, D., Bradshaw, K., 2014.
Accelerating a hydrological uncertainty ensemble model using graphics processing units (gpus).
Computers & Geosciences 62, 178 – 186.
URL: http://www.sciencedirect.com/science/article/pii/S0098300413002008, doi:https://doi.org/10.1016/j.cageo.2013.07.011.

Tu, M.Y., Hsu, N.S., Yeh, W., 2003.
Optimization of reservoir management and operation with hedging rules.
Journal of Water Resources Planning and Management-asce - J WATER RESOUR PLAN MAN-ASCE 129.
doi:10.1061/(ASCE)0733-9496(2003)129:2(86).

Tuo, Y., Duan, Z., Disse, M., Chiogna, G., 2016.
Evaluation of precipitation input for swat modeling in alpine catchment: A case study in the adige river basin (italy).
Science of The Total Environment 573, 66 – 82.

URL: http://www.sciencedirect.com/science/article/pii/S0048969716317260, doi:https://doi.org/10.1016/j.scitotenv.2016.08.034.

Turner, S.W., Ng, J.Y., Galelli, S., 2017.
Examining global electricity supply vulnerability to climate change using a high-fidelity hydropower dam model.
Science of The Total Environment 590-591, 663 – 675.
URL: http://www.sciencedirect.com/science/article/pii/S0048969717305272, doi:https://doi.org/10.1016/j.scitotenv.2017.03.022.

U.S. Soil Conservation Service, 1964.
SCS national engineering handbook.
Washington.

Vivoni, E.R., Mascaro, G., Mniszewski, S., Fasel, P., Springer, E.P., Ivanov, V.Y., Bras, R.L., 2011.
Real-world hydrologic assessment of a fully-distributed hydrological model in a parallel computing environment.
Journal of Hydrology 409, 483 – 496.
URL: http://www.sciencedirect.com/science/article/pii/S0022169411006093, doi:https://doi.org/10.1016/j.jhydrol.2011.08.053.

Vrugt, J.A., Gupta, H.V., Bastidas, L.A., Bouten, W., Sorooshian, S., 2003.
Effective and efficient algorithm for multiobjective optimization of hydrologic models.
Water Resources Research 39.
URL: https://agupubs.onlinelibrary.wiley.com/doi/abs/10.1029/2002WR001746, doi:10.1029/2002WR001746, arXiv:https://agupubs.onlinelibrary.wiley.com/doi/pdf/10.1029/

Wagener, T., 2003.
Evaluation of catchment models.

Hydrological Processes 17, 3375–3378.
URL: https://onlinelibrary.wiley.com/doi/abs/10.1002/hyp.5158, doi:10.1002/hyp.5158, arXiv:https://onlinelibrary.wiley.com/doi/pdf/10.1002/hyp.

Wagner, T., Themeßl, M., Schuppel, A., Gobiet, A., Stigler, H., Birk, S., 2016.
Impacts of climate change on stream flow and hydro power generation in the alpine region.
Environmental Earth Sciences 76, 4.
doi:10.1007/s12665-016-6318-6.

Waldman, J., Sharma, S.N., Afshari, S., Fekete, B.M., 2019.
Solar-power replacement as a solution for hydropower foregone in us dam removals.
Nature Sustainability 2, 872 – 878.

Wang, H., Zhou, Y., Fu, X., Gao, J., Wang, G., 2012.
Maximum speedup ratio curve (msc) in parallel computing of the binary-tree-based drainage network.
Computers & Geosciences 38, 127 – 135.
URL: http://www.sciencedirect.com/science/article/pii/S0098300411001919, doi:https://doi.org/10.1016/j.cageo.2011.05.015.

Wilby, R.L., Dessai, S., 2010.
Robust adaptation to climate change.
Weather 65, 180–185.
URL: https://rmets.onlinelibrary.wiley.com/doi/abs/10.1002/wea.543, doi:10.1002/wea.543, arXiv:https://rmets.onlinelibrary.wiley.com/doi/pdf/10.100

Wu, Y., Li, T., Sun, L., Chen, J., 2013.
Parallelization of a hydrological model using the message passing interface.
Environmental Modelling & Software 43, 124 – 132.

URL: http://www.sciencedirect.com/science/article/pii/S1364815213000327, doi:https://doi.org/10.1016/j.envsoft.2013.02.002.

Yamazaki, D., Kanae, S., Kim, H., Oki, T., 2011.
A physically based description of floodplain inundation dynamics in a global river routing model.
Water Resources Research 47.
URL: https://agupubs.onlinelibrary.wiley.com/doi/abs/10.1029/2010WR009726, doi:10.1029/2010WR009726, arXiv:https://agupubs.onlinelibrary.wiley.com/doi/pdf/10.1029/

Yang, Y., Wang, G., Wang, L., Yu, J., Xu, Z., 2014.
Evaluation of gridded precipitation data for driving swat model in area upstream of three gorges reservoir.
PLOS ONE 9, 1–15.
URL: https://doi.org/10.1371/journal.pone.0112725, doi:10.1371/journal.pone.0112725.

Yates, D., Sieber, J., Purkey, D., Huber-Lee, A., 2005.
Weap21,Äîa demand-, priority-, and preference-driven water planning model.
Water International 30, 487–500.
URL: https://doi.org/10.1080/02508060508691893, doi:10.1080/02508060508691893,arXiv:https://doi.org/10.1080/025080605

Zhang, A., Li, T., Si, Y., Liu, R., Shi, H., Li, X., Li, J., Wu, X., 2016.
Double-layer parallelization for hydrological model calibration on hpc systems.
Journal of Hydrology 535, 737 – 747.
URL: http://www.sciencedirect.com/science/article/pii/S002216941600041X, doi:https://doi.org/10.1016/j.jhydrol.2016.01.024.

Zhang, X., Srinivasan, R., Van Liew, M., 2008.

Multi-site calibration of the swat model for hydrologic modeling.
Transactions of the ASABE 51.
doi:10.13031/2013.25407.

Zhang, Y., Zhai, X., Zhao, T., 2018.
Annual shifts of flow regime alteration: New insights from the chaishitan reservoir in china.
Scientific Reports 8.
doi:10.1038/s41598-018-19717-z.

Zhao, G., Gao, H., Naz, B.S., Kao, S.C., Voisin, N., 2016.
Integrating a reservoir regulation scheme into a spatially distributed hydrological model.
Advances in Water Resources 98, 16 – 31.
URL: http://www.sciencedirect.com/science/article/pii/S0309170816305504, doi:https://doi.org/10.1016/j.advwatres.2016.10.014.